NTNU – Trondheim
Norwegian University of
Science and Technology

Analysis and Design of Ship Collision Barriers on a Submerged Floating Tunnel subjected to Large Ship Collisions

Jørgen Lima Hansen

Marine Technology
Submission date: June 2015
Supervisor: Jørgen Amdahl, IMT

Norwegian University of Science and Technology
Department of Marine Technology

NTNU
Norges teknisk-naturvitenskapelige universitet
Institutt for marin teknikk

MASTER THESIS 2015
for
Stud. Techn. Jørgen Lima Hansen

Analysis and Design of Ship Collision Barriers on a Submerged Floating Tunnel subjected to Large Ship Collisions

Analyse og dimensjonering av skipsbarriere for flytetunnel utsatt for støt fra store skip

Aim of study:
The aim of the Project – and Master thesis work is to quantify the response of a new concept for mooring floating bridges and submerged floating tunnels (SFT). The transition piece between the floating bridge and the SFT is especially exposed to ship collisions. A new concept for energy absorption shall be investigated on the basis of data for ship traffic and the likelihood for collision.

Background:
The Norwegian Public Roads Administration (NPRA) is running the project "Ferry free coastal route E39", where they in 2012 initiated a study to investigate the feasibility for crossings the wide fjords on the west coast of Norway, focussed on Sognefjorden. REINERTSEN AS contributed in this study and showed that crossing the Sognefjord is technically feasible.

At present, REINERTSEN is further developing this concept together with Dr.techn Olav Olsen AS, Snøhetta Oslo AS, Norsk Hydro ASA, SAPA Profiles AB and Deep Ocean AS. The artificial seabed is REINERTSEN's patent (Figure 1).

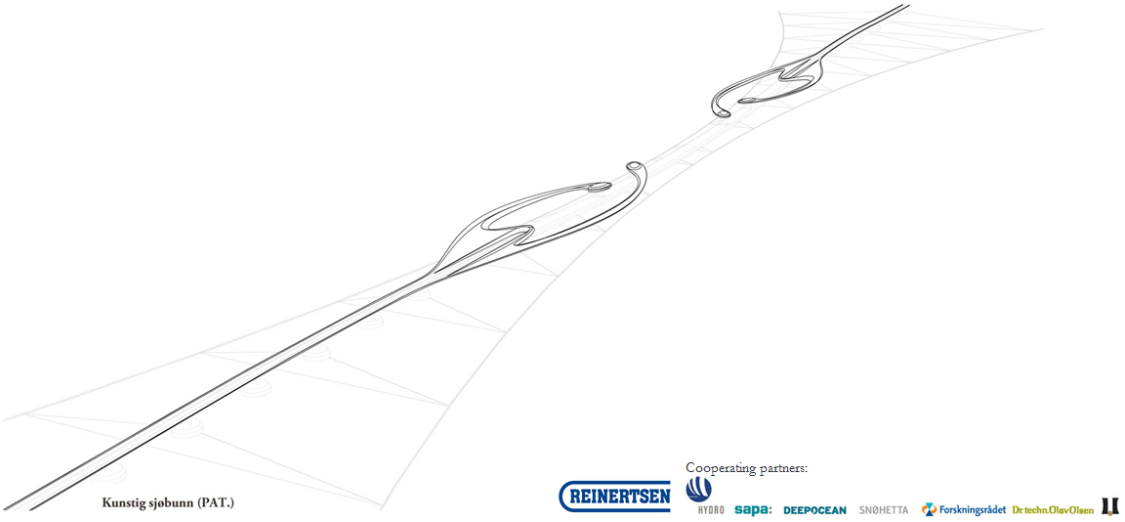

Figure 1 Concept with artificial seabed and mooring, floating bridge, submerged floating tunnel and collision barrier

This master thesis will focus on the ship collision barrier in the concept. The concept consists of a floating bridge with a submerged floating tunnel (SFT) at mid-span to allow ship traffic in and out of the fjord (Figure 2). At the border between the floating bridge and the SFT, there is need for a ship collision barrier to protect the SFT at shallow water depths before the SFT reaches a water depth where the ships can pass over without colliding with the SFT.

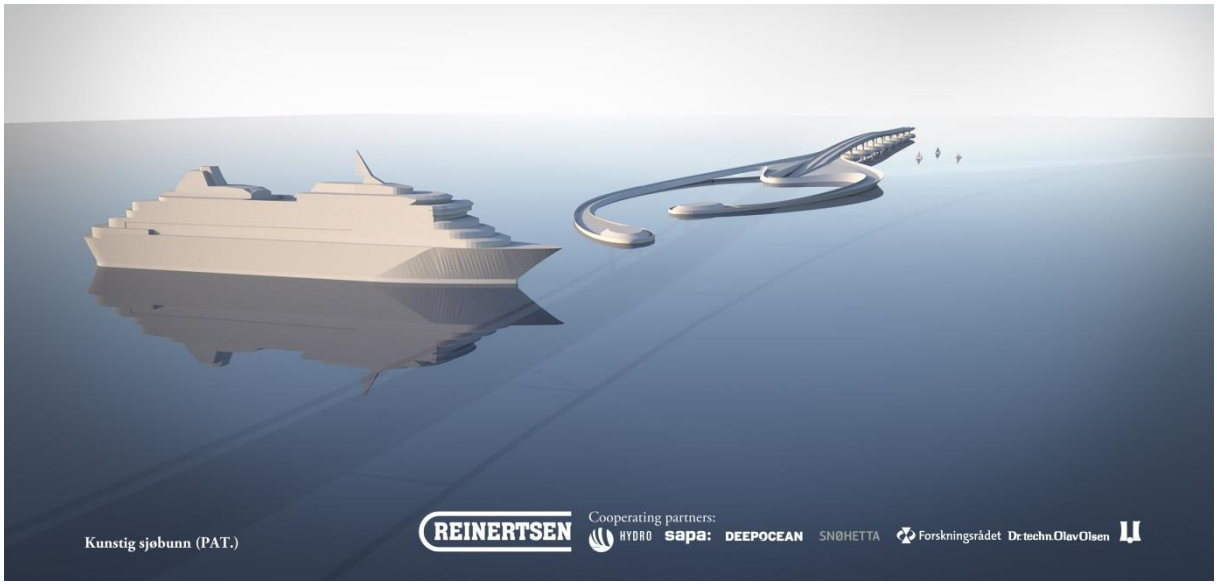

Figure 2 Collision barrier with floating bridge at rear and submerged floating tunnel with ship crossing in front

The size and speed of the large ships and design load cases at drift and collision will be taken from the reports developed by Rambøll in conjunction with the feasibility study in 2012 (will be provided the candidate upon starting the project).

The ship collision barrier needs to absorb and transfer the loads from the ship collision into the ship collision barriers itself (and down into the artificial seabed, respectively), without exceeding the allowances given in "Håndbok N400 Bruprosjektering Eurokodeutgave" issued by the NPRA (edition November 2011). Sizes and dimensions of the different components are detailed in the two project documents "Last og Lastbeskrivelse", doc. No. 2401051-02-RE-020202 and "Dimensjonering og materialbruk", doc. No. 2401051-02-RE-020203 which will be provided to the candidate upon starting the project.

The ship collision barrier is assumed to be made of aluminium (alloy 5083 and alloy 6082) and shall protect the SFT at water depths more shallow than 20m (refer "Håndbok N400 Bruprosjektering 6.13 Rørbruer"). The barrier will be thought of as a free floating structure in the water column (no moorings or fixed ends). The barrier will be a straight lined box of 380m length.

Scope of work:

1. Assess the various configurations of the barrier with respect to size, location, connection to the bridge, potential mooring to the artificial sea floor etc. How shall a weak link be designed?

2. It has been proposed to fabricate the barrier in aluminium. Describe functional requirements related to the use of aluminium in a corrosive environment and with large demands for ductility and energy absorption. Fabrication aspects shall also be addressed. Select one or two alloys/ tempers as candidate material. for particular challenges related to the use of aluminium in the collision barrier. Characterize the material properties to be used in nonlinear analysis.

3. Propose a detailed structural lay-out for the collision barrier including ballasting system. In addition to the local resistance to impact, the evaluation shall also include preliminary evaluations of the hydrostatic stability in damage condition. Special consideration should be given to how the local resistance to impact may be varied during nonlinear finite element analysis and how any ballast shall be modelled with respect to both local and global behaviour.

4. Discuss how the global motion of the barrier and the ship can be modelled for analysis in LS-DYNA. For the barrier this concerns added mass, viscous (drag) forces etc. For ship the still-water forces may be based upon manoeuvring coefficients. (A special purpose element will be developed in the winter of 2015). Modelling of the mooring/support of the barrier shall also be determined

5. For the selected barrier design and its variations perform nonlinear simulations of ship collisions with LS-DYNA for the various impact scenarios. The force-deformation (penetration) and energy dissipation in the ship bow and barrier shall be documented. The forces transferred to the bridge shall be determined and evaluated with respect to the integrity of the bridge. Compare the results with those based on simplified methods. How is the collision force compared to code requirements ((Norsok N-004, Eurocode 1, Part 1.7, AASHTO Bridge Design Specifications)?

6. Conclusion and recommendation for further work

Literature studies of specific topics relevant to the thesis work may be included.

The work scope may prove to be larger than initially anticipated. Subject to approval from the supervisor, topics may be deleted from the list above or reduced in extent.

In the thesis the candidate shall present his personal contribution to the resolution of problems within the scope of the thesis work.

Theories and conclusions should be based on mathematical derivations and/or logic reasoning identifying the various steps in the deduction.

The candidate should utilise the existing possibilities for obtaining relevant literature.

The thesis should be organised in a rational manner to give a clear exposition of results, assessments, and conclusions. The text should be brief and to the point, with a clear language. Telegraphic language should be avoided.

The thesis shall contain the following elements: A text defining the scope, preface, list of contents, summary, main body of thesis, conclusions with recommendations for further work, list

of symbols and acronyms, references and (optional) appendices. All figures, tables and equations shall be numerated.

The supervisor may require that the candidate, in an early stage of the work, presents a written plan for the completion of the work. The plan should include a budget for the use of computer and laboratory resources, which will be charged to the department. Overruns shall be reported to the supervisor.

The original contribution of the candidate and material taken from other sources shall be clearly defined. Work from other sources shall be properly referenced using an acknowledged referencing system.

The report shall be submitted in two copies:

- Signed by the candidate
- The text defining the scope included
- In bound volume(s)
- Drawings and/or computer prints which cannot be bound should be organised in a separate folder.

Supervisor NTNU:
Prof. Jørgen Amdahl

Industrial contact REINERTSEN AS:
PhD Marit Reiso

Deadline:, June 10 2015

Trondheim, January 14, 2015

Jørgen Amdahl

Preface

This master thesis is the result of Stud. Techn. Jørgen Lima Hansen's work during the spring of 2015 at the Norwegian University of Science and Technology, NTNU. This thesis is to be taken as a continuance of the project thesis which was carried out during the fall of 2014. The scope of work has been formulated as a cooperation between my supervisor at NTNU, Professor Jørgen Amdahl and my industrial contact at Reinertsen AS, PhD Marit Reiso.

The main focus in this master thesis has been to design a ship collision protection barrier in aluminium alloys. Both qualitative assessments and analysis have been carried out. The tasks have been interesting and some times a bit frustrating to work with. All tasks in the problem text have been discussed to a certain extent, in addition to issues which was coming up during the progression of the thesis.

I will specially thank my supervisor Professor Jørgen Amdahl for his guidance and discussion during the work period. I will also like to thank PhD Marit Reiso at Reinertsen AS for answering my question related to the project. In addition PhD candidate Martin Storheim has been of great help regarding the modelling and use of the nonlinear finite element program LS-DYNA.

Trondheim, 2015-06-10

Jørgen Lima Hansen

Abstract

The Norwegian Public Roads Administration (NPRA) is running the project "Ferry free coastal route E39". One of the main challenging are regarding how to cross the wide and deep fjord on the west coast of Norway. One of the bridge design considered is a combination of a floating bridge and a submerged floating tunnel. The transition zone between those structural parts is in special critical with respect to damage. This thesis focus at a ship collision barrier for protection of the transition zone.

An impact with the ship collision barrier are taken as an accidental action. The design ship is hence taken as the ship which have probability of occurrence less or equal to 1×10^{-4}. This correspond to a cruise ship with design parameter; displacement 31 456 metric ton and impact velocity 17.7 knots. The added mass coefficient was provided to be 0.2 and hence the total kinetic energy for the design ship was determined to be $1565MJ$. This is an severe amount of energy which needs to be dissipated as strain energy in the ship and then barrier. Some energy will also be dissipated by the inertia and drag forces, due to translation of the barrier.

A simplified analysis of a stiffened plate was performed by use of the nonlinear finite element program LS-DYNA. The results of the analysis shows that the strength of the stiffeners were in particular relevant for small displacements. While for larger displacement the plate carries the load by membrane forces.

The ship collision barrier needs to be designed for dissipation of large amount of strain energy. Therefore it was decided to built the structure like an ordinary ship like structure. This means that the barrier consist of decks, vertical and transverse bulkheads which all are stiffened by stiffeners. In this thesis the barrier is assumed to have a straight configuration with length $380m$, breadth $20m$, height $12m$ and a draft equal to $8m$. The barrier is assumed to be a freely floating structure only supported by buoyancy, inertia and drag forces. The barrier were decided to be built of aluminium alloys. Alloy 5083-O is considered for the plates and alloy 6082-T6 is considered for the stiffeners.

The intact stability of the barrier was verified to be good. Since the barrier is a floating structure it had to be ballasted down to the desired design draft. The aluminium cross section is a relative light cross section. When the draft of the barrier was assumed to be $8m$, the water level of ballast water inside the cross section was determined to be about $7.7m$.

By summarize the energy dissipated as strain energy in the ship and the barrier determined by a strength design and a ductility design analysis, it was shown for the considered barrier cross section that only about $1100MJ$ was dissipated. Therefore in order to dissipated the total amount of kinetic energy as strain energy a stronger cross section should be considered. If the analysis had accounted for energy lost due to translation of the barrier, the barrier cross section may have been strong enough. However, integrated shared energy analyses to verify this statement have not been completed.

Norsk sammendrag

Vegvesenet har et prosjekt som kalles for "Fergefri E39". En av hodeutfordringen i forbindelse med dette prosjektet, er relatert til hvordan de brede og dype fjordene på vest kysten av Norge kan krysses. Et av bruforslagene som er foreslått, består av en kombinasjon av en flytebro og en nedsenket flytetunnel. Det er overgangen mellom disse to delene som er spesielt kritisk med hensyn til ødeleggelse. Denne rapporten tar for seg en skipskollisjonsbarriere for beskyttelse av overgangssonen.

En kollisjon med skipsbarrieren blir behandlet som en ulykkes last. Design skipet er derfor valgt ut som det skipet som har sannsynlighet for å inntre mindre eller lik 1×10^{-4}. Dette tilsvare et cruise-skip med følgende parametere: deplasement 31 456 tonns og hastighet 17,7 knop. Tilleggsmassekoeffisienten brukt for skipet er på 0.2. Fra disse verdiene er den totale kinetiske energien beregnet til å bli $1565MJ$. Dette er en stor mengde energi som må bli tatt opp som tøyningsenergi i skipet og barrieren. I tillegg vil noe energi bli tatt opp gjennom translasjon av barrieren på grunn av masse- og drag kreftene.

En forenklet avstivet platemodell har blitt analysert med det ikke lineære element programmet LS-DYNA. Resultatene viste at bidraget fra stiverne var signifikant for små forskyvninger, mens for store forskyvninger var det platen som bar lasten ved hjelp av membran krefter.

Skipsbarrieren må designes for å kunne ta opp en stor mengde energi som tøyningsenergi. Av den grunnen ble det bestemt å bygge den lignende et skipsskrog. Det betyr at barrieren består av dekk, vertikale og transverse skott som alle er avstivet med stivere. I denne rapporten er barrieren antatt og være rett med følgende dimensjoner: lengde $380m$, bredde $20m$, høyde $12m$ og dypgang på $8m$. Barrieren er antatt å være en fritt flytende struktur som er opplagret kun på oppdrifts-, mass- og drag krefter. Det var bestemt at barrieren skal designes i aluminium. Legering 5083-O er antatt brukt for platene og legering 6082-T6 er antatt benyttet for stiverne.

Den intakte stabiliteten til barrieren har blitt beregning til å være god for det aktuelle tverrsnittet. Siden denne barrieren er en flyende struktur, behøves det å ballastere den ned til ønsket dypgang. Dette fordi aluminium tverrsnittet er et forholdsvis lett tverrsnittet. For en dypgang på $8m$, er det nødvendige vann nivået på ballasten inni strukturen beregnet til å være omtrent $7.7m$.

Ved å summere energien som ble tatt opp som tøyningsenergi i henholdsvis skipet og barrieren fra de to individuelle analysene; sterkt design (strength design) og duktilt design (ductility design). Den totale tøyningsenergien tatt opp i de to strukturene ble beregnet til omtrent $1100MJ$. For at det skal være mulig å ta opp den totale mengden kinetisk energi som tøyningsenergi, vil det være nødvendig å benytte et sterkere tverrsnitt for barrieren. Hvis analysene hadde tatt hensyn til energitap på grunn av translasjonen av barrieren, hadde resultatet muligens blitt at tverrsnittet hadde tilfredsstillende styrke. Slike integrerte delt energi analyser har ikke blitt fullført, derfor kan ikke denne påstanden bli verifisert.

Contents

Preface **i**

Abstract **iii**

Norsk sammendrag **v**

Nomenclature **xvii**

1 Introduction **1**
1.1 Background . . . 1
1.2 Concept . . . 1
1.3 Previous work . . . 2
1.4 Scope of work . . . 3
1.5 Structure of the Report . . . 3

2 Theory **5**
2.1 General ship collision theory . . . 5
2.1.1 Ship collision . . . 5
2.2 Aluminium . . . 9
2.2.1 General . . . 9
2.2.2 Special considerations . . . 12
2.3 Aluminium alloys . . . 16
2.3.1 General . . . 16
2.3.2 Specific temper classes . . . 17

3 Analysis of simplified stiffened plate **19**
3.1 Geometry . . . 19
3.2 Materials . . . 20
3.3 Modelling . . . 22
3.4 Results . . . 24
3.4.1 General . . . 24
3.4.2 Concluding remarks . . . 29
3.5 Discussion of stiffened plate analyses . . . 31

4 Design of ship collision barrier **33**
4.1 Design parameters . . . 33
4.1.1 Design Ship . . . 33

4.1.2 Barrier parameters . . . 34
4.2 Structural design . . . 36
4.2.1 Global design . . . 36
4.2.2 Local design . . . 39
4.2.3 Concluding remarks regard structural design . . . 41
4.3 Ballast considerations . . . 42
4.3.1 Required amount of ballast . . . 42
4.3.2 Water transport . . . 45
4.4 Stability . . . 46
4.4.1 Intact stability . . . 47
4.4.2 Damage stability . . . 48
4.4.3 Results and calculations . . . 49
4.4.4 Watertight bulkheads . . . 51

5 Finite element theory and modelling 55
5.1 General about finite element analysis . . . 55
5.1.1 General . . . 55
5.1.2 Solution method . . . 57
5.1.3 Elements . . . 59
5.1.4 Material models . . . 60
5.1.5 Fracture model and mesh scaling, user defined material model . . . 69
5.1.6 Contact modelling in LS-DYNA . . . 73
5.2 Modelling . . . 74
5.2.1 Ship . . . 74
5.2.2 Barrier Design . . . 77
5.2.3 Total finite element models . . . 82
5.2.4 Global Motion Interaction . . . 83
5.2.5 Inertia forces . . . 84
5.2.6 Drag forces . . . 85

6 Analysis and Results 89
6.1 Bow against rigid wall, strength design . . . 89
6.2 Rigid bow against local barrier cross section, ductility design . . . 92
6.2.1 Case 1, original cross section . . . 94
6.2.2 Case 2, further increased plate thickness . . . 95
6.2.3 Case 3, increased number of decks and bulkheads . . . 96
6.3 Shared energy design, both structural parts deformable . . . 97
6.3.1 Centric collision . . . 98
6.3.2 Collision at the barrier end . . . 98

7 Discussion 99

7.1 General 99
7.2 Element size and HAZ considerations 99
7.3 Comparison of piecewise linear and the user defined material model 100
7.3.1 Piecewise linear material model 101
7.3.2 User defined power law material model 102
7.3.3 Conclusion 102
7.4 Discussion of the nonlinear finite element analysis 103
7.4.1 General 103
7.4.2 Shared energy design, both structural parts deformable 104
7.5 Comparison with Codes and Simplified Methods 107
7.5.1 Comparison with strain energy equations in NORSOK N-004 (2004) 107
7.5.2 Comparison of Ship Collision Forces with Different Design Codes 108

8 Conclusion and Further Work **111**
8.1 Conclusion 111
8.2 Recommendation for further work 113

Bibliography **114**

Appendix A Retardation of the barrier after impact **I**

Appendix B Plastic moment capacity for the barrier **XI**

Appendix C Additional results **XIII**
C.1 Shared energy approach based on strength design and ductility design XIII
C.1.1 Force-indentation curves for a simplified shared energy approach XIII
C.1.2 Energy-deformation curves for a simplified shared energy approach . . . XV

List of Figures

1.1 Concept showing artificial seabed, floating bridge, submerged floating tunnel and ship collision barrier (Provided by Reinertsen AS) 1
1.2 Concept showing the ship collision barrier together with the transition part (Provided by Reinertsen AS) 2

2.1 Relative strength - installation/ship (NORSOK N-004, 2004) 6
2.2 Dissipation of strain energy in ship and installation (NORSOK N-004, 2004) . . . 8
2.3 Stress-strain curve obtained by using Ramberg-Osgood equation plotted together with experimental values (Mazzolani, 1995) 10
2.4 Difference in stress-strain curves between mild steel and aluminium (Moan, 2003) 12
2.5 Recommendation for corrosion protection for various exposure condition and durability ratings (Eurocode 9: Part 1-1, 2007) 15

3.1 Stiffened plate 19
3.2 True stress-strain curves for all the different aluminium alloys 21
3.3 True stress-strain curves for alloy 6082 applied to the stiffeners 21
3.4 True stress-strain curves for alloy 5083 applied to the plate 22
3.5 Figure shows the rigid sphere which is applied as the load for the stiffened plate . 23
3.6 (a) Force-deformation curve and (b) energy-displacement curve for alloy 5083-O in plate 24
3.7 (a) Force-deformation curve and (b) energy-displacement curve for alloy 5083-H12 in plate 25
3.8 First failure occur at the middle point in the stiffener 26
3.9 Second failure occur close to the middle point in the plate. The figure is to be taken as a illustration since the level of displacement varies between the analysis. This particular Figure shows alloy 5083-H12 without HAZ 26
3.10 Total failure of analysis with alloy 5083-O in the plate. (a) without HAZ modelled fails locally between the stiffeners. (b) with a 40 mm extent of HAZ in the plate fails after the two outer stiffeners fails and fails therefore at a larger global displacement compared to (a) 27
3.10 Total failure of analysis with alloy 5083-O in the plate. (a) without HAZ modelled fails locally between the stiffeners. (b) with a 40 mm extent of HAZ in the plate fails after the two outer stiffeners fails and fails therefore at a larger global displacement compared to (a) 28

3.11 Force-deformation curve for alloy 5083-O. It is included a curve where the critical effective stress to failure is increased from 23 % to 30 % when the stiffeners are modelled without HAZ 30
3.12 Force-deformation curve for alloy 5083-H12. It is included a curve where the critical effective stress to failure is increased from 16 % to 23 % when the stiffeners and the plate are modelled without HAZ 30

4.1 Cross section of the barrier, one closed symmetrical cross section and one cross section with skirt 35
4.2 Simplified model for the global analysis 37
4.3 Deformed shape when plastic hinge have been formed 38
4.4 Local design (illustration) 40
4.5 Four different cross sections used for the calculations 43
4.6 Amount of ballast filled in the cross section for case 4 45
4.7 The figure shows an example of how the manholes or cutouts in transverse bulkheads for case 4 can be introduced, it will be similar cutouts in decks and vertical bulkheads 46
4.8 Stability of the barrier cross section 47
4.9 Flooding of one compartment between two watertight bulkheads, the fracture is shown by the two dotted lines at the middle tank 53
4.10 Longitudinal position of the watertight transverse bulkheads 54

5.1 Example of boundary non linearity (Moan, 2003) 57
5.2 The calculation cycle for time integration in LS-DYNA (Hallquist, 2006) 58
5.3 Construction of element coordinate system for the co-rotational formulation of Belytschko-Lin-Tsay (Hallquist, 2006) 60
5.4 Comparison of the stress-strain curve obtained from Ramberg-Osgood equation and from the modified power law expression used for the user defined material model for aluminium alloy 5083-O 67
5.5 Comparison of the stress strain curve obtained from Ramberg-Osgood equation and from the modified power law expression used for the user defined material model for aluminium alloy 6082-T6 67
5.6 Comparison of experimental true stress-strain curve and a stress-strain curve obtained from the modified power law expression, the comparison is performed for mild steel (EN 10025 S275) (Alsos et al., 2008) 71
5.7 Volume averaged strain when necking has occurred (Alsos et al., 2009) 72
5.8 Bow model shown with different views (a) 75
5.9 Converting of bulbous stiffeners (Konstali, 2014) 76
5.10 Bow model (Konstali, 2014) 77
5.11 Local barrier design, total view (a) transverse bulkheads with stiffeners (b), vertical bulkheads and decks with stiffeners (c), detailed view of a corner (d) 78

5.12 The Figure shows the modelling of stiffeners in the local model, the blue region is equal to 20mm height and represent the HAZ region 79
5.13 The figure shows the global model which will be attached to the local model . . . 82
5.14 The different total models used for the finite element analysis 83
5.15 The nodes where the drag forces are applied to the structure for the centric collision scenarios, (the black points represents the nodes where the drag force are attached) 86
5.16 The nodes where the drag forces are applied to the structure for the collision scenarios where the ships hits at one of the barrier ends, (the black points represents the nodes where the drag force are attached) 87
5.17 A representative velocity for each barrier part er calculated by taking the average of the nodes shown by the yellow point in the figure 87
5.18 A representative velocity for each barrier part er calculated by taking the average of the nodes shown by the yellow point in the figure 87
5.19 The Figure shows an illustration of the drag load. The load will first be significant after the barrier have got a significant velocity. This curve is only an illustration since it is drawn for a case where mass scaling is applied. 88

6.1 Time collapse of collision between ship and rigid wall, the figures (c)-(f) are plotted with the same height so the relative indentations is clearly shown 90
6.2 Force and energy curves for collision of a bow against a rigid wall 91
6.3 Illustration of the bow against a rigid wall where only a part of the model is crushed 92
6.4 Time collapse of collision between rigid ship and local barrier cross section, (c) and(d) is plotted from top without displaying the rigid ship 94
6.5 The figure shows the curves for the cross section discussed in 4.2.2 95
6.6 The figure shows the curves for a cross section with increased plate thickness . . 96
6.7 The figure shows the local barrier which intentional should be considered with respect to energy dissipation 97
6.8 The figure shows the global mode for the centric collision scenarios. Mass scaling has been applied for the bow so the shown deformation is not real. 98
6.9 The figure shows the global mode for the collision scenario at the barrier end. Mass scaling has been applied for the bow so the shown deformation is not real. 98

7.1 The figures shows the difference in the stiffeners when HAZ is modelled or not . 100
7.2 Curves for collision a rigid bow against the barrier, when the piecewise linear material model is applied without mesh scaling and only a simplified fracture criterion 101
7.3 Curves for collision a rigid bow against the barrier, when the modified power law material model is applied utilising mesh scaling and a RTCL fracture criterion102
7.4 Force-deformation curve for the ship and barrier. Both the barrier cross section considered are included 105

7.5 Force-deformation curve for the ship and barrier. The measured indentation of each structural parts at the end of the analysis is shown. 105
7.6 Energy-deformation curve for the ship and barrier. Both the barrier cross section considered are included 106

A.1 Cross section of the barrier with and without skirt IV
A.2 Velocity vs. distance plot for a closed-cross section with different drafts IV
A.3 Velocity vs. distance plot for a closed cross-section with draft 8 meter and with variable effective draft of the included skirt V
A.4 Kinetic energy vs. distance for different drafts V
A.5 Kinetic energy vs. distance for different drafts with skirt VI
A.6 Drag force vs. distance for different drafts VI
A.7 Drag force vs. distance for different drafts with skirt VII
A.8 Characteristic velocity vs. distance plot as a function of the parameters VII

B.1 Simplified model for the global analysis XI
B.2 Deformed shape when plastic hinge have been formed XI

C.1 Force-deformation curve for the ship and barrier. Each curve based on the rigid analysis. The curve for the barrier is for the cross section discussed in section 4.2.2XIII
C.2 Force-deformation curve for the ship and barrier. Each curve based on the rigid analysis. The curve for the barrier is for the case with increased thickness XIV
C.3 Force-deformation curve for the ship and barrier. Both the barrier cross section considered are included XIV
C.4 Energy-deformation curve for the ship and barrier. Both the barrier cross section considered are included XV

List of Tables

2.1 Comparison of properties for aluminium alloys and common mild steels (Mazzolani, 1995) . . . 11

3.1 Material properties for stiffened panel analysis . . . 20

4.1 Design ship parameters, (Ramboll, 2011) . . . 33
4.2 Design barrier parameters . . . 36
4.3 Parameter used for ballast and stability calculations . . . 44
4.4 Results of the required ballast calculations for the different cross sections . . . 44
4.5 Results of stability calculations in intact condition . . . 50
4.6 Calculation of the necessary distance between watertight bulkheads . . . 53

5.1 Material properties for MAT_003 Plastic Kinematic and MAT_028 Resultant Plasticity . . . 62
5.2 Material properties for steel using MAT_046 User Defined Material Model . . . 63
5.3 Material properties for aluminium using MAT_046 User Defined Material Model 68
5.4 Approximate dimensions of the ship used for the bow model (Konstali, 2014) . . . 75
5.5 Model input for the local detailed model . . . 80
5.6 Global model . . . 81
5.7 Comparison of cross section properties in the global and local model . . . 81

A.1 Input parameter for the simplified analysis . . . II

Nomenclature

Abbreviations

AASHTO	American Association of State Highway and Transportation Officials
ALS	Accidental Limit State
BWH	Bressan-William-Hill instability criterion
DWT	Deadweight tonnage of the ship
HAZ	Heat Affected Zone
MIG	Metal Inert Gas
NPRA	Norwegian Public Roads Administration
RTCL	Rice-Tracy-Cockcroft-Latham damage criterion
TIG	Tungsten Inert Gas
ULS	Ultimate Limit State

Capital letters

$\dot{D}$	Rate of damage	$[1/s]$
A	Area	$[m^2]$
A_p	Projected area	$[m^2]$
A_{cs}	Cross section area of the barrier	$[m^2]$
B	Breadth of the barrier	$[m]$
C_d	Drag coefficient	[-]
C_m	Added mass coefficient	[-]
D	Damage	[-]
D_{cr}	Critical damage level	[-]
E	Young's modulus	[Pa]
E_{imp}	Energy which have to be absorbed by plastic deformations	[J]
E_{kin}	Kinetic energy	[J]
$E_{strain,i}$	Strain energy installation	[J]
$E_{strain,s}$	Strain energy ship	[J]
E_{strain}	Total strain energy	[J]
F_0	Reference collision force	[MN]
F_d	Drag Force	[N]
F_{bow}	Largest bow impact force	[MN]
GM	Metacentric height	$[m]$

GZ	Righting arm	$[m]$
H	Height of the barrier	$[m]$
I	Second moment of area	$[m^4]$
K	Power law constant	[Pa]
L	Total length of the barrier	$[m]$
L_s	Characteristic element length	[m]
L_{pp}	Length between perpendicular	[m]
M_P	Plastic moment capacity	[J]
$M_{heeling}$	Heeling moment	$[Nm]$
$M_{restoring}$	Restoring moment	$[Nm]$
P_s	Equivalent static impact force	[kips]
R_i	Collision force installation	[N]
R_s	Collision force ship	[N]
T	Stress triaxiality	[-]
V	Ship impact velocity	[feet per second]
V_n	Volume of local neck	$[m^3]$
V_r	Element volume outside the necking region	$[m^3]$
V_{al}	Total volume of aluminium in the barrier	$[m^3]$
V_{el}	Total element volume	$[m^3]$
W_e	External virtual work	[J]
W_i	Internal virtual work	[J]
W_P	Plastic section of modulus	$[m^3]$

Greek Symbols

α_p	Plastic cross-section shape factor	[-]
Δt_e	Time step	[s]
Δ	Tonnage of the barrier	[kg]
$\dot{\epsilon}_{eq}$	Rate of the equivalent plastic strain	$[1/s]$
ϵ	Strain	[-]
ϵ_{eq}	Equivalent plastic strain	[-]
ϵ_0	Strain parameter which which allows the plateau and power law expression to intersect	[-]
ϵ_{eq}	Equivalent strain	[-]
ϵ_{plat}	Equivalent plastic strain at strain plateau exist	[-]
∇	Displacement	$[m^3]$
ρ'	Density of liquid in the tank	$[kg/m^3]$
ρ_{eff}	Artificial material density of the material model applied for the global cross section to account for added mass and ballast	$[kg/m^3]$
σ	Stress	[Pa]

σ_1	Major principal stress	[Pa]
σ_m	Hydrostatic stress	[Pa]
σ_Y	Yield stress	[Pa]
σ_{eq}	Equivalent stress	[Pa]
θ	Angle of rotation	

Small letters

a	Added mass	[kg]
a_i	Added mass installation	[kg]
a_s	Added mass ship	[kg]
c	Acoustic wave speed	[m/s]
d	Draft of the barrier	[m]
dw_i	Indentation installation	[m]
dw_s	Indentation ship	[m]
i	Second moment of area of the tank	[m^4]
m	Mass	[kg]
m_i	Mass installation	[kg]
m_s	Mass ship	[kg]
m_X	Mass plus added mass	[kg]
m_{al}	Total mass of aluminium in the barrier	[kg]
m_{bal}	Required mass of ballast	[kg]
m_{total}	Mass of the whole barrier including ballast water and added mass	[kg]
n_p	Material constant for Ramberg-Osgood law	[-]
n_{pow}	Power law exponent	[-]
n_{tb}	Number of transverse bulkheads	[-]
q	Distributed load	[N/m]
s	Distance translated	[m]
t_{tb}	Thickness of transverse bulkheads	[m]
v	Velocity	[m/s]
v_0	Velocity before impact	[m/s]
v_i	Velocity of installation	[m/s]
v_s	Velocity of ship	[m/s]
$v_{i,s}$	Velocity of ship and installation after impact	[m/s]
w	Deflection	[m]
w_0	Deflection at the middle position	[m]

1 Introduction

1.1 Background

The Norwegian Public Roads Administration (NPRA) is running the project "Ferry free coastal route E39". One of the main challenging are regarding how to cross the wide and deep fjord on the west coast of Norway.

In 2012 NPRA initiated a study to investigate the feasibility for crossing the wide and deep fjords on the west coast of Norway, focussed on Sognefjorden. Different solutions were considered and the conclusion was that the crossing was technically feasible.

1.2 Concept

Reinertsen AS in cooperation with partners developing a concept which consist of a combination of a floating bridge and a submerged floating tunnel. Due to the large water depth the bridge could not be anchored to the sea bottom and it was not practical to only be anchored at the abutment due to the wide fjord. Therefore it was developed a concept called "Artificial Seabed", which is an anchoring system for the bridge, see Figure 1.1.

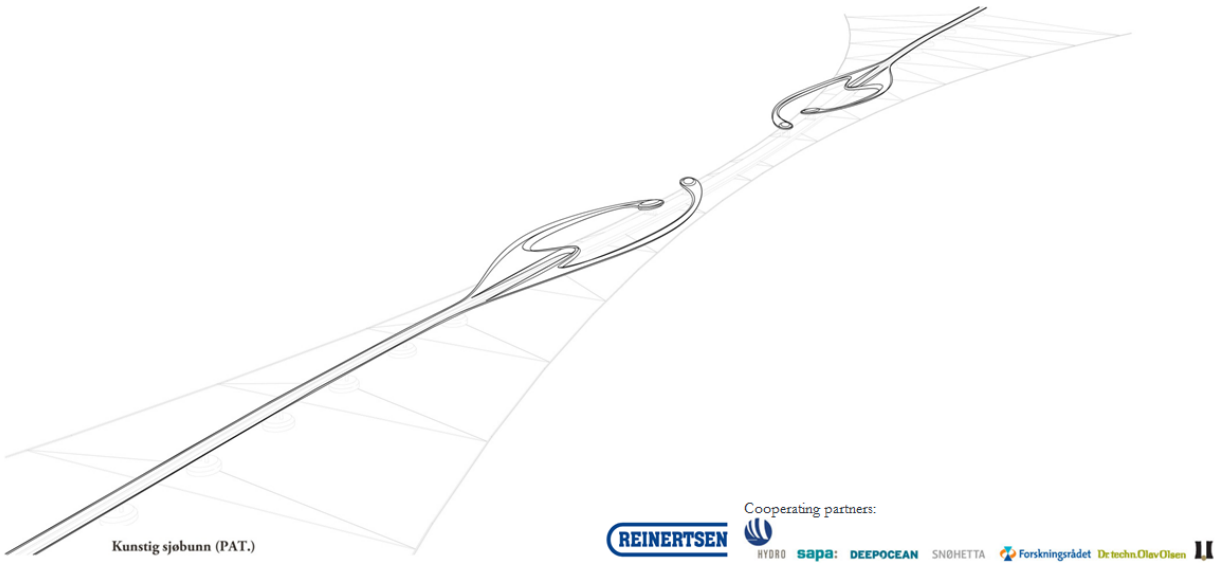

Figure 1.1: Concept showing artificial seabed, floating bridge, submerged floating tunnel and ship collision barrier (Provided by Reinertsen AS)

As mentioned in the previous paragraph the bridge consist of two different parts, a floating bridge and a submerged floating tunnel. The floating bridge consist of pontoons and bridge way which is anchored to the artificial seabed. The floating submerged tunnel consist of a large concrete tunnel anchored to the artificial seabed. In practical the tunnel is designed to be neutrally loaded in water, this means that the main function of the anchoring is to keep the tunnel at the desired position. The reason to have a submerged floating tunnel is to let ship passing the bridge independent of the height of the ship.

In addition to those two sections, the bridge have a transition part from the floating bridge to the submerged floating tunnel. This part is most critical with respect to ship collision and it will therefore be necessary to install a ship collision barriers to protect the transition parts, see Figure 1.2.

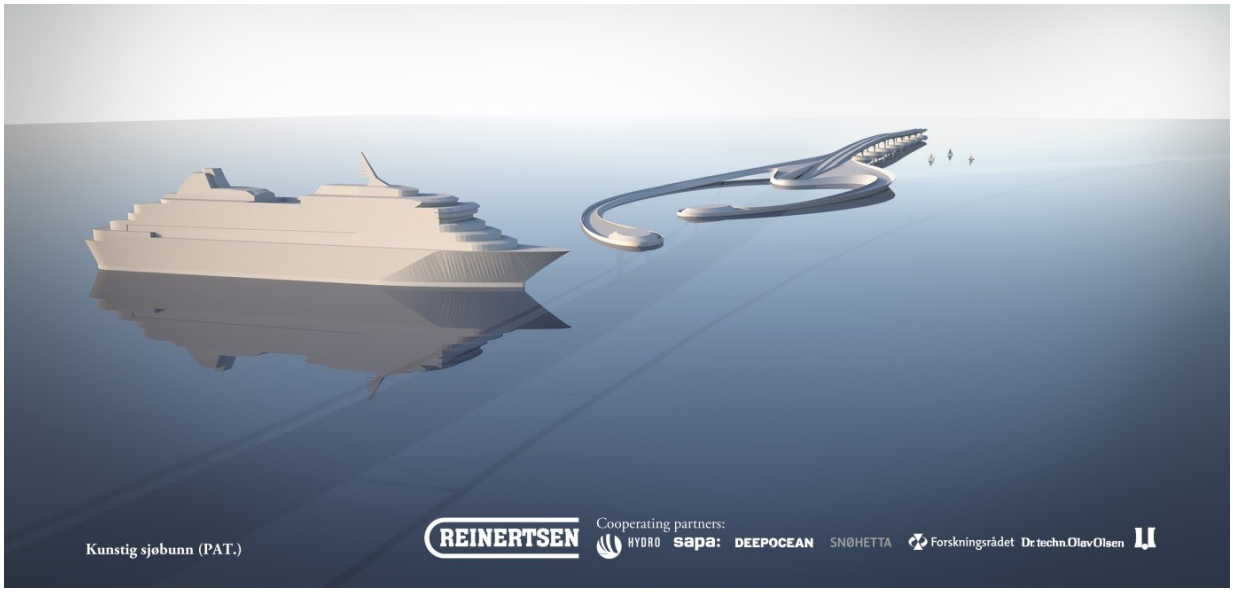

Figure 1.2: Concept showing the ship collision barrier together with the transition part (Provided by Reinertsen AS)

1.3 Previous work

Last year during the spring of 2014 a master thesis was carried out on the same topic by Ørjan Konstali (Konstali, 2014). The main task of this master thesis was to design the ship collision barrier in steel and use a geometric configuration equal to the barrier shown in Figure 1.1 and Figure 1.2. The barrier was assumed to be rigidly connected to the transition zone between the floating bridge and the submerged floating tunnel. On the other side the barrier is connected to a pontoon which again is connected by weak links down to the artificial seabed. For simplicity the ship collision barrier was assumed to be rigidly connected at the pontoon end for the analysis carried out by Konstali (2014).

The conclusion of the work carried out by Konstali (2014) was that the kinetic energy in the design ship was too large to be taken by the ship alone. Therefore the barrier cross section needs to be designed to carry large amount of energy. The total energy should hence be taken totally by the barrier as a ductility design or as a shared energy design between the barrier and the ship. At the end of Konstali's master thesis it was concluded that it was technical feasible to design a ship collision barrier to dissipate the total kinetic energy in the design ship.

1.4 Scope of work

The main focus in this master thesis is related to design of the ship collision barrier against ship collisions. The ship collision barrier is decided to be build up consisting of aluminium alloys. In this master thesis the barrier is assumed to have a straight configuration and to be a freely floating structure only supported by buoyancy, inertia and drag loads. Other environmental loads will be neglected. The barrier is assumed to be connected by a weak link at the initial position. This weak link will snap of for a small force relative to the force applied from the collision ship. Therefore the anchoring is neglected as a first approach.

Some of the same topics covered by Konstali (2014) are recovered in this master thesis. This in order to obtain the necessary background to design a ship collision barrier made of aluminium alloys.

First a literature study related to ship collision theory will be conducted. A study of aluminium alloys will also been performed. Thereafter simplified calculation on the ship collision barrier together with qualitative discussion will be performed. At the end modelling and simulations of different ship collision scenarios will be conducted by applying the nonlinear finite element program LS-DYNA.

All the nonlinear finite element analysis have not been completed. The shared energy analysis where the total barrier and the bow is included have not been completed. Such analyses are recommended as a further work.

1.5 Structure of the Report

Chapter 2 gives general background theory related to ship collision. In addition the behaviour of aluminium alloys with focus on accidental limit state are reviewed.

In chapter 3 a simplified stiffened plate made of the two aluminium alloys which are considered for the ship collision barrier have been analysed. The purpose of this chapter is to determine the influence of applying different tempers and also which influence the heat affected zone (HAZ) has to the ultimate strength of the stiffened plate.

The different design parameters for the ship and the barrier are discussed in chapter 4. In this chapter ballast considerations and stability are also discussed.

Chapter 5 is related to the nonlinear finite element analyses conducted with the program LS-DYNA. This includes a short review of general nonlinear finite element theory, in addition to how the different models have been built.

The results and analysis which have been conducted are shown in chapter 6. The results is further discussed in chapter 7.

In chapter 8 the work is summed up in a conclusion together with a list including the recommendations for further work.

2 Theory

This chapter contains theory relevant for the scope of work. This include a brief review of general ship collision theory and theory related to use of aluminium in accidental limit states.

2.1 General ship collision theory

This section contains general theory related to ship collision as an accidental action event, referring to Annex A in NORSOK N-004 (2004).

2.1.1 Ship collision

The characteristic value related to ship collision is kinetic energy, see equation (2.1). For simplicity it is often assumed that the entire change in kinetic energy is converted to strain energy, which is a conservative assumption since it always will be some losses to the environment like friction and temperature losses. For structures which are able to move some of the energy will remain as kinetic energy after impact.

$$E_{kin} = \frac{1}{2} \cdot (m + a) \cdot v^2 \tag{2.1}$$

Where:

m: Mass

a: Added mass

v: Velocity

E_{kin}: Kinetic energy

Design principle

It is common to distinguish between three different design principle. Each principle is related to how the strain energy is distributed between the structures, see Figure 2.1.

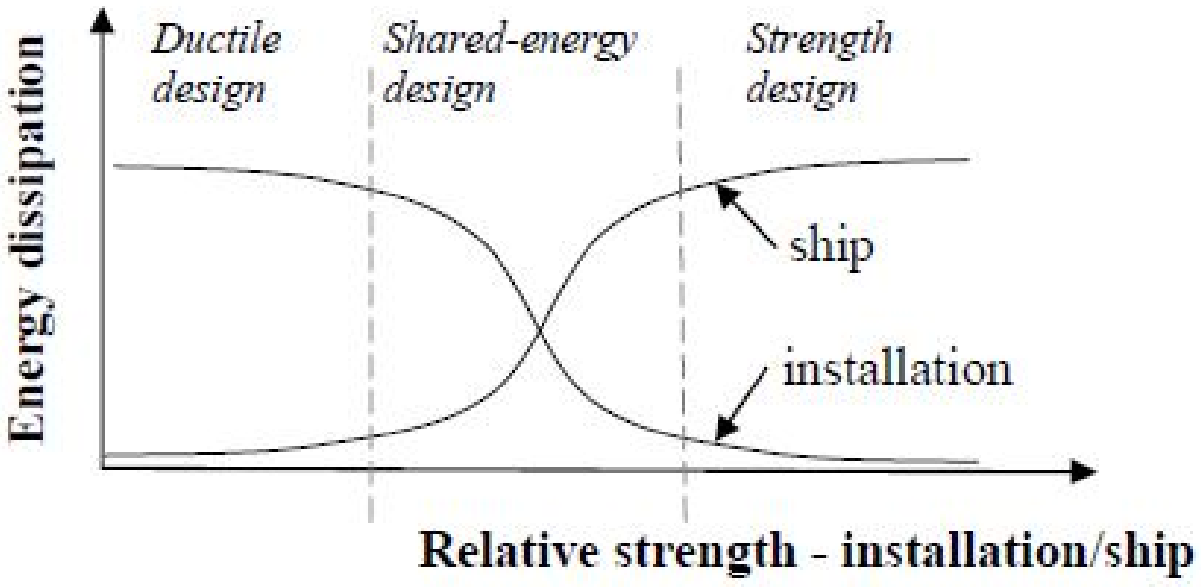

Figure 2.1: Relative strength - installation/ship (NORSOK N-004, 2004)

Strength design implies that the installation is rigid and major part of the energy is taken as deformation in the ship. **Ductility design** implies the opposite, major part of the energy is taken as deformation in the installation. In the middle **shared-energy design** should be applied, which means that both the ship and the installation undergo some deformation. Hence, this case is more complicated and complex than the other two design principle.

It is convenient, related to calculation difficulties to assume either ductility or strength design as a first approach. In reality most of collision events will be characterised by shared-energy design, but still ductility or strength design can be used since it may be a conservative assumption.

Collision mechanics

To be able to solve collision events with simplified methods, the analysis are often split into two step. External mechanics which applies conservation of momentum and conservation of energy to calculate the amount of kinetic energy which are to be taken as strain energy by the structures. The second step is related to internal mechanics, which describe how the strain energy is distributed in both the ship and the installation.

External mechanics The external collision mechanics determine the amount of kinetic energy to be dissipated as strain energy. Usually the strain energy dissipated in the structures is smaller than the kinetic energy, mainly because of loss to the environment and remaining kinetic energy in the structures.

A central impact is assumed with the purpose of showing the principle of external mechanics, this means that the force vector acts through the center of gravity of both the ship and the installation.

Conservation of momentum:

$$(m_i + a_i) \cdot v_i + (m_s + a_s) \cdot v_s = (m_i + a_i + m_s + a_s) \cdot v_{i,s} \tag{2.2}$$

Conservation of energy:

$$\frac{1}{2} \cdot (m_i + a_i) \cdot v_i^2 + \frac{1}{2} \cdot (m_s + a_s) \cdot v_s^2 = \frac{1}{2} \cdot (m_i + a_i + m_s + a_s) \cdot v_{i,s}^2 + E_{strain} \tag{2.3}$$

Combining equation (2.2) and (2.3) to get an expression for the strain energy (E_{strain}). The solutions is taken from Annex A in NORSOK N-004 (2004).

Compliant installations:

$$E_{strain} = \frac{1}{2} \cdot (m_s + a_s) \cdot v_s^2 \cdot \frac{(1 - \frac{v_i}{v_s})^2}{1 + \frac{m_s + a_s}{m_i + a_i}} \tag{2.4}$$

Fixed installations:

$$E_{strain} = \frac{1}{2} \cdot (m_s + a_s) \cdot v_s^2 \tag{2.5}$$

Where:

a_i: Added mass installation

a_s: Added mass ship

m_i: Mass installation

m_s: Mass ship

v_i: Velocity of installation

v_s: Velocity of ship

$v_{i,s}$: Velocity of ship and installation after impact

E_{strain}: Strain energy

According to NORSOK N-004 (2004), the installation can be assumed compliant if the duration of impact is small compared to the fundamental period of vibration of the installation. In the opposite condition, when the duration of impact is long compared to the fundamental period of vibration of the installation, the installation can be assumed fixed.

Internal mechanics As already mentioned, the internal mechanics determine the energy dissipation in the structures.

The structural response of the impact event can be represented as a load-deformation curve, see Figure 2.2. Each of those two curves are usually established independently of each other by assuming that the other object is infinity rigid.

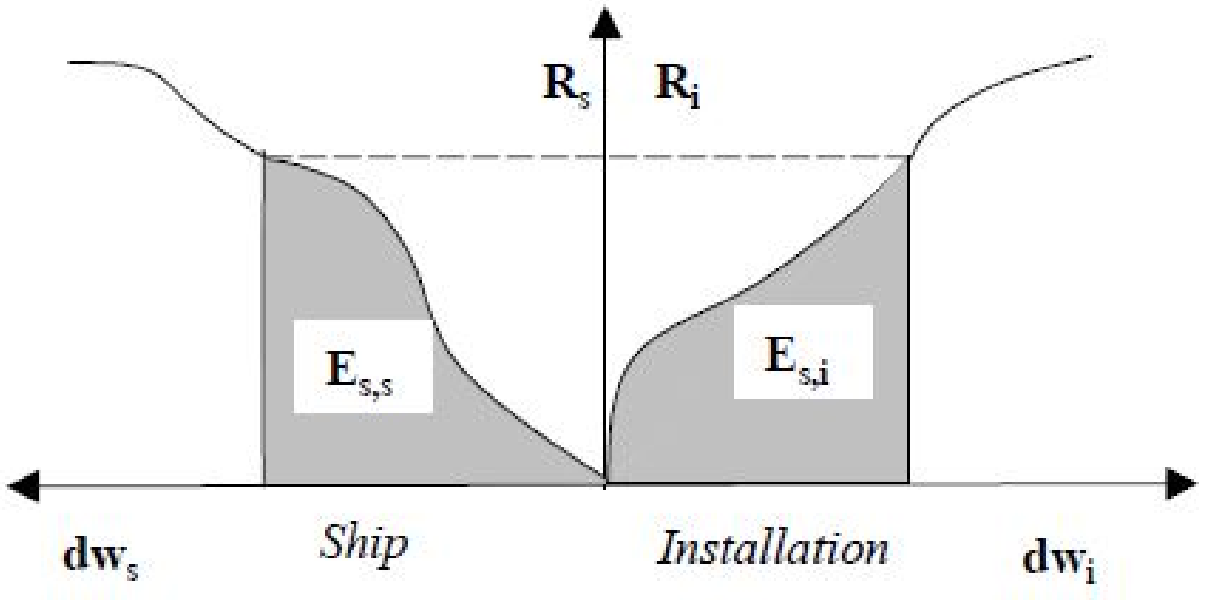

Figure 2.2: Dissipation of strain energy in ship and installation (NORSOK N-004, 2004)

$$E_{strain} = E_{strain,s} + E_{strain,i} = \int_0^{w_{s,max}} R_s \cdot dw_s + \int_0^{w_{i,max}} R_i \cdot dw_i \tag{2.6}$$

Where:

R_i: Collision force installation

R_s: Collision force ship

dw_i: Indentation installation

dw_s: Indentation ship

E_{strain}: Total strain energy

$E_{strain,s}$: Strain energy ship

$E_{strain,i}$: Strain energy installation

As can be seen from equation (2.6) and Figure 2.2, the total strain energy are calculated as the sum of the strain energy dissipated by the ship and the strain energy dissipated by the instal-

lation. This is done by utilising that the collision force on the ship and the installation will be equal at the end of the collision event according to fundamental low of mechanics.

Concluding remarks regarding the method given in Norsok N-004

The method described above has several weakness as stated in NORSOK N-004 (2004). One of them is that both structures will dissipate some energy regardless of the relative strength. The general trend is that the method overestimate the deformation of the stronger part and underestimate the deformation of the weakest part. Large deformation of the softer part will give a larger contact surface, and hence the force is distributed over a larger area. Accordingly the resistance of the strong structure increases and hence the load-deformation curve is not fully valid. As a concluding remark, care should be exercised when load-deformation curves are used. This fact is stated in NORSOK N-004 (2004).

To get a detailed solution it is therefore recommended to apply a nonlinear finite element analysis (NLFEA).

2.2 Aluminium

It has been proposed to fabricate the ship collision barrier in aluminium. This section contains functional requirement related to use of aluminium in a floating ship collision barrier exposed to accidental action. It is suggested to apply aluminium alloy 5083 for the plates and alloy 6082 for the profiles. Those two alloys will be further discussed in section 2.3.

2.2.1 General

Aluminium is a light material compared to for instance ordinary construction steel. Therefore it has traditional been used in structure which are weight sensitive, for instance airplane and high speed vessel.

The stress-strain relationship for aluminium alloys is different from the curves obtained for ordinary mild steel, see Figure 2.4. One of the main differences are the lack of strain plateau in the curves representing aluminium alloys. To describe the stress-strain relation for aluminium, Ramberg-Osgood equation can be used, see equation (2.7). The Ramberg-Osgood law is widely used because the predicted behaviour are very close to the actual behaviour of aluminium alloys. The Ramberg-Osgood curve gives value at a lower bound and close to the experimental values and are hence on the conservative side. The energy absorption will then also be on the conservative side.

For an illustrations of Ramberg-Osgood curves see Figure 2.3. A typical true stress-strain relationship for aluminium are monotonic increasing until fracture, no stress loss until fracture. An aluminium cross section may obtain fracture in one fibre before the cross section is fully plastic utilised. Therefore it is no or small indication before the fracture occurs and hence aluminium can be taken as a brittle material. A comparison of the nominal stress-strain curves for steel and aluminium is given in Figure 2.4.

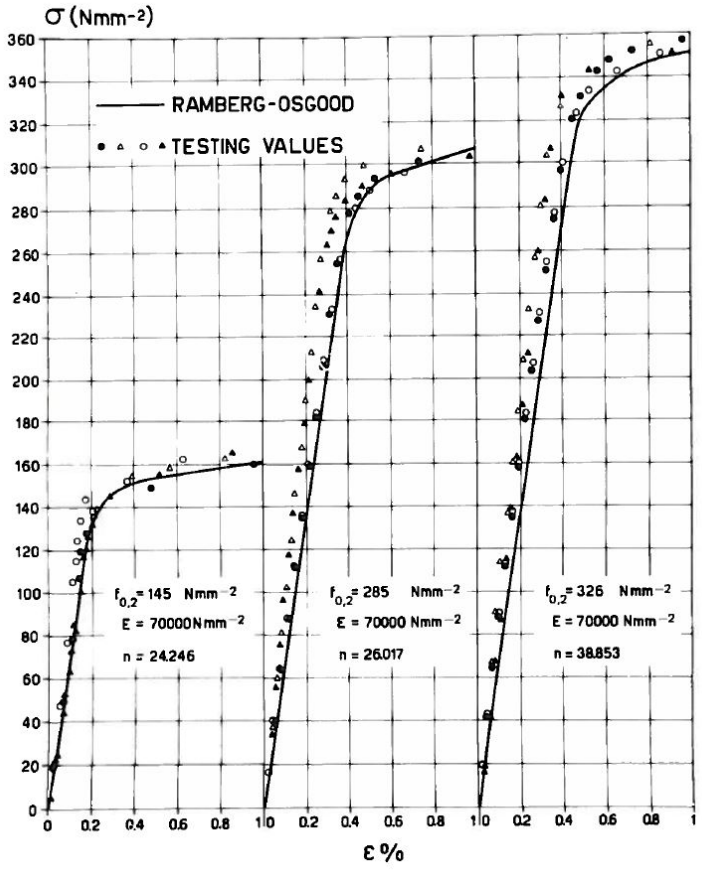

Figure 2.3: Stress-strain curve obtained by using Ramberg-Osgood equation plotted together with experimental values (Mazzolani, 1995)

$$\epsilon = \frac{\sigma}{E} + (\frac{\sigma}{B})^n \tag{2.7}$$

where:

ϵ: Strain

σ: Stress

E: Young's modulus

B, n: Material constants, have to be determined by experiment

The material constant B has its physical meaning to be the limit stress for the elastic part of the curve when $n = \infty$. In Eurocode 9: Part 1-1 (2007) this parameter is written as a function of the yield stress, σ_Y, this will be shown later in equation (3.1). The exponent n is related to the strain hardening part of the stress-strain curve.

A comparison between aluminium alloys and a couple of steel grades are shown in Table 2.1, the table is taken from Mazzolani (1995). From this table it is clearly shown that aluminium alloys usually have lower yield and tensile strength and ultimate strain compared to construction steel. Alloys with high strength have generally lower ultimate strain. This means that the ultimate strain decrease as the strength increases in generally. This is the same tendency as between mild and high strength steel. One of the largest difference between aluminium alloys and mild steel with respect to material properties, is that steel have a elasticity modulus of about three times the modulus for aluminium alloys. It is also a great difference in coefficient of thermal expansion, α and the specific weight, γ. Figure 2.4 shows the difference in the stress-strain curves for the two materials. One advantage aluminium have in addition to the reduced specific weight compared to steel is that it has no transition temperature. This means that it will not appear as more brittle at low temperatures. As have been mentioned it is the difference in ultimate strain which are of greatest importance related energy absorption and hence also related to accidental actions. A further discussion of the properties of aluminium will be discussed in the next section, (section 2.2.2).

Table 2.1: Comparison of properties for aluminium alloys and common mild steels (Mazzolani, 1995)

	Aluminium alloys		Steel	
$f_{0.2}(f_y)$	AlMg4.5Mn	~140	F360	~235
[MPa]	AlMgSi1	~260	F510	~350
	AlZnMg1	~360		
f_t	AlMg4.5Mn	~280	F360	~360
[MPa]	AlMgSi1	~320	F510	~510
	AlZnMg1	~410		
E	70 000 MPa		206 000 MPa	
ϵ_t	10-25%		25-30%	
γ	26 500 N/m^3		77 000 N/m^3	
α	0.000 02		0.000 01	

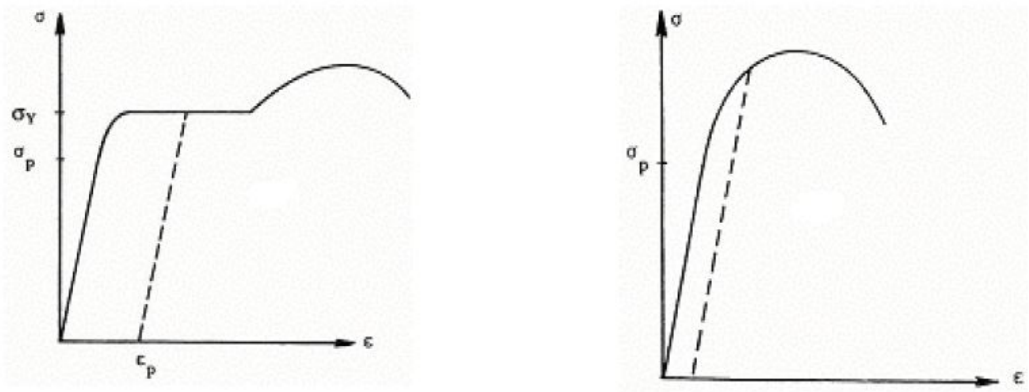

a) Mild steel b) High strength steel, aluminium

Figure 2.4: Difference in stress-strain curves between mild steel and aluminium (Moan, 2003)

2.2.2 Special considerations

Heat Affected Zone (HAZ)

HAZ is one of the main concerns related to aluminium alloys. This is because a lot of aluminium alloys has a strong reduction in HAZ, this means that material properties such as yield strength and tensile strength is reduced. HAZ is critical with respect to energy dissipation and structural integrity of the structure. If the reduction is large the tensile strength in HAZ could be lower than the yield strength of the base material. If that occur the strains will be confined to the relatively narrow HAZ and the base material will only carry a small amount of the load. Even if the behaviour is ductile in HAZ, the structure may exhibit brittle behaviour in a global sense, due to this effect.

If the amount of strength reduction is moderate and the material has considerable hardening, it is likely that the stress in HAZ will be large enough to expand the yield zone into the base material. If this is the case HAZ is not that critical with respect to the structural integrity and the structure will be able to dissipate more strain energy.

Aluminium in load bearing structure which are heat treated can loose up to 70 % of the strength in HAZ. To take this effect into account in calculation it is usually applied a constant reduced value for the material properties with a width of HAZ equal to about 25 mm on each side of the weld. According to Eurocode 9: Part 1-1 (2007) the width of the HAZ differs for different welding method and plate thickness, but it usually is about 25 mm.

For instance the extent of HAZ according to Eurocode 9: Part 1-1 (2007) section 6.1.6.3 (3) for MIG weld:

$0 < t \leq 6mm$: $b_{haz} = 20mm$

$6 < t \leq 12mm$: $b_{haz} = 30mm$

$12 < t \leq 25mm$: $b_{haz} = 35mm$

$t \geq 20mm$: $b_{haz} = 40mm$

For TIG weld according to 6.1.6.3 (6):

$0 < t \leq 6mm$: $b_{haz} = 30mm$

The reason why TIG welds gives a larger HAZ compared to MIG, is that the heat input is greater during the TIG weld process. A larger heat gives consequently a larger HAZ.

For additional information related to the extent of HAZ it is referred to section 6.1.6.3 in Eurocode 9: Part 1-1 (2007).

As stated above aspects related to HAZ are crucial to take into account. The general trend related to aluminium alloys is that higher strength of base material gives a larger strength loss in the HAZ.

Use of aluminium alloys in accidental limit state

Aluminium may not be treated in the same way as is common for mild steel, when it is applied in structure exposed for ALS. The reason is because the stress-strain relationship for aluminium alloys are a continuity between the quasi-elastic and the inelastic hardening behaviour. This is compared to mild steel which have a strain plateau between the elastic and plastic zone.

For steel structure the plastic capacity of a cross section can be defined by the shape parameter α_p, see equation (2.8). This equation is no longer valid when working with aluminium alloys. The reason is that there is not logical to define a fully plastic section, because the fibres of the cross section may not reach a bound characterised by yielding of the whole cross section. Instead the stresses grows for higher values of deformation until failure is reached in the highly stressed fibres. In other words this means that the equation (2.8) lose its mechanical meaning while keeping its geometrical meaning for aluminium alloys. If equation (2.8) should be applied to aluminium cross sections it therefore needs to be assumed that the whole cross section could reach a bound characterised by yielding, which in fact could be a non-conservative assumption.

$$\alpha_p = \frac{M_{pl}}{M_e} = \frac{Z}{W} \tag{2.8}$$

Because of the effects described above there are difficult to predict the actual plastic moment capacity for a aluminium cross section compared to the same cross section made of mild steel.

For many aluminium alloys the difference in value between the yield and tensile stress are small, the stress-strain curve looks quite similarly as an elastic perfectly plastic stress-strain curve. When this is the case the redistribution of stress in the plastic zone may not be satisfied and hence the structure may fails for a strain level lower that the ultimate strain.

Use of aluminium in a corrosive environment

Generally aluminium alloys by nature have a good corrosive protection in mild environments. This is a main advantage of applying aluminium alloys compared to mild steel. When the corrosive protection is good this will implies less maintenance costs. The reason why the corrosive protection is good for aluminium alloys are because of the protective oxide film which forms on the surface of the metal immediately on exposure to air. In some conditions this film can be broken down and the aluminium alloys lose their protection. For such conditions there will be necessary to add additional corrosive protection to the structure.

The ship collision barrier considered in this thesis is to be taken as a floating structure which is to be made of aluminium. There are proposed two aluminium alloys, alloy 5083 and alloy 6082, which will be further discussed in section 2.3. Both alloys need to be protected against seawater either in a passive or active manner. The structure is a floating structure and it has to be ballasted down to a certain design draft. For common cases seawater is used as ballast. Therefore it will be seawater both outside and inside the structure.

Eurocode 9: Part 1-1 (2007) gives requirement for use of aluminium alloys in different environment. The need for corrosive protection are given from which durability rating the alloy is characterised as and in which environment it will be operated. The durability rating of several alloys are specified in Table C.1 in Eurocode 9: Part 1-1 (2007). According to this table alloy 5083 and alloy 6082 respectively have durability rating A and B. Further Table D.1 in Eurocode 9: Part 1-1 (2007) gives the recommendation for corrosion protection for various exposure condition and durability ratings. Table D.1 is reprinted as Figure 2.5. This table shows that alloy 6082 normally require corrosion protection when it is immersed in seawater. For alloy 5083 the need for protection depends on if there are special conditions for the structure. Such need should be stated in the specification for the structure.

Table D.1 - Recommendations for corrosion protection for various exposure conditions and durability ratings

Alloy durability rating	Material thickness mm	Protection according to the exposure							
		Atmospheric						Immersed	
		Rural	Industrial/urban		Marine			Fresh-water	Sea water
			Mode-rate	Severe	Non-industrial	Mode-rate	Se-vere		
A	All	0	0	(Pr)	0	0	(Pr)	0	(Pr)
B	< 3	0	0	(Pr)	(Pr)	(Pr)	(Pr)	Pr	Pr
	≥ 3	0	0	0	0	0	(Pr)	(Pr)	Pr
C	All	0	0 [2)]	(Pr) [2)]	0 [2)]	0 [2)]	(Pr) [2)]	(Pr) [1)]	NR

0 Normally no protection necessary

Pr Protection normally required except in special cases, see D.3.2

(Pr) The need for protection depends on if there are special conditions for the structure, see D.3.2. In case there is a need it should be stated in the specification for the structure

NR Immersion in sea water is not recommended

1) For 7020, protection only required in Heat Affected Zone (HAZ) if heat treatment not applied after welding

2) If heat treatment of 7020 after welding is not applied, the need to protect the HAZ should be checked with respect to conditions, see D.3.2.

NOTE For the protection of sheet used in roofing and siding see prEN 508-2:1996.

Figure 2.5: Recommendation for corrosion protection for various exposure condition and durability ratings (Eurocode 9: Part 1-1, 2007)

The corrosive protection of aluminium alloys can be increased in different ways. Eurocode 9: Part 1-1 (2007) states that the type of corrosion protection should be adapted to the corrosion mechanis; surface corrosion, galvanic induced corrosion, crevice corrosion and corrosion due to contamination by other building materials. Some of the methods commonly used to combat corrosion includes passive film formation, chromating, cathodic protection, organic coatings and inhibitors. All methods are not suitable for protection in seawater. For instance the formation of passive film is the self protection condition for aluminium alloys when there are exposed to air (oxygen). When this film is exposed for seawater the chlorine ions in the seawater will broke down some of the passive films and the aluminium alloy will not be able to formate a new passive film in this area and hence the corrosion protection of the structure is broken. This means that different protection methods have its own special application area.

In Eurocode 9: Part 1-1 (2007) part D.3.4.5 it is stated that aluminium alloys which should be immersed in seawater should preferable be of durability rating A, which are the case for alloy 5083 which should be applied in the plates in the ship collision barrier.

As already mentioned alloys of durability rating A may not need any corrosion protection. The ship collision barrier may therefore only need to have corrosion protection inside the structure in the tanks filled by seawater as ballast, since the profiles are to be made up of alloy 6082 which has durability rating B.

Other consideration

If comparing aluminium alloys to mild steel. Aluminium has a low ratio of stiffness to strength, young's modulus (E) divided by yield stress (σ_Y). Since almost every aluminium section are made to be slender, they are susceptible to local and global buckling. Fatigue could also be an issue as a result of the high ratio of live load to dead weight.

Fabrication Aspect

The fabrication method should be taken into consideration when designing an aluminium structure. As mentioned in previous sections, there are some challenges which need to be overcome when using aluminium as a construction material compared to ordinary mild steel. A way to compensate for the material strength reduction in HAZ is to locally increase the thickness in the HAZ area. This may not be as easy as it sounds, for instance if the HAZ region is localised in the middle of a continuous plate.

The HAZ will be localised close to the welds and the joints. It will therefore be preferable to place the joints if possible in position which are less severe with respect to the total structural integrity. Longitudinally welds compared to the loading direction have small influence on the strength reduction compared to transversal placed welds. This is related to how cracks will propagate in the structure. Therefore the welds should if possible be positioned in the same direction as the loading direction.

2.3 Aluminium alloys

2.3.1 General

It exist several different aluminium alloys with different material properties. The differences are related to which metals the alloys consist of in addition to aluminium. Adding different metals affects the material properties. Some metals increase the strength while other is added to increase for instance the corrosive resistance.

All aluminium alloys are characterised by four numbers which represent the materials the alloy consist of. It should be remark that even for a specific aluminium alloy the material

properties could various within a given range. The reason is that the amount of substitution metals could also be vary within a given range. This means that for instance an alloy 5083 produced by one factory, may not have the same material properties as an alloy 5083 produced by another factory.

Tempering class

Most aluminium alloys can be temperated in different ways. The material properties will differ regarding how the alloy has been treated. In general there are four different temper types associated with aluminium alloys. Each types are characterised by a capital letter. There are different class within each temper types and this classes are given by numbers following the capital letter, for instance H12.

- F: As-Fabricated
- O: Annealed
- H: Strain-Hardened
- T: Solution Heat-Treated

When designing for accidental action it is important to remember that it is not the yield strength or tensile strength which should be used as the characteristic value. In accidental actions it is the material ability to dissipate energy which should be taken as a design parameter, this is related to the area below the stress-strain curve. The effect of using high strength steel or high strength aluminium alloys is beneficial related to conventional ultimate limit state design (ULS), but the beneficial is lost considerably when designing against accidental limit state (ALS) as is the case for the ship collision barrier. The reason why it is not beneficial to use high strength aluminium alloys is mainly because of HAZ and the lower ultimate strain. It is better to have moderate flow stress distributed over a large area and large strains, than having large stress in a small area. High strength aluminium alloys have commonly less ability to absorb energy.

2.3.2 Specific temper classes

Two of the most common aluminium alloys applied for floating structure is alloy 5083 and alloy 6082. Therefore those two alloys have been selected for the ship collision barrier. Alloy 5083 is used for the plates and alloy 6082 is applied for the profiles.

Alloy 5083

Alloy 5083 is one of the commercial aluminium-magnesium alloys with the greatest strength (Hatch, 1984). The alloy is characterised as an aluminium-magnesium alloy (4.4 wt% magnesium), but it also contains small amount of manganese (0.7 wt%) and chromium (0.7 wt%) (Hatch, 1984). This alloy is a non-heat treatable alloy.

As stated above aluminium alloy 5083 is an alloy containing magnesium and traces of manganese and chromium. It is therefore highly resistant to attack by seawater. The alloy has among the highest strength of the non-heat treatable alloys, but it is not recommended for use in temperature in excess of 65 °C. Alloy 5083 is usually used in plates, including skin plates for high speed vessels.

One of the big properties for the 5000 class is that they are used in welded structure since their strength is not drastically decreased in the HAZ. For the temper class O, where the total alloy is assumed to have the same properties as the HAZ zone, it is no reduction of material properties in HAZ. That is preferable with respect to distribution of stresses in the material. Other common temper for the alloy 5083 is for instances temper H12 and H22.

Alloy 6082

Alloy 6082 is characterised as an aluminium-magnesium-silicon alloy, since it mainly consist of those three materials. In addition this alloy could consist of for instance small amount of manganese. Aluminium alloy 6082 is a medium strength aluminium alloy with good corrosion resistance. It has the highest strength out of the 6000 series.

The most relevant temper for alloy 6082 is T6. T6 means a heat treatable alloy which is solution heat-treated and then artificially aged. The temper have a large reduction of material properties in HAZ, about 50 %, the reduction parameter will slightly differ with respect to welding method and plate thickness. Due to the large decrease of material properties in HAZ, this would be one of the main concerns and challenging of applying aluminium alloy 6082-T6 in a welded aluminium structure.

Aluminium alloy 6082 is a common used alloy for profiles. Therefore this alloy have been selected for the stiffeners in the ship collision barrier.

3 Analysis of simplified stiffened plate

This chapter contains analysis of a stiffened plate made of aluminium alloys. The analysis have been carried out with the nonlinear finite element program LS-DYNA. The purpose of including analysis of a stiffened plate in this thesis is to investigate the influence of use of different material parameters, the effect of including HAZ both on the stiffeners and the plate and the effect of variable extent of HAZ. The results of the analysis is discussed with respect to ultimate capacity and the ability to dissipate energy in the stiffened plates. The theory behind the finite element program LS-DYNA is discussed together with the modelling of the ship collision barrier in chapter 5 and is therefore not included in this chapter. This chapter is to be taken as a stay alone chapter, where both the procedure, results and the discussion related to the analysis of the stiffened plate are included.

3.1 Geometry

The geometry consist of a squared plate stiffened by three L-stiffeners. The plate has dimension 2x2 meter and a plate thickness equal to 12 mm. The L-stiffeners have dimensions 200x90x11.5x15 mm and spacing equal to 500 mm. The HAZ area is modelled with a extent of either 0 mm, 20 mm or 40 mm. A model where the thickness is locally increased in HAZ have also been considered. The model of the stiffened plate is shown in Figure 3.1.

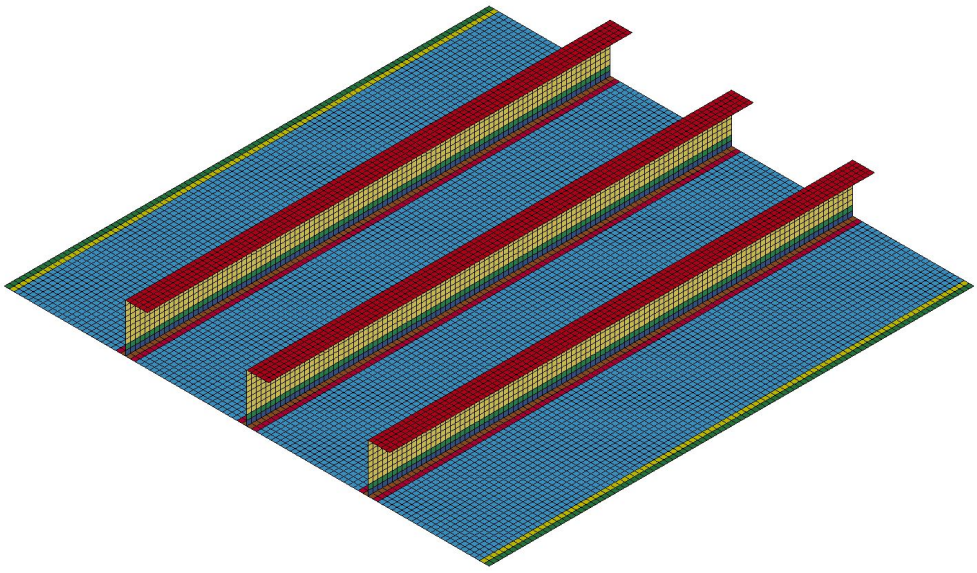

Figure 3.1: Stiffened plate

3.2 Materials

The material parameter for the aluminium alloys are taken according to Eurocode 9: Part 1-1 (2007), in particular with respect to table 3.2a and 3.2b in this standard. Alloy 5083 are used for the plate and alloy 6082 in the stiffener. For alloy 5083 the influence of applying two different tempers have been investigated, O and H12. For alloy 6082 mainly the T6 temper are investigated, but in additional a custom made alloy have been applied with the ultimate stress capacity in HAZ larger than the yield stress in the base material. Then the yield zone will be able to be distributed into the base material and hence the base material will contribute to the load bearing structure. The relevant material properties are given in Table 3.1. In order to obtain all the necessary input for the NLFEA analysis some assumption have been applied for the HAZ area. The materials are assumed to have the same ductile properties in HAZ as in the base material, this means that the ultimate strain in HAZ are assumed equal to the base material. By this assumption the exponent in the Ramberg-Osgood equation (n_p) for the HAZ is measured by applying curve fitting.

Table 3.1: Material properties for stiffened panel analysis

Alloy	Temper		Material Properties Base	Material Properties HAZ
5083	O/H111	ρ	2700 kg/m^3	2700 kg/m^3
		E	70 000 MPa	70 000 MPa
		σ_Y	125 MPa	125 MPa
		σ_{ult}	275 MPa	275 MPa
		ϵ_{ult}	0.23	0.23
		n_p	6	6
5083	H12	ρ	2700 kg/m^3	2700 kg/m^3
		E	70 000 MPa	70 000 MPa
		σ_Y	250 MPa	155 MPa
		σ_{ult}	305 MPa	275 MPa
		ϵ_{ult}	0.16	0.16
		n_p	22	7.68
6082	T6	ρ	2700 kg/m^3	2700 kg/m^3
		E	70 000 MPa	70 000 MPa
		σ_Y	260 MPa	125 MPa
		σ_{ult}	310 MPa	185 MPa
		ϵ_{ult}	0.16	0.16
		n_p	25	11.238

The properties in HAZ are assumed to be constant in the HAZ region. This is a common used assumption when accounting for HAZ in analysis. However in the real world the properties varies over the width, the shape of the variation depends among other factors on the welding technique. Due to the variations, there are hard to assume a correct distribution and therefore the variations in the HAZ region usually is assumed constant.

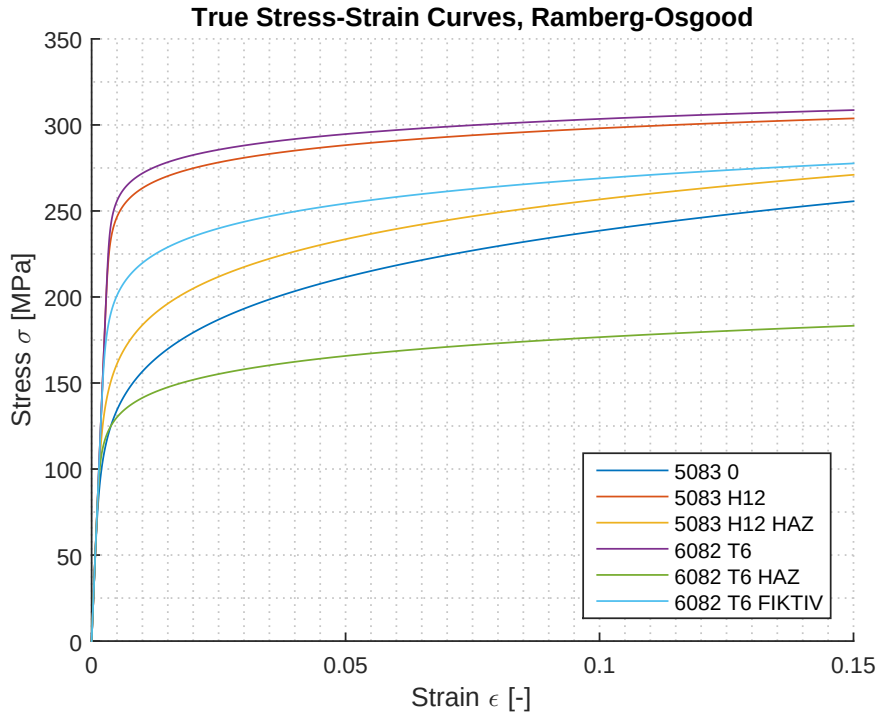

Figure 3.2: True stress-strain curves for all the different aluminium alloys

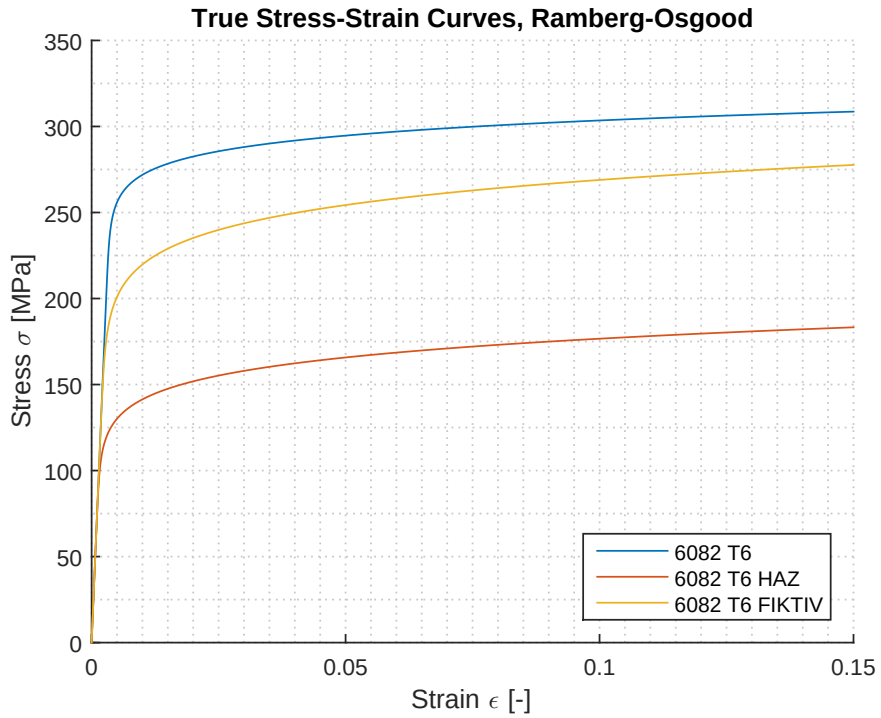

Figure 3.3: True stress-strain curves for alloy 6082 applied to the stiffeners

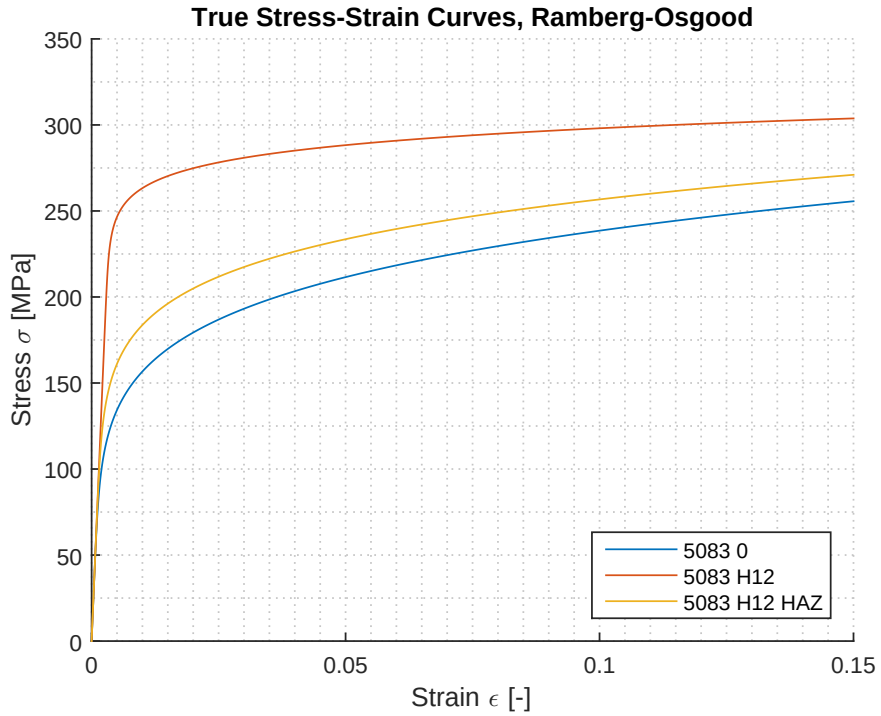

Figure 3.4: True stress-strain curves for alloy 5083 applied to the plate

3.3 Modelling

The model is build up of thin shell elements according to Belytschko-Tsay theory. An evenly distributed mesh with element size 20x20 mm are applied. There are applied five integration points through the thickness for all elements.

It has been applied fixed boundary condition along all edges, both against translation and rotation. The proposed boundary condition may be questionable if the stiffened plate are to be taken as a part of a bigger structure, as is the case for the ship collision barrier which will be discussed further in chapter 4. A more realistic boundary condition could be to use fixed with respect to rotation along all edges. Then applying fixed translation in plane, but allow the plate to translate out of plane. However, the analysis in this section is related to investigate the influence of applying different material properties and for a such comparison fixed boundary condition will give acceptable results.

To predict failure a simplified fracture criterion based on the effective plastic strain is applied as a first approach. When one integration point in an element reach the given strain level, LS-DYNA is designed such that this element will be deleted from the structure and will hence not contribute to the strength of the structure. A simple fracture criterion based on a critical strain level will not always give a correct solution since the element may not always fail in tension. To account for failure in compression a more detailed fracture criterion needs to be applied.

This could for instance be a Rice-Tracy-Cockcroft-Latham (RTCL) damage criterion as will be discussed further in section 5.1.5. However, the simplified strain fracture criterion gives a first approach and it is assumed to give acceptable results for the comparison of material properties performed in this section.

The material model which are used in LS-DYNA is a model called piecewise linear plasticity. The material curves are drawn as Ramberg-Osgood curves from the parameters given in Table 3.1. The Ramberg-Osgood equation used is taken according to section E.2.2.2 (3) in Eurocode 9: Part 1-1 (2007), and reprinted as equation (3.1). The 0.2 % proof stress is assumed equal to σ_Y.

$$\epsilon = \frac{\sigma}{E} + 0.002 \cdot (\frac{\sigma}{\sigma_Y})^{n_p} \tag{3.1}$$

The extent of HAZ varies between the analysis. Analysis have been conducted without HAZ, for 20 mm extend of HAZ and for 40 mm extent of HAZ. For some analysis the HAZ are only represented in the stiffener web. The differences between analysis and a qualitative discussion of the results are further discussed in the next section.

The load are applied as a rigid sphere with radius 500 mm, see Figure 3.5. The sphere is moved in z-direction, normal to the stiffened plate, with a constant velocity. The reason to use such a large sphere is to let the plate take the load globally and have a smaller angle of inclination between the first and second point on the sphere which impact the stiffened plate. The total normal contact force between the rigid sphere and the plate is determined. The results which will be discussed in the next section are given as load-deformation curves between the normal contact force and the translation of the rigid sphere.

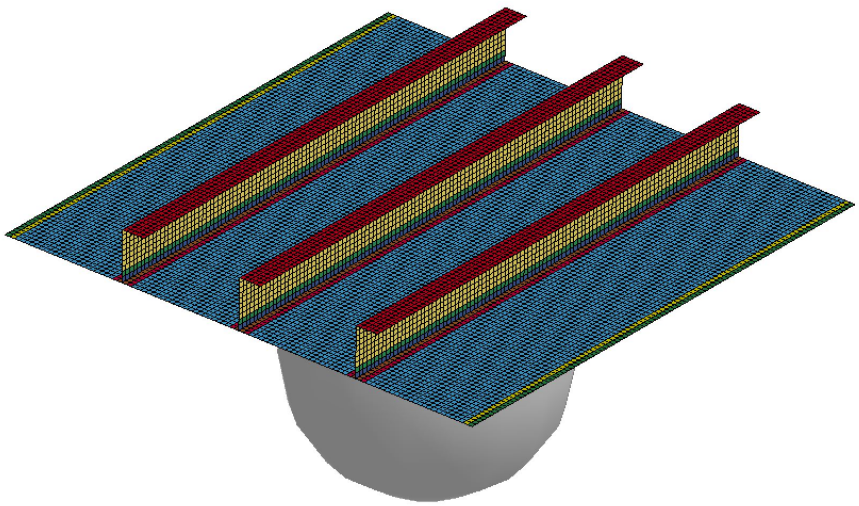

Figure 3.5: Figure shows the rigid sphere which is applied as the load for the stiffened plate

3.4 Results

3.4.1 General

The results will be discussed as force-deformation curves and also with respect to some energy-deformation curves. The normal contact force between the rigid sphere and the stiffened plate are plotted against the displacement of the sphere. The reason to use rigid sphere as reference for the displacement and not the center node on the plate is because the node on the plate are allowed to slide at the surface and may therefore not have constant coordinates during the deformation. The center node on the plate could also be deleted from the structure if a integration point reach the critical strain value in this node.

The force-deformation and energy-deformation curves for alloy 5083-O and alloy 5083-H12 in the plate and both with alloy 6082-T6 in the stiffeners are shown in Figure 3.6 and Figure 3.7. Several more analysis were carried out, for instance analysis with a custom made alloy in the stiffeners and analysis with increased thickness in HAZ. Results for those analysis are not included in this section, in particular the results achieved from those analysis are similar as does which will be discussed with respect to Figure 3.6 and Figure 3.7.

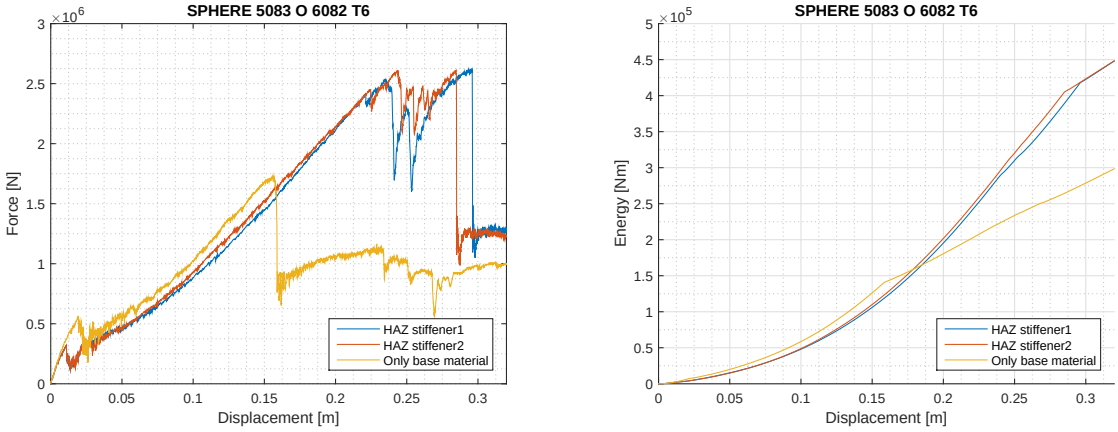

(a) Force-displacement curve

(b) Energy-displacement curve

Figure 3.6: (a) Force-deformation curve and (b) energy-displacement curve for alloy 5083-O in plate

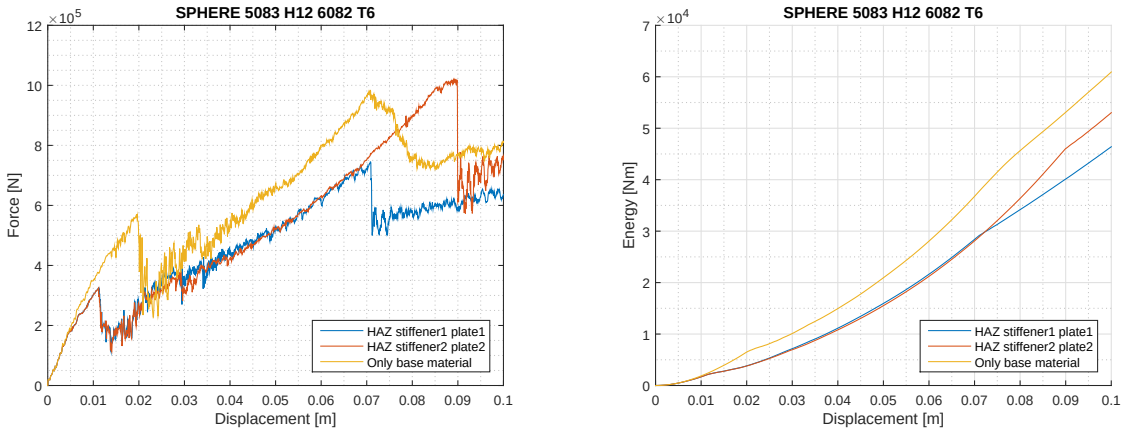

(a) Force-displacement curve

(b) Energy-displacement curve

Figure 3.7: (a) Force-deformation curve and (b) energy-displacement curve for alloy 5083-H12 in plate

In Figure 3.6 and Figure 3.7 stiffener1, stiffener2 and plate1 and plate2 means respectively an extent of HAZ in the stiffener or/and the plate of 20 mm or 40 mm. For the results given in the figures there have not been assumed any HAZ at the edges. However this may not be totally correct, if the stiffened plate are to be taken as a part of a bigger structure, it will be introduced a HAZ regions at the edges.

From Figure 3.6 and Figure 3.7 it is clearly shown that all the curves have a local peak near zero displacement relative to the total displacement. From investigation of the graphic representation of the analysis, it is verified that the first peek is the strength of the stiffened plate until the first element in the stiffener fails. There are the two elements connected to the center node of the plate which fails first. This position is the first position where the rigid sphere impact the plate and it will hence have the largest displacement when the first failure occur, see Figure 3.8. The strength until failure is then mainly due to the strength and material properties of those two elements. It is seen that the analysis with only base material in the stiffener web gives the largest strength until first failure. It is more interesting that it is no difference in strength until first failure when the extent of HAZ is 20 mm or 40 mm, this is due to the fact that there are only the elements in the stiffener web closest to the plate which is critical with respect to first failure.

Comparison of the first drop in Figure 3.6 and Figure 3.7 shows that the peak are almost exactly at the same magnitude and occur for the same displacement. This verifies that the first failure is almost only depending on the properties in the stiffener web close to the plate.

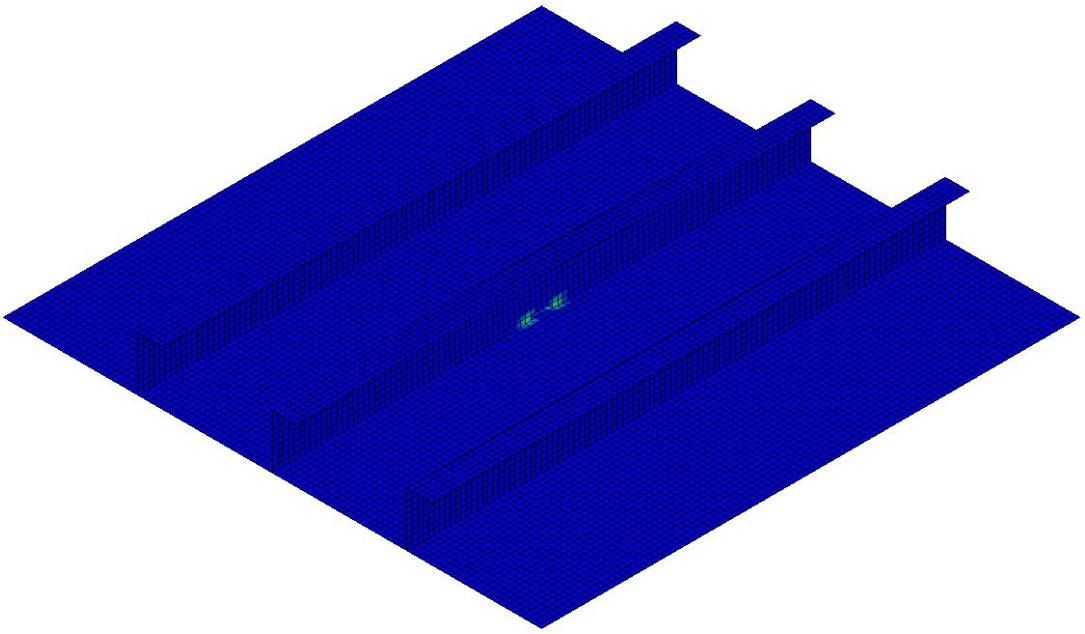

Figure 3.8: First failure occur at the middle point in the stiffener

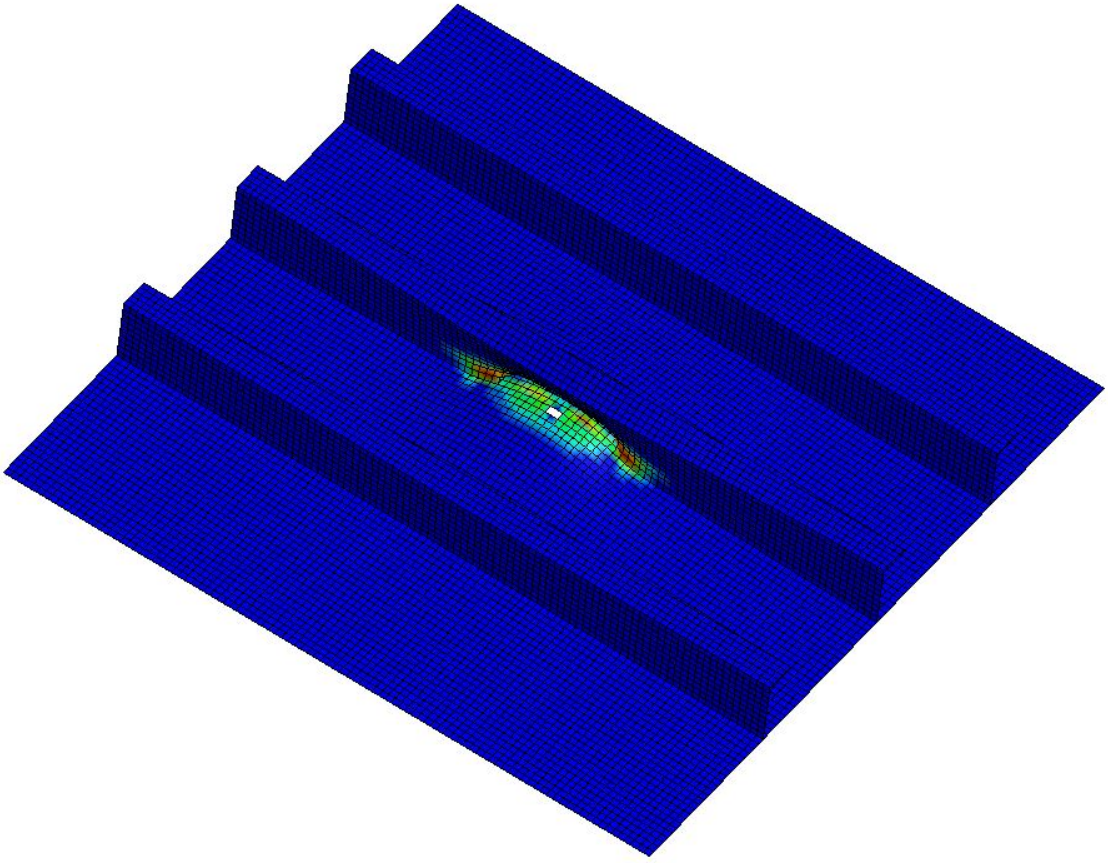

Figure 3.9: Second failure occur close to the middle point in the plate. The figure is to be taken as a illustration since the level of displacement varies between the analysis. This particular Figure shows alloy 5083-H12 without HAZ

The second significant drop is due to failure of the plate and is hence characterised as the ultimate capacity of the stiffened plate. From Figure 3.9 it is clearly shown that the failure in the plate occur close to the center, which seems reasonable since it is in that area the surface displacement is largest.

Figure 3.6 shows that the analysis without HAZ modelled fails at the smallest displacement level and for a smaller contact force compared to the analysis where HAZ is included. The reason why the material without HAZ fails for a smaller displacement compared to the analysis with HAZ for alloy 5083-O in the plate is due to the fact that the plate fails more locally, see Figure 3.10. For the analysis with HAZ include also the stiffeners at each side fails before the plate fails. The plate is therefore able to have a larger global displacement before it reach the critical strain locally in an element. For the analysis without HAZ the stiffeners at each sides does not fails before the plates fail. Hence an element in the plate reach the critical strain for a smaller global displacement level. However it is impossible to account for this effect in a reasonable manner when doing a design. The reason is that which failure mode occurring is really sensitive with respect to material properties and spacing between the stiffeners. Therefore it sounds most convenient and as a conservative assumption to use the values measured from a failure mode similarly to that one shown in Figure 3.10(a).

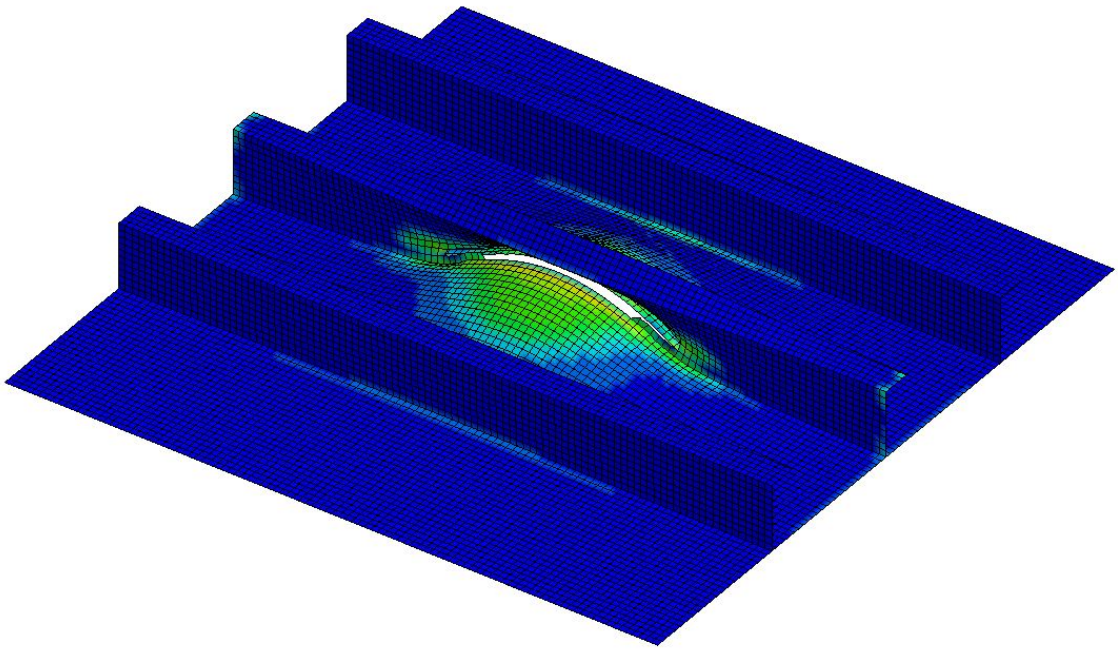

(a) Only base material

Figure 3.10: Total failure of analysis with alloy 5083-O in the plate. (a) without HAZ modelled fails locally between the stiffeners. (b) with a 40 mm extent of HAZ in the plate fails after the two outer stiffeners fails and fails therefore at a larger global displacement compared to (a)

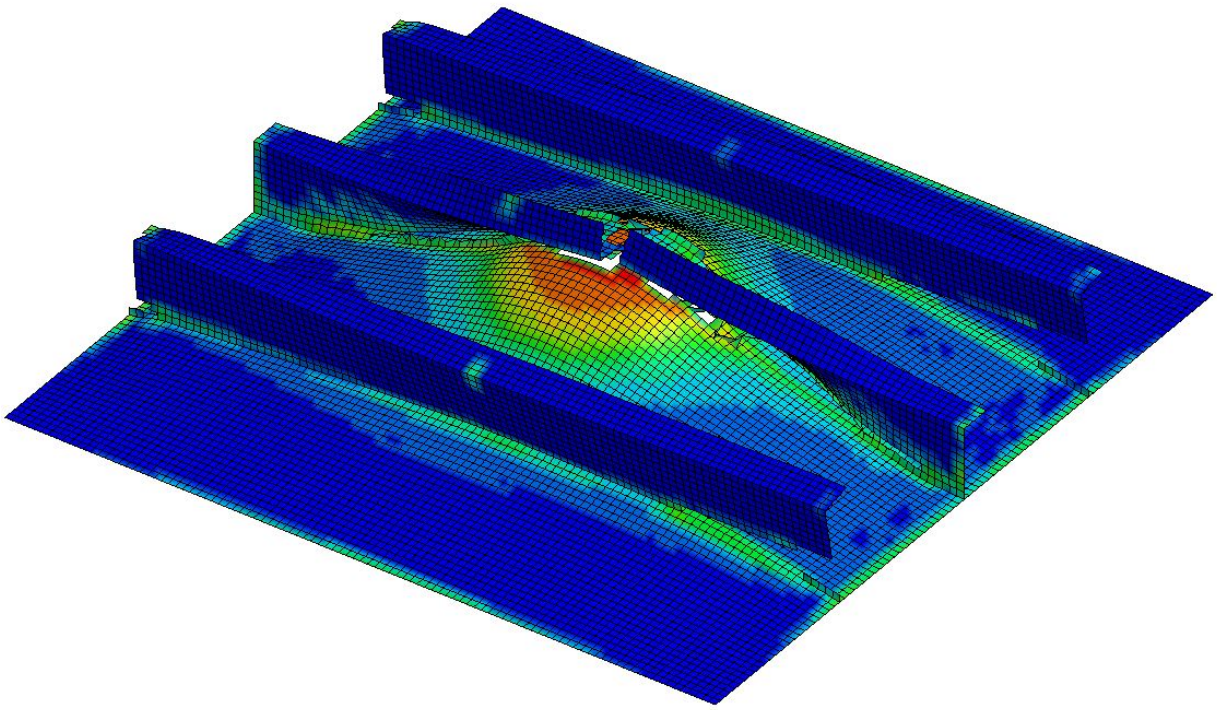

(a) Stiffener2

Figure 3.10: Total failure of analysis with alloy 5083-O in the plate. (a) without HAZ modelled fails locally between the stiffeners. (b) with a 40 mm extent of HAZ in the plate fails after the two outer stiffeners fails and fails therefore at a larger global displacement compared to (a)

The effect shown for alloy 5083-O where the global displacement significantly increase until failure when HAZ is modelled is not shown for alloy 5083-H12. The reason is that all the analysis with this alloy fails in the plate before any of the two outer stiffener fails. An interesting observation in Figure 3.7 is that the analyses with the largest extent of HAZ fails at the largest displacement. The reason why the analysis with an extent of HAZ of 40 mm have a larger strength compared to the one with 20 mm extent could be because a larger HAZ range gives a larger area with same material properties. The HAZ area could therefore carry more load before the stresses needs to be distributed into the base material. However, the results may also be due to numerical inconsistency in the analysis and it is therefore not possible to do a conclusion based on this results.

A comparison of the second peaks in Figure 3.6 and Figure 3.7 shows that alloy 5083-H12 fails at a smaller displacement. This sounds reasonable since the critical effective plastic strain are assumed smaller compared to alloy 5083-O (16 % to 23 %). Another remark is that for the same displacement level the analysis without HAZ gives a larger contact force for alloy 5083-H12 compared to the same curve for alloy 5083-O. This is logically since alloy 5083-H12 have larger yield and ultimate stress compared to alloy 5083-O. The same tendency between the curves exist when HAZ is modelled, but the difference is less significant.

3.4.2 Concluding remarks

From the analysis where the HAZ is omitted the plate utilising alloy 5083-O will fails at a larger global displacement compared to the plate with alloy 5083-H12 even that alloy 5083-H12 have larger material properties such as yield and tensile strength and both plates fails with the same mode, similar to that one shown in Figure 3.10(a). The reason is that alloy 5083-O is a softer material and are allowed to obtain larger strains until failure. From this it is clearly shown that it is beneficial to apply the softer material temper O compared to temper H12 in the plate with respect to energy dissipation. This implies that temper O is more beneficial to be applied for structures exposed to accidental loads. This is also verified by the energy-displacement curves shown at the right side of Figure 3.6 and Figure 3.7. Temper O is also beneficial since it has no reduction of material properties in HAZ. Another beneficial of applying alloy 5083-O is that this have larger difference between the yield and ultimate stress. This implies that the hardening zone is larger which is beneficial in connection to redistribution of forces. Alloy 5083-H12 have a small difference between the yield and ultimate stress and will hence have a stress-strain curve which looks quite similar to a linear elastic perfectly plastic material curve.

From Figure 3.6 it seems to be conservative to not include HAZ in the stiffener when alloy 5083-O is used in the plate. However, as have been shown in Figure 3.10 the differences between the curves are related to the global mode of the stiffened plate at failure. What it actual shows is that it is beneficial for the energy dissipation in the plate that the two outer stiffeners fails at a small displacement in order to distribute the strains in the plate over a larger area. What which should be conducted from this discussion is that care should be managed when post processing results of NLFEA to verify that the structure fails in a reasonable manner.

In generally the stiffeners will fail at a small displacement level compared to the ultimate displacement level where the plate fails. The reason why plates is stiffened by stiffeners is to counteract buckling when it is subjected to life loads, such as for instances hydrostatic pressure load and wave loads. This implies that the stiffeners properties are important to the structure when loads are within the elastic range. After the stiffener have failed the plate have to more or less carry the total load introduced as membrane forces.

One of the main uncertainty for the analysis carried out in this section is regarding the fracture modelling. The model which is used is as already mentioned a simple criterion based on a critical effective strain level. It exist several difficulties related to use of a simplified fracture model. The model is for instance very sensitive regarding the critical strain chosen as input. The value used in those analysis are picked in conformity with Eurocode 9: Part 1-1 (2007).

Figure 3.11 shows the force-displacement curve where the critical effective stress to failure is increased from 23 % to 30 % for the alloy 5083-O when the stiffeners are modelled with-

out HAZ. It is clearly seen that this increase have a great influence on the displacement until fracture. The same tendency is shown for alloy 5083-H12 in Figure 3.12.

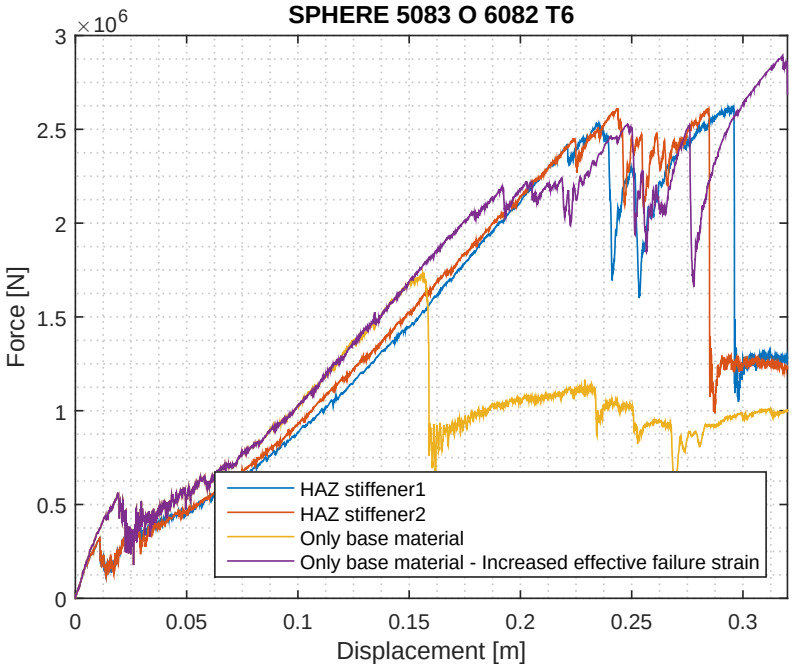

Figure 3.11: Force-deformation curve for alloy 5083-O. It is included a curve where the critical effective stress to failure is increased from 23 % to 30 % when the stiffeners are modelled without HAZ

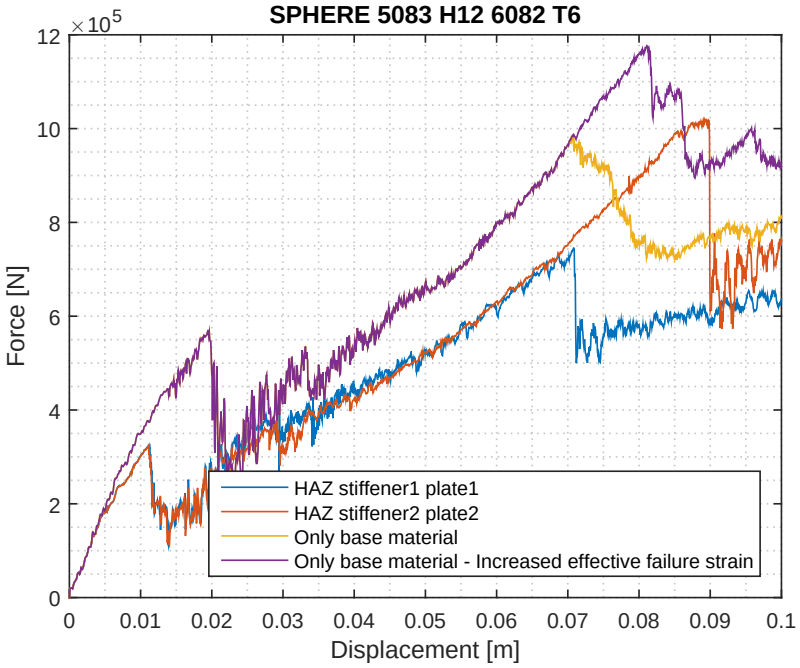

Figure 3.12: Force-deformation curve for alloy 5083-H12. It is included a curve where the critical effective stress to failure is increased from 16 % to 23 % when the stiffeners and the plate are modelled without HAZ

In this chapter it have been shown that the stiffeners fails at a relative small displacement and will hence have small influence of the total energy dissipated in the stiffened plate. It is the plate which needs to be able to dissipate most of the energy. Hence when picking a material for the plate it is important to pick a material with large hardening, which means great difference between the yield and ultimate strength. It will also be important to chose a material which is characterised as ductile. A conclusion may therefore be that almost any kind of material can be applied for the stiffeners, but the plate material should be picked carefully. From this section the analysis have greatly shown that alloy 5083-O is preferable for the plate since it has large hardening and is relative ductile.

3.5 Discussion of stiffened plate analyses

By the author knowledge minor research have been performed on plates made of aluminium alloys subjected to lateral loads with respect to the ultimate capacity of the plate. Therefore the validation of the results obtained are limited to ensure that the correct theory have been applied for the NLFEA. Due to that reason also the trend found according to the results is more important than the actual values predicted. However, research have been performed on stiffened plate made of aluminium alloys with respect to buckling. Analysis have been performed for stiffened plates subjected to axial compression, transverse compression, lateral pressure and a combination of two or more of those loads. Researches of such analysis are for instance conducted by Kristensen (2001) and Chen (2011).

The general trend verified by Kristensen and Chen was; when the amount of reduction of the material properties in HAZ this will give an increased reduction of ultimate strength of the plates with respect to buckling. It is not really practical to compare the trend observed from buckling of stiffened plates made up of aluminium alloys with the analysis performed in this chapter. For buckling analysis the stiffness of the panel and hence the strength of the stiffeners are of great importance with respect to buckling strength and that is what which have been shown by Kristensen and Chen.

Chen (2011) shows that the amount of reduction in strength when HAZ is introduced varies significantly depending on the welds and where the welds was positioned. The amount of reduction also depends significantly on the slenderness parameter for the stiffened panel. This because for slender panels the ultimate capacity in buckling is governed by elastic buckling.

For investigation the influence of the extent in HAZ, Chen (2011) used alloy 6082-T6 with a reduction of 50% of the material properties in HAZ. It was shown that the amount of reduction of ultimate capacity depends on the orientation of the welds. For strength in the welding direction the effect of increase the extent of HAZ from 20 mm to 40 mm have a minor influence. However regarding the capacity normal to the welds the effect is significant according

to (Chen, 2011). The increase from 20 mm to 40 mm are approximately doubled the reduction of strength normal to the weld (9.70% to 18.63%), while the strength in the welding direction is decreased by about 3% (19.52% to 20.54%). The research regarding extent of HAZ is performed for a panel with closed stiffeners and it will not be totally correct to draw a general trend valid for all kind of stiffeners based on this research. However, the trend will probably be the same for a plate stiffened by L-stiffeners subjected to lateral loads.

4 Design of ship collision barrier

The main function of the ship collision barrier is to protect the transition zone between the floating bridge and the submerged floating tunnel. The barrier should protect against ships with larger energy. The design ship considered is a cruise ship. Due to the risk of human life it is desirable to cause a minor damage to the ship. By this reason the barrier needs to absorb large amount of energy through large local deformation in order to reduce the contact force and cause a minor damage to the ship.

4.1 Design parameters

Some of the design parameter were provided by Reinertsen AS upon the start of the author's project thesis during the fall of 2014. This includes the design parameters for the ship, while all the parameters for the barrier where not provided and the author was recommended to do reasonable choices.

4.1.1 Design Ship

The design ship in accidental limit state (ALS), is taken as the ship which have probability of occurrence less or equal to 1×10^{-4}. The design ship was provided by Reinertsen AS through a report made by Ramboll (2011), the relevant ship parameters from this report are reprinted in Table 4.1.

Table 4.1: Design ship parameters, (Ramboll, 2011)

Length [m]	208
Breadth [m]	29
Displacement [metric ton]	31456
GT	20000-50000
Speed [knots]	17.7
Draught [m]	8.8

In this report the added mass was taken to be 20% of the mass. The total kinematic energy is then calculated according to equation (2.1) to be $1564.9 MJ$.

4.1.2 Barrier parameters

Reinertsen AS provided that the barrier should have a minimum length of 380 meter in order to cover the whole transition zone. It was also provided that the barrier should be a floating structure and have a straight configuration. The barrier should be assumed freely floating at the time of impact. Hence, the barrier is assumed to be only supported by inertia and drag forces for all practical calculations and discussions in this master thesis.

The breadth of the barrier have a small influence on the drag force acting on the barrier. However, the breadth have large influence on how much energy the barrier are able to absorb locally. The barrier are assumed to have a breadth equal to 20 meter, which is the same assumption used by Konstali (2014) and was by Konstali taken according to drawings provided by Reinertsen AS.

Somehow the barrier needs to be attached to the bridge or/and the artificial seabed at its initial position. The most reasonable method to create a such connection is to use a weak-link. The weak-link needs to be strong enough to carry all weather loads on the barrier during the decided design life time. It should also be strong enough to withstand loads from impact of small boats. When the barrier is subjected to accidental load, then the load will be too large and the weak-link is snap off. Therefore the barrier is in practical assumed to be a freely floating beam when it is subjected to accidental actions.

Intentionally it would have been preferable to place the ship collision barrier as far as possible from the transition zone. The reason is that for a longer distance more energy could be dissipated when the barrier is translated by drag forces and other viscous forces. It may however be impossible to position the barrier that far from the tunnel to have zero velocity and energy when it hits the tunnel. If the energy still is larger than the tunnel can handle, the barrier should be anchored in a secondary way in addition to the weak-link discussed for the initial position. This could be managed in several ways. For instance could the barrier be anchored such that the anchoring lines are activated after the barrier has translated a given distance. The anchoring force may still be of significant amount, but it is reasonable that this force will be smaller compared to if the anchoring force is activated at the initial position of the barrier. Such configuration was briefly conducted in the author's project thesis (Hansen, 2014). A more detailed discussion related to anchoring of the ship collision barrier is not covered in this thesis.

The kinetic energy in the striking ship need to be absorbed locally as strain energy by local deformations in the barrier and in the ship bow. In additional remaining kinetic energy in ship and the barrier could as already mentioned be dissipated by drag forces and other viscous effect.

A qualitative discussion and some simplified calculations related to the retardation of the barrier were discussed in the author's project thesis during fall of 2014 (Hansen, 2014), the par-

ticular chapter are reprinted in appendix A. This discussion was done with respect to a centric collision scenarios. In that case the draft of the barrier was taken as a variable. Two different cross sections were discussed, see Figure 4.1. One closed symmetrical cross section and one where the draft was increased by adding a skirt.

Figure 4.1: Cross section of the barrier, one closed symmetrical cross section and one cross section with skirt

The advantage by using a closed cross section is that it is a symmetrical cross section about both axis, and hence the fabrication will be regular for the whole section. The disadvantage is that the displacement will be larger and hence it requires a lot more ballast water, in addition is more material regarded. For the cross section with skirt the most critical structural member with respect to design will be how to design the skirt. This have to withstand large forces and moments. The connection between the skirt and the main body of the cross section have to be done in such a way that the forces will be carried by the whole main body and not be localised in a small area.

In the author's project thesis, (Hansen, 2014), it was stated that a cross section with skirt have benefits compared to a closed cross section when the draft became large. A benefit for the closed cross section which not was mentioned in project thesis is that a heavy cross section will probably have smaller responses when subjected weather loads such as waves and it will hence be less exposed to fatigue loads.

Even that the benefits of using a cross section with skirt could be large it is decided to use a closed cross section as a first approach in the analysis carried out later in this thesis.

To decide the draft of the barrier it is important to consider the draft of the design ship which according to table 4.1, is 8.8 meter. Therefore the draft of the barrier, should be at least 8 to 9 meter. Hence the main part of the bow impact the barrier and then the energy which the ship and the barrier have to dissipate is distributed over as large as possible area. Another input parameter provided by Reinertsen AS is that the distance from waterline to top of the barrier should be at least 4 meter. All the design parameter used for the barrier i summed up in Table 4.2. The displacement is calculated by multiplying the breadth, draught, length and the density of seawater.

Table 4.2: Design barrier parameters

Length [m]	380
Breadth [m]	20
Displacement [metric ton]	62320
Total height [m]	12
Draught [m]	8

Table 4.2 give a first approach for the relevant global design parameters for the ship collision barrier. Most of the values are to be taken a guidance value and can be changed at a later design stage.

4.2 Structural design

The barrier is to be taken as a floating structure which locally need to dissipate a large amount of energy. The global strength should be designed such that the retardation force acting on the barrier will be as large as possible. The barrier are decided to be built of two different aluminium alloys. For the plate it is suggested to use alloy 5083-O, while for the stiffeners it is suggested to use alloy 6082-T6.

The ship collision barrier is assumed to be a freely floating structure at the time where the ship impacts. Therefore the barrier is only supported by inertia and drag forces. The inertia forces will dominate straight after impact due to the large mass of the barrier including added mass and ballast. Since the velocity is small straight after impact the drag forces will be approximately zero at that moment. The drag forces will be more important when the ship and the barrier more or less have emerged into one part and it have got a stable velocity of some magnitude.

In the following subsections the local and global design of the barrier will be briefly discussed with respect to the different cross sectional properties. In addition procedure for how the global and local strength can be estimated is included. Results from such simplified approach are not included.

4.2.1 Global design

The global strength of the ship collision barrier is important in order to ensure as large as possible retardation force. Therefore it is preferable that the barrier remains straight after impact in order to maximise the drag and other viscous forces. However in reality it will not be practical or possible to built a barrier with so large global strength. The barrier will therefore form a global mode, but the global strength is still important to ensure that the barrier does not fail in a global manner.

The global strength of a straight beam only supported by drag and inertia forces will probably be a mode with formation of a hinge at the middle position, see Figure 4.3. This is valid for the ship collision scenarios where the ship impact the barrier at the center position of the barrier. This scenarios will be the most critical scenarios with respect to global strength of the barrier, this is shown in appendix B. A simplified approach for estimation of the global strength is discussed in the following subsection. The topic was briefly discussed in the authors project thesis (Hansen, 2014).

Global strength

It is possible to apply plastic theory to get an estimation of the global strength. The solution will give the plastic moment capacity which can be used as an input to the local design analysis in order to design a barrier cross section. The moment capacity (M_P) will not be totally correct due to simplification, but it will be valid as a first approach.

An additional uncertainty is introduced for this particular ship collision barrier since it should be built of aluminium alloys. Therefore it will not be practical to assume a fully plastic cross-section as have been discussed in chapter 2. The procedure for the centric collision event is discussed in the following sections, and a deduction for an arbitrary impact position is included in appendix B.

For the centric collision event a simplified model is shown in Figure 4.2. In this figure the point load represent the ship and the line load is the drag and inertia forces which is distributed over the length. The position of the ship is assumed as the support. In a perfect centric collision the resultant from both the ship and the distributed forces acts through the same point and hence all the energy will participate in developing of a plastic hinge.

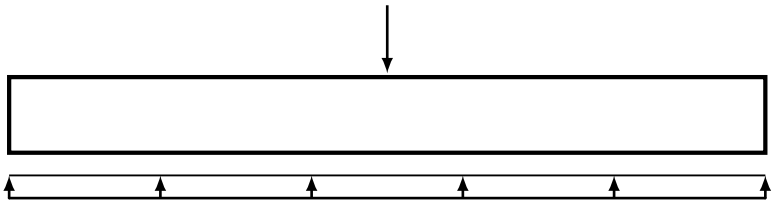

Figure 4.2: Simplified model for the global analysis

Figure 4.3 shows a configuration with a plastic hinge formed at the middle position at the collision barrier. Most of the relevant dimensions are given in the figure, but in addition the rotation in point 2 is assumed to be $2 \cdot \theta$ and the rotation in point 1 and 3 is equal to θ. By using small angle assumptions $w_0 = \theta \cdot \frac{L}{2}$.

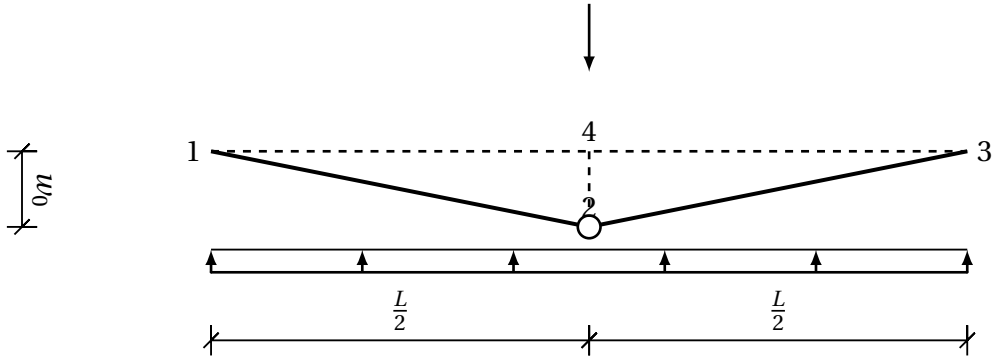

Figure 4.3: Deformed shape when plastic hinge have been formed

When the deformed shape is assumed, see Figure 4.3, it is now possible to establish an equation for calculation of the plastic moment capacity (M_P). This establishment is based on applying equilibrium between the internal and external work and then solve with respect to M_P. The calculation sequence follows.

Internal virtual work:

$$W_i = M_P \cdot 2 \cdot \theta \tag{4.1}$$

External virtual work:

$$W_e = \int_0^L \cdot q \cdot w(x) \cdot dx = \frac{1}{2} \cdot q \cdot w_0 \cdot L \tag{4.2}$$

Where:

$$w_0 = \theta \cdot \frac{L}{2} \tag{4.3}$$

Gives the external virtual work:

$$W_e = \frac{1}{4} \cdot q \cdot L^2 \cdot \theta \tag{4.4}$$

Setting the internal and external virtual work equal and get an expression for M_P:

$$M_P = \frac{1}{8} \cdot q \cdot L^2 \tag{4.5}$$

Where:

W_i: Internal virtual work

W_e: External virtual work

M_P: Plastic moment capacity

θ: Angle of rotation

w_0: Deflection at the middle position

w: Deflection

q: Distributed load

L: Length

Equation (4.5) gives the minimum regarded plastic moment capacity for the barrier cross section. From this equation it is clearly shown that the regarded plastic moment capacity is depended on the barrier length squared and linearly depended on the distributed load which again particularly means that it is linear dependent on the mass. The reason is that the inertia forces will dominate straight after impact.

4.2.2 Local design

The local cross section need to be designed such that it can withstand large energy locally. The barrier needs to be soft enough to not totally crush the the bow of the ship. It also needs to be strong enough so the ship not more or less are sailing straight through the barrier. The ship collision barrier have to be a light structure since it is a floating structure and also in order to keep the material cost at a reasonable level. By those arguments it seems more than reasonable to design the barrier more or less as a ship hull like structure. This implies a cross section build up by stiffened plates, supported by decks, transverse bulkheads and longitudinal bulkheads.

Qualitative discussion of the influence from various structural members on the local resistance to impact

This subsection gives a qualitative discussion related to how local resistance to impact may be varied during nonlinear finite element analysis. A discussion is done with respect to each structural member and to which influence the different members have on the local strength.

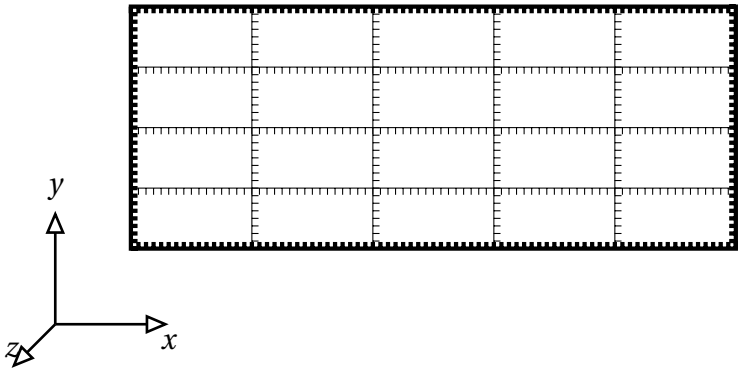

Figure 4.4: Local design (illustration)

The different structural members have various influence on the barrier, both the global strength and the local strength depends on how the local cross section is designed.

Vertical longitudinal bulkheads are relevant with respect to the global strength. The reason is because the number and position of the vertical decks will have great influence on the sectional modulus about the vertical axis (y-axis in Figure 4.4). Both the decks and the transverse bulkheads influence the local strength against impact. The reason is that those two structural members influence the span width of the vertical bulkheads. A smaller span width increase the local strength. The stiffeners main function are to increase the local strength in additional to counteract local buckling.

The configuration of the local cross section is not only important with respect to the local strength and global stiffness. It will also have an influence on the ballast system and how the ballast is split into several tanks. Hence it will also be important regarding the stability of the barrier. To disregard the negative influence on stability which is connected to free surface effect, it is wanted that each tank filled with water is close to full. Due to stability requirement it will be preferable to have small surface area in the tanks. One of the reasons is related to damage stability. If flooding occurs between two ballast tanks due to penetrating, the new effective surface will be the sum of those two tanks. Therefore if the tanks surfaces are large it will give a larger free surface effect and hence be more critical with respect to damage stability. Stability is further discussed in section 4.4.

Some of the transverse bulkheads should be designed watertight. This is in order to keep the barrier stable after impact when water have flooded into a compartment of the barrier. A further discussion regarding the spacing is performed in section 4.4.4.

Regarding which parameters related to the barrier which most easily could be changed during the finite element analysis, it will in principle be able to change all of them. However, in order to do as little extra modelling as possible some changes are more preferable than others. Therefore it may be a good solution to assume the number of decks and longitudinal bulkheads to be constant. The reason is due to the ballast system and the stability calculation which is more or less calculated independently on the rest of the barrier parameters. There-

fore the parameters which most easily can be varied without have a severe influence on the on the ballast system and/or the stability will be to change the thickness of each plate, the dimension and spacing of the stiffeners and to change the spacing and the number of transverse bulkheads.

Estimation of local strength

The plastic moment capacity is known from the global design analysis. From the plastic moment the regarded plastic section of modulus (W_P) can generally be calculated by rewriting equation (4.6).

$$M_P = W_P \cdot \sigma_y \tag{4.6}$$

Where:

W_P: Plastic section of modulus

The barrier is to be built up by two different alloys (alloy 5083 and 6082) which have different material properties. However, since the calculations in this section are only to give a brief estimate for the regarded cross section it may therefore be good enough to use the same yield stress for all the cross sectional members.

The plastic section of modulus for a cross section configuration similarly to that in Figure 4.4 can be calculated according to equation (4.7). The axis are referring to the system of coordinates in Figure 4.4. Since the cross section is bending about the y-axis the relevant plastic section of modulus with respect to plastic deformation needs also to be calculated about this axis.

$$W_P = \int_A |x| \cdot dA \tag{4.7}$$

4.2.3 Concluding remarks regard structural design

More detailed analysis of the structure needs to be performed in order to verify the structural properties estimated according to the method discussion in the previous section. Most often it will be an iteration process. Making reasonable assumption related to the structural configuration is preferable as a first approach. The reason is that the finite element analysis of relevant configurations are time consuming, therefore it is preferable to have as few as possible iteration operations with a finite element program.

4.3 Ballast considerations

Since the barrier is build up as a ship like structure, the weight relative to the volume is small. Therefore ballast is required in order to obtain the desired design draft ($8m$) for the ship collision barrier, see section 4.1.2 and Table 4.2. Ballast is in fact weight added to the structure with the only purpose of increase the total weight of the structure. It is possible to use different kind of ballast to add weight to a structure, but water is mostly used. Therefore it is naturally to assume that salt water is applied as ballast for this structure. However, if the stability are determined to be critical other heavier ballast could be considered in order to lower the center of gravity. Salt water is assumed in the following sections.

4.3.1 Required amount of ballast

The regarded amount of ballast depends on the weight of the structure itself, which means the weight of aluminium.

$$m_{bal} = \Delta - m_{al} = \rho_{sw} \cdot L \cdot B \cdot d - m_{al} \tag{4.8}$$

Where:

m_{bal}: Required mass of ballast [kg]

Δ: Tonnage of the barrier [kg]

m_{al}: Total mass of aluminium in the barrier [kg]

ρ_{sw}: Density seawater [kg/m^3]

L: Length of the barrier [m]

B: Breadth of the barrier [m]

d: Draft of the barrier [m]

From equation (4.8) it is shown that the first term, Δ is constant independently on how the cross section is built up. While the second term m_{al} depends on the thickness and number of decks, vertical and transversal bulkheads and the stiffeners.

To estimate the required amount of ballast four different cross sections were considered, see Figure 4.5. The global parameter were taken according to Table 4.2 for all the cases. By using a different amount of decks and vertical bulkheads m_{al} is slightly varied. The main reason by investigating different cross sections is related to the stability consideration, see section 4.4.

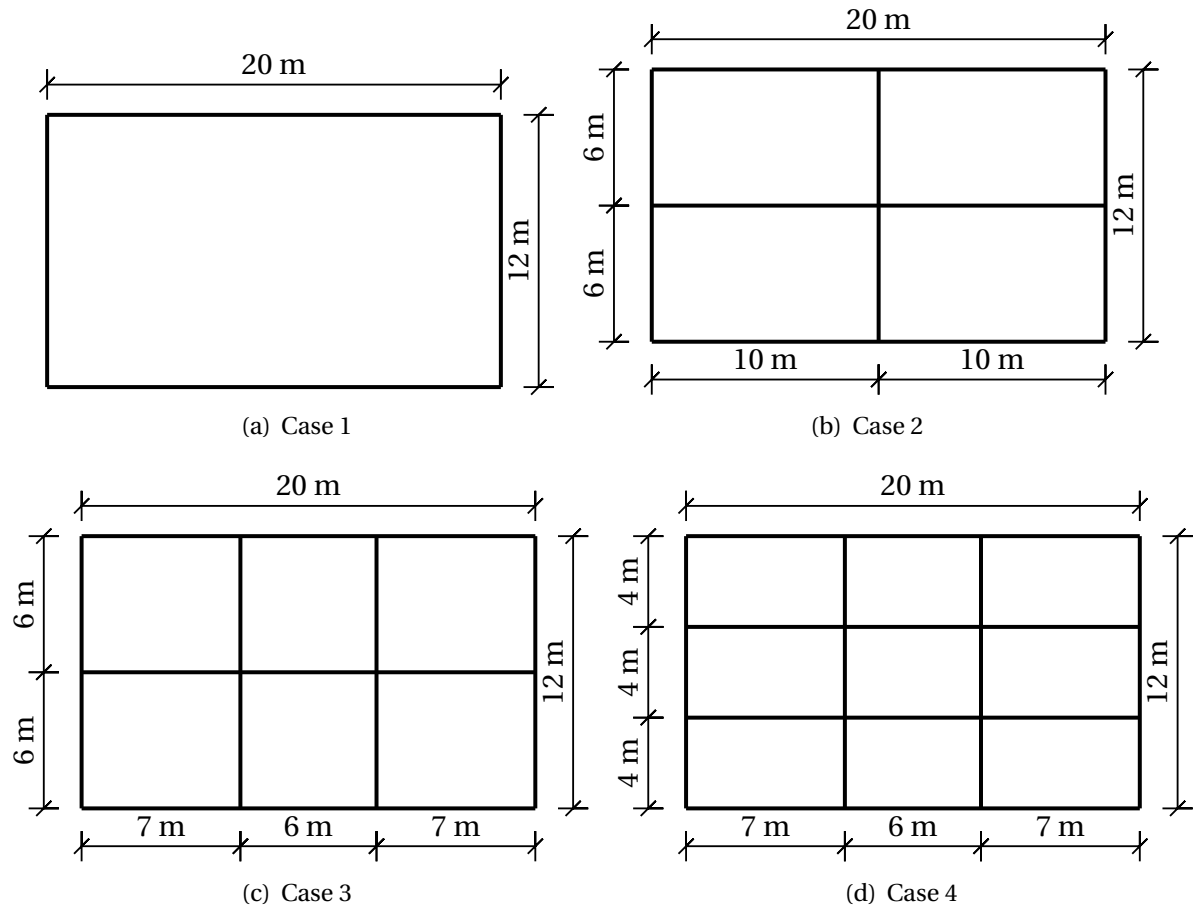

(a) Case 1 (b) Case 2

(c) Case 3 (d) Case 4

Figure 4.5: Four different cross sections used for the calculations

The calculation and consideration done within this section is taken according to a unit width of the cross sections. This implies that the weight and area of the transverse bulkheads are disregarded from the calculations, which means that the required amount of ballast will slightly be overestimated, and hence also the center of gravity will slightly low and the stability GM will be overestimated. However the difference is small and since the number of transverse stiffeners not yet is desired it was decided to look at a unit length of the cross section and disregard the transverse bulkheads.

The dimensions used to calculate the required ballast are given in Table 4.3. The stiffeners is for simplicity assumed smeared to the plate, the effective thickness obtained from the smearing process are used in the calculations.

Table 4.3: Parameter used for ballast and stability calculations

Height, H $[m]$	12
Breadth, B $[m]$	20
Length, l $[m]$	1
Draft, d $[m]$	8
ρ_{al} $[kg/m^3]$	2700
$\rho_{sw}[kg/m^3]$	1025
t_{eff} $[mm]$	20

The mass of displaced volume for the cross section:

$$m_{total} = \Delta = B \cdot l \cdot d \cdot \rho_{sw} = 20 \cdot 1 \cdot 8 \cdot 1025 = 164000kg \tag{4.9}$$

The results for the different cross sections in Figure 4.5 are given in Table 4.4.

Table 4.4: Results of the required ballast calculations for the different cross sections

	Case 1	Case 2	Case 3	Case 4
Weight of aluminium m_{al} $[kg]$	3456	4752	5238	6048
Necessary weight of ballast m_{bal} $[kg]$	160 544	159 248	158 762	157 952
Necessary volume of ballast, when using salt water V_{bal} $[m^3]$	156.62	155.36	154.89	154.10
Percent ballast mass of total mass	97.9 %	97.1 %	96.8 %	96.3 %
Ballast height, distance from the bottom of the cross section $[m]$	7.85	7.78	7.76	7.72

From Table 4.4 it is clearly shown that the amount of ballast is significant, more than 95 % of the total mass for all the cross sections considered. This is shown with an illustration in Figure 4.6. The large amount of ballast implies that the ballast have the biggest influence on the position of the center of gravity. When the outer dimensions is equal for all four cases the number of inside decks, vertical and transversal bulkheads have small influence on the regarded amount of ballast. The reason is that the weight of ballast is dominated even for case 4 which has the greatest amount of bulkheads and decks.

In section 4.4 it is shown that the number and position of bulkheads will have great influence on the stability. The reason is that the different cases implies different surface area and hence also affect the free surface effect.

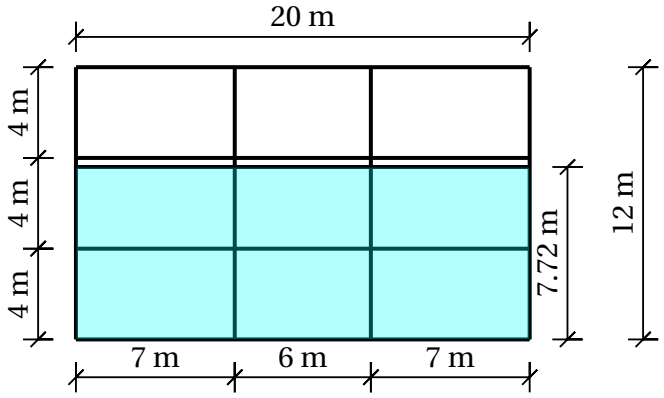

Figure 4.6: Amount of ballast filled in the cross section for case 4

4.3.2 Water transport

Water is a nearly incompressible fluid. Imagine a tank which is full of water and closed, then the water are not allowed to flow out from the tank. If this tank get an indentation and the volume decreases, the forces from the water on the structure will be increasingly large. This will then cause failure of the tank at an earlier stage compared to an empty tank. This simple example shows that the ballast water need to have an escape route from the tanks if the volume of the tank decreases. This in order to counteract failure due to forces from the water at the structure.

The common passive way to let water be transferred between tanks is by applying manholes, cutouts and ventilation pipes. It is beneficial to apply several cutouts or manholes in stead of one large hole, due to stability consideration. For an illustration of cutouts in the ship collision barrier see Figure 4.7.

If large openings are applied the tanks can not be assumed separately since the water transport from one tank to another will happen really quick. If the openings between tanks are small the water transport will happen slower and it will therefore be a good assumption that the tanks still are assumed as two individually tanks. Konstali (2014) carried out a simplified approach for the number of required cutouts by considering Bernoulli's equation, see equation (4.10).

$$\frac{1}{2} \cdot \rho_{sw} \cdot v^2 + \rho_{sw} \cdot g \cdot z + p = C \tag{4.10}$$

The position of the cutouts should be selected carefully. The reason is to avoid water transport into tanks which are empty. The reason is because those tanks will then get a free surface effect and will then have a negative influence on the stability. Any further discussion related to water transport have not been carried out in this thesis.

Structural lay-out

An example of how the cutouts or manholes can be organises in the decks and the bulkheads are shown in Figure 4.7. Any further discussion of the lay-out is omitted. Due to the size of the cutouts and common practise non of the cutouts are included in the finite element analysis carried out in this thesis. The common way to take into account cutouts in large finite element analysis are to reduce the effective thickness in the area where cutouts should have been introduced.

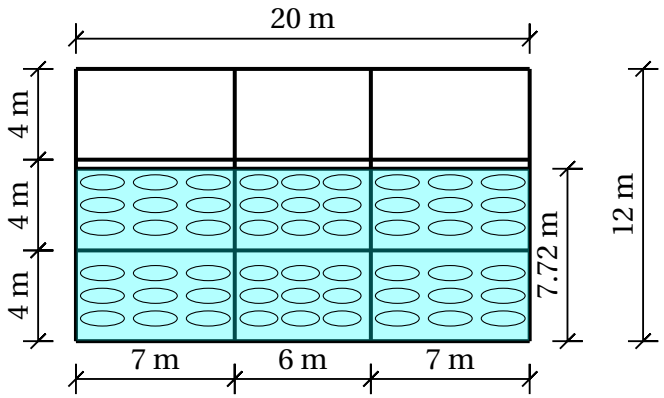

Figure 4.7: The figure shows an example of how the manholes or cutouts in transverse bulkheads for case 4 can be introduced, it will be similar cutouts in decks and vertical bulkheads

4.4 Stability

Assessing the stability of the barrier in both intact and damage condition is an important design check. In this section the hydrostatic stability will be discussed with respect to simplified assessment and qualitative discussions. All considerations will be carried out with respect to the four cross sections discussed with respect to ballast considerations, see Figure 4.5. The discussion is mainly focusing on the stability in transverse direction, this means the stability of the cross section, see Figure 4.8. The longitudinal stability will only briefly be mentioned, the reason is that the longitudinal stability will almost never be critical if the transverse stability is satisfying.

The skip collision barrier is a more and less permanently structure which will float with small or no heeling angle, by that reason it sounds reasonable to assume small heeling angles when the simplified hand calculations are carried out.

For the transverse stability in intact condition the transverse bulkheads have been omitted and the calculations are carried out for a unit length of the cross section. It should be aware that some transverse bulkheads have to be included and some of them needs to be applied as watertight bulkheads. This will be further discussed in section 4.4.4.

4.4.1 Intact stability

The fundamental stability equation is given in equation (4.11). This is valid for small angles, $\theta \leq \pm 10^{\circ}$, and exactly correct for $\theta = 0$. As already mentioned it will be assumed small angles for the calculation of this particular ship collision barrier. The fundamental stability requirement is $GM > 0$.

As a comment to Figure 4.8, for most of ship cross sections the center of gravity is above the center of buoyancy, but for this ship collision barrier it has been calculated that the center of buoyancy will be placed above the center of gravity and therefore it is drawn like this in Figure 4.8.

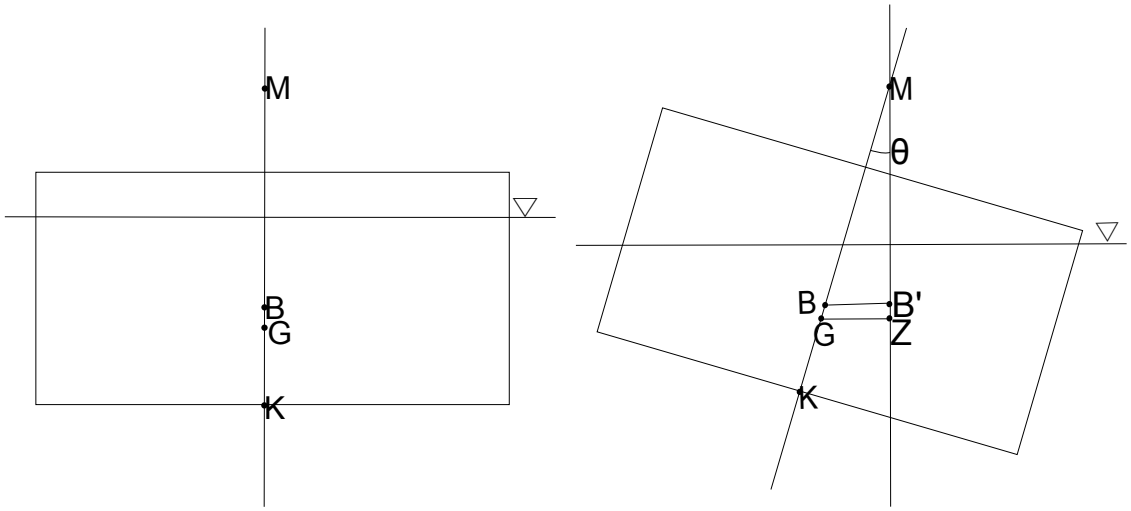

(a) No heeling (b) With heeling

Figure 4.8: Stability of the barrier cross section

$$GM = KB + BM - KG \tag{4.11}$$

Where BM can be calculated according to equation (4.12).

$$BM = \frac{I}{\nabla} \tag{4.12}$$

Where:

I: Second moment of area $[m^4]$

∇: Displacement $[m^3]$

GM: Metacentric height $[m]$

When the metacentric height, GM have been measured the righting arm, GZ can be calculated as follows:

$$GZ = GM \cdot \sin(\theta) = GM \cdot \theta \tag{4.13}$$

The last term is only valid when small angles are assumed.

Inserting for GM:

$$GZ = (KB + BM - KG) \cdot \theta \tag{4.14}$$

Free surface effect

When the floating structure contains tanks with liquid and the tanks are not completely filled the metacentric height have a negative contribution from the free surface effect. It is therefore preferable to fill the tanks more or less completely full (98% to 99%). If the tanks does not are completely full the structure will get a virtual extension of the gravity point from G to G". This could be taken into consideration by using equation (4.15). The equation can be deducted by use of the center of mass theorem.

$$GG'' = \sum \frac{\rho' \cdot i}{\rho \cdot \nabla} \tag{4.15}$$

Where:

ρ': Density of liquid in the tank $[kg/m^3]$

ρ: Density of seawater $[kg/m^3]$

i: Second moment of area of the tank $[m^4]$

∇: Displacement of the structure $[m^3]$

4.4.2 Damage stability

The damage stability considerations are more calculation demanding compared to the intact stability calculations. In this thesis only assessments with simplified considerations are applied. At a late design state it should be carried out detailed analysis of the stability in damaged condition. This could be done by use of an advanced computer program or a set of equations to consider all the different scenarios and take as many as possible effects into considerations. However such detailed calculations related to damage stability of the barrier is out of the scope of this master thesis. Therefore several simplifications needs to be carried

out in order to be able to due estimations related to damage stability of the barrier cross sections. Generally all assumptions performed in this section is based up on conservatism.

The fundamental relation used in damage stability calculations is that the restoring moment should be greater or equal to the heeling moment (overturning moment), see equation (4.16).

$$M_{restoring} \geq M_{heeling} \tag{4.16}$$

First assumption is that the greatest allowed heeling angle, θ, is when one of the upper corner of the cross sections hits the water. This is close to the angle shown in Figure 4.8(b). The second assumption applied is that the draft of the barrier is assumed constant. The reason why this assumption is applied is because the height of the ballast water inside the structure is close to the draft value, as have been shown in section 4.3. Third assumptions is that the flooded tanks gives zero contributions to the buoyancy force. Fourth assumptions is that all the tanks including those which have been flooded contributes to heeling moment.

The maximum restoring moment of the cross section is calculated at the largest healing angle. The moment is calculated as the contribution from the buoyancy force (flooded tanks gives zero contribution), the force acting through the point B' in Figure 4.8(b) multiplied with the righting arm GZ.

Accordingly the heeling moment will be determined as the contribution from the ballast water in the tanks and due to the gravity of the structure.

The calculation and discussion with respect to damaged stability is further discussed in the next section.

4.4.3 Results and calculations

In section 4.3 related to ballast considerations it is stated the necessity to have cutouts in bulkheads and decks in order to allow water transport. For simplicity in this section the cutouts have been neglected and all bulkheads are assumed watertight. This may be reasonable with respect to short duration since the cutouts are small relative to the bulkheads and it will therefore take time for water to transport from one tank to another.

Intact stability

The results for the intact stability calculations are given in Table 4.5. The intact stability of the barrier is only just stable for the cross section without any internal bulkheads and decks,

see Figure 4.5. Since this value is near zero, it is recommended to use at least an internal longitudinal bulkhead.

Table 4.5: Results of stability calculations in intact condition

	Case 1	Case 2	Case 3	Case 4
KG [m]	3.97	3.95	3.95	3.94
KB [m]	4	4	4	4
I [m^4]	666.67	666.67	666.67	666.67
∇ [m^3]	160	160	160	160
BM [m]	4.17	4.17	4.17	4.17
Metacentric height without accounting for free surface effect, GM [m]	4.20	4.21	4.22	4.23
i [m^4]	666.67	166.67	75.17	75.17
GG" [m]	4.17	1.04	0.47	0.47
Metacentric height accounted for free surface effects, G"M [m]	0.03	3.17	3.75	3.76

The equation (4.11) was also applied for calculation of the longitudinal stability. Even for a simplified cross section with no bulkheads either in transverse or longitudinal direction, see Figure 4.5(a), the longitudinal intact stability gives a metacentric height, GM equal to about $1500m$. For a barrier with length ($95m$) the longitudinal stability metacentric height is above $90m$. This means that the longitudinal stability will not be critical in intact position.

Damaged stability

Initially at the moment when the impacts happen, the stability will probably not be critical. The ship will impact the barrier with a great amount of energy and the deformation of the barrier will be large. The barrier may therefore not be allowed to get any additional heeling angle since the ship and barrier will emerge together as one single unit during impact. The two parts will not be allowed to transform relatively at each other due to contact forces between the parts such as friction forces. The ship will therefore probably act like a plug in the penetrated barrier and only minor water will be allowed to flood into the barrier. However, the damaged stability needs to be verified. If for instances an impact cause small damage globally, but the local damage is large enough to penetrate the skin plate in the barrier. Then the barrier will be flooded and it will loose stability. This means that the critical scenario with respect to stability is after the collision are finished and the ship and barrier are detached. Then the water is allowed to flood into the barrier and influence the hydrodynamic stability of the barrier. This is the scenarios which is briefly discussed bellow.

The damaged stability should be measured to verified and ensured that the restoring moment is larger than the heeling moment. The equations for establishment of those to moments are shown bellow. The moments are calculated for the assumed worst case.

The general equation for the restoring moment due to buoyancy:

$$M_{restoring} = g \cdot \rho_{sw} \cdot B \cdot d \cdot (L - l_{flooded}) \cdot l_{arm} \tag{4.17}$$

The general equation for the heeling moment consist in particular in three terms, the weight of the material itself, the contribution from the ballast water and the contribution from the flooded tanks. How the contribution from ballast and flooding is calculated depends on how the local cross section is arranged. The different cross sections considered are shown in Figure 4.5.

$$M_{heeling} = M_{material} + M_{ballast} + M_{flooding} \tag{4.18}$$

The calculation performed in this section are related to how close the watertight bulkheads needs to be positioned in order to keep the barrier stable after flooding of two compartments. The reason for the requirement of two compartments is because it is the worst case scenarios. If impact occurs at a watertight bulkhead, then the barrier will get a flooding of two compartments.

The intact stability calculation showed that case 1 in Figure 4.5 does not satisfied the intact stability criterion and this cross section was therefore not considered with respect to damaged condition. For the other three cases the damaged stability was determined with applying the simplified method described above. Calculation have determined the critical length between the watertight bulkheads to be approximately $95m$ for case 2. This implies that three watertight bulkheads will satisfying the requirement with respect to damage stability. It will be recommended to increase this number to four or five watertight bulkheads evenly distributed over the barrier length, see Figure 4.10. For case 3 and 4 the stability will be even better. The conclusion is therefore that using four to five watertight bulkheads will be enough as long as it exist at least one longitudinal bulkheads in order to keep the barrier stable in damaged condition. However the calculations are simplified and it should at a later design state be performed more advanced calculations to verify the results.

4.4.4 Watertight bulkheads

This section contains considerations relating to positioning of watertight bulkheads. First some more thought related to the ship collision barrier. If the barrier is hit by a ship and it occurs severe damage to the barrier, then the barrier any how needs to be repaired or replaced. Therefore a relevant question may be; is the transverse stability of the barrier really important? Do the barrier need to float with correct side of the cross section above the water, or it is satisfying that the barrier is still floating after collision?

As long as the barrier is floating it will still absorb energy both as strain energy and due to viscous effects from the water. The forces from the water at the structure may in fact increases since the projected area may increase and then also the drag forces increases. However this is just a consequence and could not be applied in a design check. If the ship collision barrier is required to remain floating after damage it will not cause any damage to the subsea installations, such as the artificial seabed and the submerged floating tunnel. Another beneficial of keeping the barrier floating after impact is that it will be easy to access and remove the ship collision barrier after damage in order to due some repairs.

The requirement related to about the damage stability are important or that the only requirement in damage condition should be to keep the structure floating, is depending on how the ship collision barrier is be taken as a part of the total barrier structure. If the barrier is to carry people as a view point or similarly as shown in Figure 1.2, the assessment of damage stability will be a question of human life. Then it will be important to have good stability of the barrier in damage condition.

Bellow is a brief discussion on the position of the watertight bulkheads when the only requirement is to stay floating after collision included.

The buoyancy of the structure should be larger than the total mass of the structure including added mass.

$$m_{buoyancy} - m_{structure} \geq 0 \tag{4.19}$$

With the minimum requirement:

$$m_{buoyancy} = m_{structure} \tag{4.20}$$

For simplicity it is here assumed that the ship penetrate the ship at the center position, and that it is no longitudinal bulkheads so the water is free to flood the whole cross section. It is also assumed only two transverse bulkheads symmetrically installed about the center line. The calculations is done with respect to an equilibrium position where the center tank is totally filled by water and the new draft of the whole ship collision barrier is $12m$, which is the same as the height of the barrier. The global configuration of the barrier is still assumed to be intact. For an illustration see Figure 4.9. Also in this section the discussion is related to the four cross sections shown in Figure 4.5. The resultant distance between the watertight transverse bulkheads are shown in Table 4.6 and the calculations is done to satisfy equation (4.20).

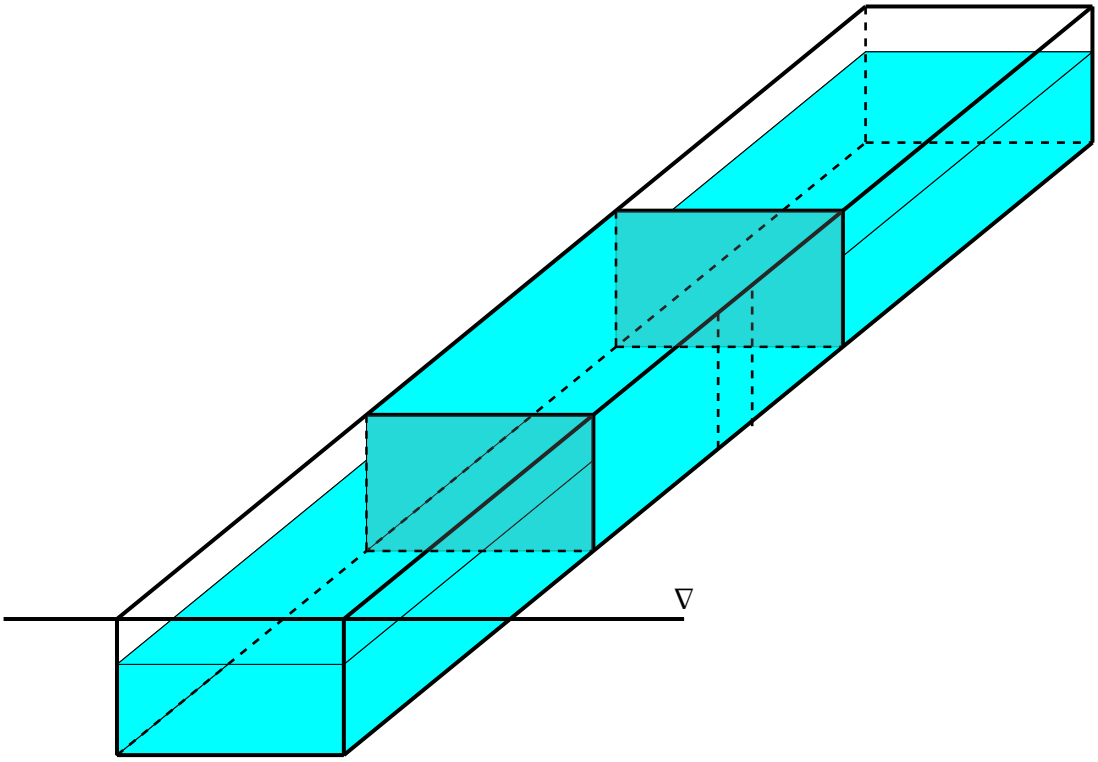

Figure 4.9: Flooding of one compartment between two watertight bulkheads, the fracture is shown by the two dotted lines at the middle tank

Table 4.6: Calculation of the necessary distance between watertight bulkheads

	Case 1	Case 2	Case 3	Case 4
Mass structure $m_{structure}$ $[kg]$	3 780 506	5 120 539	5 612 786	6 421 123
Weight buoyancy $m_{buoyancy}$ $[kg]$	3 780 506	5 120 539	5 612 786	6 421 123
Distance between watertight transverse bulkheads $[m]$	364.6	359.2	357.2	353.9

In Table 4.6 the $m_{structure}$ is equal to $m_{buoyancy}$. This is the requirement according to equation (4.20).

$m_{structure}$ includes the total mass of aluminium and the ballast water in the tanks which not have been flooded, which means the two tanks at the ends of the barrier, see Figure 4.9. The buoyancy and the mass of ballast in the tank which have been flooded are assumed to not contribute to $m_{buoyancy}$ or $m_{structure}$. The may be a slightly non-conservative assumption to disregard the weight of the water in flooded tank in $m_{structure}$. However, when equilibrium is reach the water inside the flooded tank will be in equilibrium with the water outside the structure.

Table 4.6 shows that it will not be necessary to have more than two bulkheads in order to keep the barrier floating after flooding of one compartments. However with only two tanks and if the ship impact at the position of one of the bulkheads two tanks will then be flooded

and then the ship collision barrier will sink. Therefore it is suggested to insert at least five watertight transverse bulkheads symmetrically distributed in the barrier length direction, see Figure 4.10. Four bulkheads will probably be enough based on the discussion above, but five is suggested in order to have one in redundancy.

As a final comment related to stability and position of watertight bulkheads, is that the required amount of watertight bulkheads are the same in the estimation of damaged stability in section 4.4 as for the discussion in section 4.4.4 when the only requirement was to keep the barrier stable after impact. However, the configuration of the local cross section have small influence on the requirement of only remain floating after impact, while for damage stability the configuration of the local cross section have great influence.

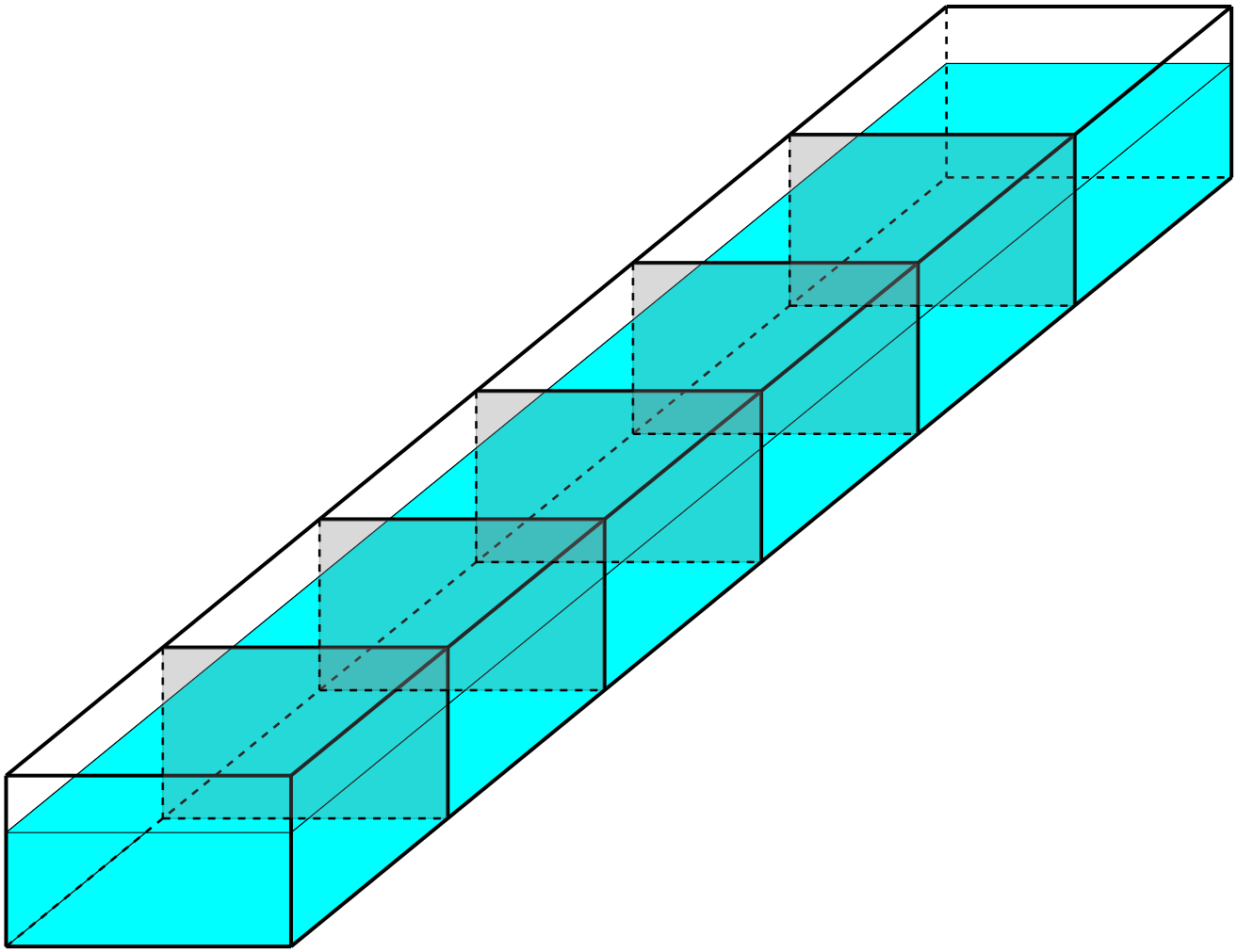

Figure 4.10: Longitudinal position of the watertight transverse bulkheads

5 Finite element theory and modelling

In the first section general theory related to finite element analysis are briefly reviewed. Then nonlinear finite element theory special related to the analysis performed in this thesis with the program LS-DYNA are discussed.

In chapter 4 the various design parameters and the concept have been discussed. A first approach for the geometrical parameters for the ship collision barrier have also been discussed. This chapter summarise how the various models have been modelled in order to perform finite element analysis in the nonlinear finite element program LS-DYNA. The work carried out by Konstali (2014) has been used as a basis and inspiration for the models used in this thesis.

5.1 General about finite element analysis

5.1.1 General

Finite element analysis is a method to solve problems which are too complicated or too time consuming to be solved analytical. The problems are solved in space by utilise discretization of the problem into smaller elements. The three fundamental principles of finite element analysis are:

- Equilibrium
- Kinematic compatibility
- Stress-strain relationship

Any detailed review of finite element formulation will not be conducted in this master thesis. However a short review of the different non-linearities in connection with nonlinear finite element formulation are reviewed in the following subsections. The topics related to finite element which are reviewed in this section are topics related to the particular analyses carried out in this thesis. The theory is mainly reviewed from the LS-DYNA theory manual (Hallquist, 2006). For further information related to nonlinear finite element theory the reference is made to the LS-DYNA theory manual (Hallquist, 2006).

Nonlinear finite element analysis

Compared to linear analysis where the stiffness matrix and the load matrix are independent of the displacement, nonlinear formulation is more comprehensive. For instance due to the non-linearities the stiffness matrix needs to be updated during the analysis and the strains can not be found just by taking the derivative of the displacement. Non-linearity means simply that the displacement can not be assumed to be linearly dependent on the load, which is a governing assumption in linear structural finite element analysis.

It is mainly three classes of non-linearities which is accounted for in connection with nonlinear finite element analysis. References for this subsection is made to Moan (2003).

- Geometry
- Material
- Boundary condition

Geometry non linearity Linear analysis is based on a small displacement assumption and in this region the geometry will hence act linearly since it will not be any redistribution of stresses. While for analysis of a collision event the deformations in region will be severe and large deformations and displacement will occur. Then the stresses will be redistributed and carried by the structure in a different manner. Membrane forces can be introduced through redistribution of stresses. For instance a beam or a shell can then carry load both with membrane forces and bending forces instead of only bending forces. Hence the load bearing capacity of the element will increase. The geometry non linearity have been discussed in chapter 3 for the stiffened plate analysis, and is the effect why the plate will contribute in a larger extent to the total capacity of the stiffened plate compared to the stiffeners.

Material non linearity It means that the material stress-strain relationship is nonlinear. This means that the analysis take into account the hardening area and the plastic region of the stress-strain relationship. An example of a stress-strain curve is for instance given in Figure 2.4.

Material non-linearity is mainly accounted for three rules when account for in a NLFEA.

- **Yield criterion:** States the value for onset of yielding
- **Hardening rule:** Describes how the yield point changes due to accumulation of plastic strain
- **Flow rule:** Relates stresses and strains

Boundary non linearity This non-linearity is related to when a displacement became large and contact occurs. Therefore this kind of non-linearity is also commonly named contact non-linearity. Boundary non-linearity occur in most contact problems where two surfaces come into or out of contact. The displacement and stresses which occur between two contacting bodies are usually not linearly dependent on the applied load and nonlinear effect is hence introduced. In fact boundary non-linearity can occur even if the materials itself are assumed to be linear and the displacements are infinitesimal. The reason is that the size of the contact area is not linearly dependent on the load. If friction is accounted for in the analysis and it gets slick-slip behaviour an additional nonlinear complexity is added which is normally dependent on the loading history. For an illustration of boundary non-linearity see Figure 5.1.

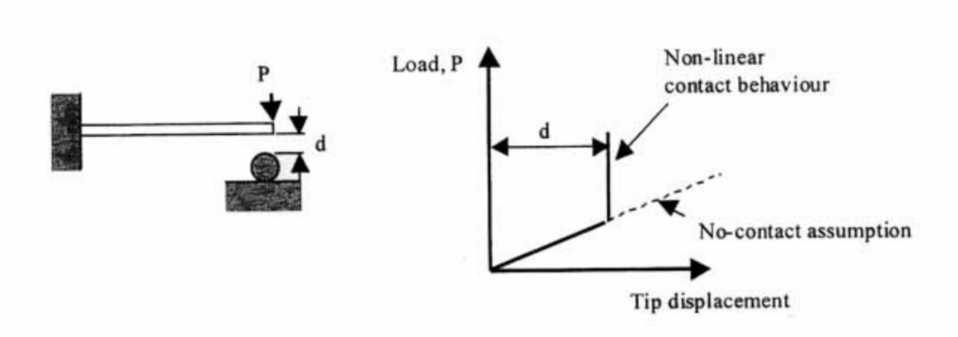

Figure 5.1: Example of boundary non linearity (Moan, 2003)

5.1.2 Solution method

In LS-DYNA the user can choose to solve the problem by either using an implicit or an explicit solver. The analysis carried out in this thesis is done by utilise the explicit solver in LS-DYNA, but a short review of both solvers are included below.

Implicit solver In an implicit finite element formulation the displacement at the new time step are expressed by the velocities and accelerations at the new time step, in addition to the historical information at previous time step. Many of the implicit methods are unconditionally stable, the restriction of time step are only due to requirement of accuracy.

An implicit solver have typically 100 to 10 000 times fewer time steps compared to an explicit solver. A disadvantage is that the cost per time step is unknown since the speed depends mostly on the convergence behaviour of equilibrium which can vary widely between problems.

Explicit solver In an explicit solver the displacement at the new time step, can be obtained by the displacement, velocity and accelerations of the previous time step. Explicit methods

are only stable at very low time step.

One of the main motivations for utilising explicit time integration compared to an implicit time integration is because it is in some cases preferable to avoid inverting of the stiffness matrix. The reason is that inverting of matrices will be cost and time consuming for large finite element models, such as for instances collision events.

Since the explicit solver is only conditional stable and require small time step to be stable, LS-DYNA have implemented stability criterion with respect to the size of the time step. The equations given below are valid for shell elements in LS-DYNA, criterion for other element is included LS-DYNA theory manual (Hallquist, 2006).

Minimum time step size:

$$\Delta t_e = \frac{L_s}{c} \tag{5.1}$$

Where:

Δt_e: Time step

L_s: Characteristic element length

c: Acoustic wave speed

Time integration

The analyses performed by LS-DYNA are solved in time. The calculations cycle for time integration in LS-DYNA, which are running through for each time step is shown in Figure 5.2.

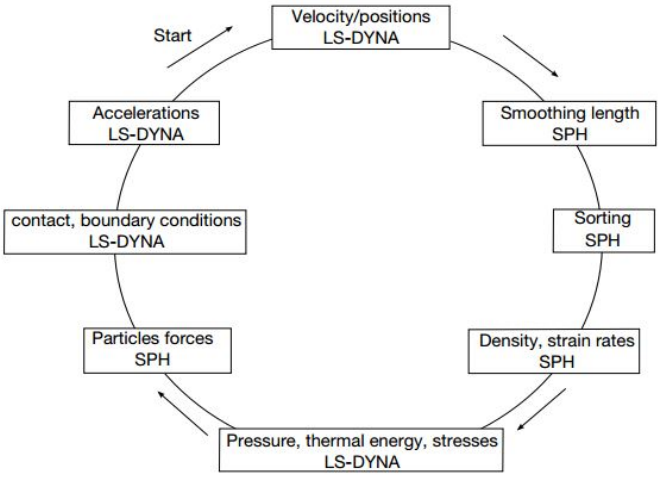

Figure 5.2: The calculation cycle for time integration in LS-DYNA (Hallquist, 2006)

5.1.3 Elements

Three different elements formulation are applied to the finite element model in this thesis. Two different beam formulation and one shell formulation. The element formulations for the beam are of minor importance for the total structure and will hence have a small influence on the energy and force distribution in the total structure. Those two element formulations will only shortly be mentioned in this section. The element formulation used for the most of the structure Belytschco-Lin-Tsay shell elements will be reviewed in some more detail. For further detail related to all element formulations which could be utilised in LS-DYNA, references are made to the LS-DYNA theory manual (Hallquist, 2006).

Beam elements

There are used two kind of beam elements to represent a few elements in the bow model.

The formulations used are Belytschko-Schwer tubular beam with cross section integration for the tubular beams, and Belytschko-Schwer resultant beam for the square hollow profiles.

Shell elements, Belytschco-Lin-Tsay

The major part of the total model is built up by this element formulation. All the shells for both the bow and the barrier model utilise this shell formulation.

The Belytschko-Lin-Tsay shell formulation is the default choice for shells in LS-DYNA. The reason is due to the computationally efficiency compared to other shell formulations as for instances Hughes-Liu shell elements which was the default choice of shell elements in an earlier version of LS-DYNA. An example of how efficient the Beltschko-Lin Tsay is compared to the Hughes-Liu elements for a shell element with five through thickness integration points is given in LS-DYNA theory manual (Hallquist, 2006). The Belytschko-Lin-Tsay requires 725 mathematical operations, while the under integrated Hughes-Liu element require 4050 operations and the selective reduced integration formulation of the explicit Hughes-Liu element requires 35 350 mathematical operations. The Belytschko-Lin-Tsay is well known for its accuracy in the class of mean quadrature elements, but the elements loose accuracy when the elements are subjected to warping distortion. To retain the accuracy the element formulation needs then to be modified and the computational efficiency compared to other formulations is then decreased.

Belytschko-Lin-Tsay shell elements uses discrete Mindlin shell theory to describing displacements and rotations. The displacements and rotations are utilised to find the stress and strains. The element formulation is a so called C^0 class element, (the 0 in C^0 is related to

how many times the the derivative of the interpolation polynomials of the element have to be defined in order to satisfy the fundamental criterion for finite element analysis). In the history of shell elements, the class of C^0 shell elements based on Mindlin theory have become very popular because of its accuracy and efficiency. Thin as well as thick shells are modelled accurately because shear deformation is included. The computational cost are low when simple bilinear shape functions are used.

When the Belytschko-Lin-Tsay shell formulation is used to represent thin shell, the κ parameter which is the shear factor in Mindlin theory is used as a penalty parameter to enforce the Kirchhoff normality condition as the shell becomes thin.

The Belytschko-Lin-Tsay shell element formulations is based on a combined co-rotational and velocity-strain formulation. The efficiency of this element formulation is obtained due to the mathematical simplifications from those two kinematic assumptions.

The co-rotational formulation avoids the complexities of the nonlinear mechanics by embedding a coordinate of the system, see Figure 5.3. An embedded element coordinate system that deform with the element is defined in terms of the four corner nodes of each element. Figure 5.3 shows how the procedure for construction the co-rotational coordinate system. The co-rotational technique in the element formulation is used to treat large rotation. This technique is a method of separating the deformation displacement and the rigid body displacements. Only the deformation displacements give rise to strains and generation of strain energy.

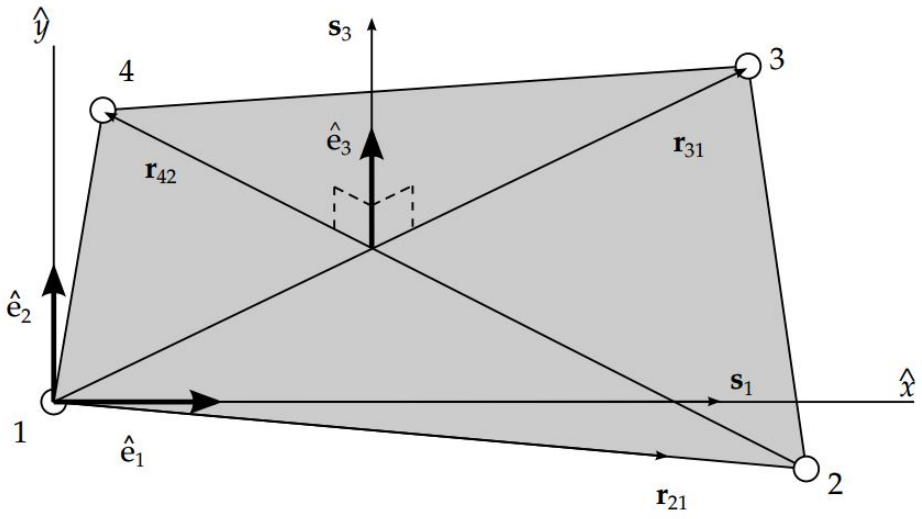

Figure 5.3: Construction of element coordinate system for the co-rotational formulation of Belytschko-Lin-Tsay (Hallquist, 2006)

5.1.4 Material models

The five different material models which are used for the analyses performed by LS-DYNA are shortly described in the following sections. For additional and more detailed information

about each material model, see LS-DYNA theory manual (Hallquist, 2006).

MAT_RIGID

This material model is used for the bow model for the ductility analysis, where only the barrier is allowed to deform. The model are also applied to the rigid wall in the strength design, when the bow is crushed against a rigid wall.

The model is as the name explain a totally rigid model. The density, elasticity module and the poison ratio are given as input in order to account for the sliding effect in the contact interface with the non-rigid elements.

MAT_024 Piecewise Linear Plasticity

For this material model the true stress-strain curve is given as an input file and as the name of the material model indicates the curve will be assumed linear between each points. If the input file includes a large number of points, it will in practical be quite equal to the true stress-strain curve obtained by using a continuous model to establish the material model.

Relevant material parameters such as density, elasticity modulus, poison ration, yield stress are given as input. In addition a simplified failure criterion based on effective plastic failure strain could be applied.

In this thesis this material model was used for the aluminium alloys in the simplified stiffened plate model in chapter 3. The relevant input parameters for this material model was discussed in that chapter and references are made to Table 3.1. This material model have also been discussed in that chapter, chapter 3.

MAT_003 Plastic Kinematic and MAT_028 Resultant Plasticity

Those material models are used for the beams in the bow model. The plastic kinematic model is applied for the tubular beams and the resultant plasticity model is applied for the square hollow beams. Both models are simplified material models, however Konstali (2014) showed that the energy absorbed during an analyse of those two material models were small (about 0.20 MJ) in comparison with the total energy in the collision event. The relevant material properties for those two material models are given in Table 5.1.

Table 5.1: Material properties for MAT_003 Plastic Kinematic and MAT_028 Resultant Plasticity

	MAT_003 Plastic Kinematic	MAT_028 Resultant Plasticity
ρ [kg/m^3]	7 850	7 850
E [MPa]	207 000	207 000
σ_Y [MPA]	275	275
ν Poisson's ratio [-]	0.3	0.3
E_T Tangent E-modulus [MPa]	2 000	2 000
$\epsilon_{failure}$ [-]	0.15	

MAT_046 User Defined Material Model

The last material model considered to describe the material behaviour is a material model implemented in LS-DYNA by Hagbart S. Alsos (Alsos et al., 2009) at the Department of Marine Technology. The model utilise a modified power law equation (Eq. (5.2)) for describing the true stress strain-curve, see Figure 5.6. The beneficial of using this material model compared to for instance the Piecewise Linear Plasticity material model is that this user defined material model includes a more advanced fracture criterion, The RTCL (Rice-Tracy-Cockcroft-Latham) damage criterion. This is in opposite to the built material models in LS-DYNA which base the fracture only on a strain criterion.

$$\sigma_{eq} = \begin{cases} \sigma_Y & \text{if } \epsilon_{eq} \leq \epsilon_{plate} \\ K_{pow} \cdot (\epsilon_{eq} + \epsilon_0)^{n_{pow}} & \text{Otherwise} \end{cases} \tag{5.2}$$

Where:

K: Power law constant [Pa]

n_{pow}: Power law exponent [-]

σ_Y: Yield stress [Pa]

ϵ_{eq}: Equivalent strain [-]

ϵ_0: Strain parameter which which allows the plateau and power law expression to intersect [-]

ϵ_{plat}: Equivalent plastic strain at strain plateau exist [-]

$$\epsilon_0 = (\frac{\sigma_Y}{K})^{\frac{1}{n_{pow}}} - \epsilon_{plat} \tag{5.3}$$

In additional to an advanced fracture criterion this material model also applies mesh scaling. The reason to apply mesh scaling is because it is impossible to have small enough element to obtain an accurate representation of the element fracture and necking zone large finite element models. This because the computational cost will be too large. For a large finite element model the mesh size will typical be 5 – 10 times the shell thickness and such mesh size will be too large in order to detect local instabilities. Therefore as a remedy for problems related to local instabilities mesh scaling of the rupture criterion is applied in this user defined material model. For further review of the theory behind the RTCL fracture criterion and the mesh scaling technique applied for this material mode references is made to section 5.1.5.

As a comment to this material model; it is developed with respect to steel material, so the use of this material model in connection with aluminium alloys should be questionable. The main reason is that aluminium alloys does not have the same behaviour as steel with respect to failure. Research have shown that aluminium alloys mostly fails in a different manner than structure made up by construction steel.

Steel The input parameters for the steel model are given in Table 5.2. The steel material applied in this thesis are standard values for mild steel given by the European steel grade s235 and also taken according to the article (Alsos et al., 2009). The steel material is applied for the shell elements in the bow model.

Table 5.2: Material properties for steel using MAT_046 User Defined Material Model

ρ $[kg/m^3]$	7 850
E [MPa]	207 000
σ_Y [MPA]	275
ν Poisson's ratio	0.3
Bulk modulus B [MPa]	172 500
Shear modulus G [MPa]	79 615
Power law strength coefficient K [MPA]	740
Power law exponent n_{pow}	0.24
Equivalent plastic strain at strain plateau exit ϵ_{plat}	0.01
Critical strain ϵ_{crit}	0.71

Aluminium The input parameters for the different aluminium alloys are given in table 5.3. The parameters for the different aluminium alloys are primarily taken according to Eurocode 9: Part 1-1 (2007).

The reason why it was desired to use the user defined material model to describe the aluminium alloys was as already mentioned that this model utilises mesh scaling and that a fracture criterion based on RTCL was implemented. To be able to apply this material model for the aluminium alloys an assumption that the aluminium will fail in a similar way as a steel structure have been assumed. This however are from the authors knowledge not necessary

correct. Some reasons are that the aluminium alloys commonly have no yield plateau and that it may fails in yielding before the total cross section have reach yield. In spite of this uncertainties it was decided to apply this material model for the aluminium alloy. This because the user defined material model were the most correct material model available upon the work with this thesis. However, care should be conducted when investigating the results from the analysis where this material model is applied for the aluminium alloys.

The user defined material model utilise a modified power law expression, the relevant input parameters for this model could not be picked directly from Eurocode 9: Part 1-1 (2007). Therefore some calculations and fittings of curves were needed in order to describe the true stress-strain curve by the power law expression. An example of the modified power law expression is shown in Figure 5.6 for mild steel. The procedure to rewrite the true stress-strain curve from a Ramberg-Osgood curve to a power law expression are discussed in the following paragraph.

The Ramberg-Osgood equation is a continuous true stress-strain relation where the strain are given as a function of the stress, see equation (3.1) and Figure 3.2. For a stress-strain curve given by the modified power law expression, see equation (5.2), the stress is given as a function of the strain. See Figure 5.6 for an illustration of the modified power law stress-strain curve.

The stress-strain curve obtained from Ramberg-Osgood and the power law expression looks quite similar if the parameters in the power law expression is fitted to the Ramberg-Osgood curve. However, it is still some main difference between the two stress strain curves. For the Ramberg-Osgood formulation the contribution from the plastic zone is assumed to contribute to the stress-strain curve from zero strain and stress since the curve is a continuous function. The plastic contribution is according to the second term in equation (3.1), but the exponent n is chosen so the contribution is small in the range where the material normally is assumed to be linearly elastic. The modified power law formulation as shown in equation (5.2) assumes that the curves following a linear elastic behaviour in the range bellow a given equivalent stress. The plastic contribution starts to act after stress have reach the given equivalent stress, and eventually after it has reach a given strain which characterises th end of the yield plateau. For an illustration of a power law curve references is made to Figure 5.6.

Due to the differences between the Ramberg-Osgood equation and the power law expression as have been described above it was necessary to do some assumption and regression in order to establish the necessary power law parameters. A further discussion follows.

The first assumption made is that aluminium alloys are assumed to not have a strain plateau. It is also applied that yielding occur when the stress reach the yield stress. The transition from the elastic range to the plastic range are assumed to be at the strain level where the equivalent

strain are equal to the yield strain:

$$\epsilon_{eq} = \epsilon_Y = \frac{E}{\sigma_Y} \tag{5.4}$$

The power law stress-strain curve is then assumed to be written on the following form:

$$\sigma(\epsilon) = \begin{cases} E \cdot \epsilon & \text{for } \epsilon \leq \epsilon_Y \\ K_{pow} \cdot \epsilon^{n_{pow}} & \text{for } \epsilon > \epsilon_Y \end{cases} \tag{5.5}$$

Rewriting the equation be a function of the stress:

$$\epsilon(\sigma) = \begin{cases} \frac{\sigma}{E} & \text{for } \sigma \leq \sigma_Y \\ (\frac{\sigma}{K})^{(\frac{1}{n_{pow}})} & \text{for } \sigma > \sigma_Y \end{cases} \tag{5.6}$$

Using the Ramberg-Osgood curve on the form according to equation (3.1) which is reprinted bellow:

$$\epsilon(\sigma) = \frac{\sigma}{E} + 0.002 \cdot \left(\frac{\sigma}{\sigma_Y}\right)^n \tag{5.7}$$

The plastic contribution in the Ramberg-Osgood curve acts from stress equal to zero, but with a small amount. Therefore it sounds as a reasonable assumption to split the Ramberg-Osgood equation into a combined equation in order to get it on a similar form as the modified power law expression in equation (5.2). The divided Ramberg-Osgood equation is given bellow:

$$\epsilon(\sigma) = \begin{cases} \frac{\sigma}{E} & \text{for } \sigma \leq \sigma_Y \\ 0.002 \cdot (\frac{\sigma}{\sigma_Y})^n & \text{for } \sigma > \sigma_Y \end{cases} \tag{5.8}$$

The parameters in the power law expression, n_{pow} and K, could then be estimated with approximated values from comparison of equation (5.6) and equation (5.8). From the two stress-strain formulations, there are clearly shown that they both are assumed to have the same form in the elastic region. Therefore the parameters for the power law expression is done with respect to the curves behaviour in the plastic region. The deduction of n_{pow} and K follows.

$$0.002 \cdot \left(\frac{\sigma}{\sigma_Y}\right)^n = \left(\frac{\sigma}{K}\right)^{(\frac{1}{n_{pow}})} \tag{5.9}$$

Which could be written:

$$\left(\frac{0.002^{(\frac{1}{n})} \cdot \sigma}{\sigma_Y}\right)^n = \left(\frac{\sigma}{K}\right)^{(\frac{1}{npow})} \tag{5.10}$$

By further investigate this equilibrium equation, both the two unknown parameter, K and n_{pow}, in the modified power law equation could be estimated as a function of the Ramberg-Osgood parameter, n, and the known yield stress, σ_Y, of the material.

$$\frac{1}{n_{pow}} = n \Rightarrow n_{pow} = \frac{1}{n} \tag{5.11}$$

And,

$$\frac{1}{K} = \frac{0.002^{(\frac{1}{n})}}{\sigma_Y} \Rightarrow K = \frac{\sigma_Y}{0.002^{(\frac{1}{n})}} \tag{5.12}$$

Where:

ϵ_{eq}: Equivalent strain

ϵ_Y: Yield strain

E: Elasticity modulus

ϵ: Strain

K_{pow}: Power law constant

n_{pow}: Power law exponent

σ: Stress

σ_Y: Yield stress

n: Ramberg-osgood exponent

The resultant power law parameters together with the rest of the material parameters used to describe the user defined material model discussed in this section are given in Table 5.3.

A comparison of the true stress-strain curve drawn from the Ramberg-Osgood equation and the curve drawn according to the modified power law equation (equation (5.5)) with the power law parameters estimated in this section are shown in Figure 5.4 and Figure 5.5 for respectively the aluminium alloy 5083 and alloy 6082.

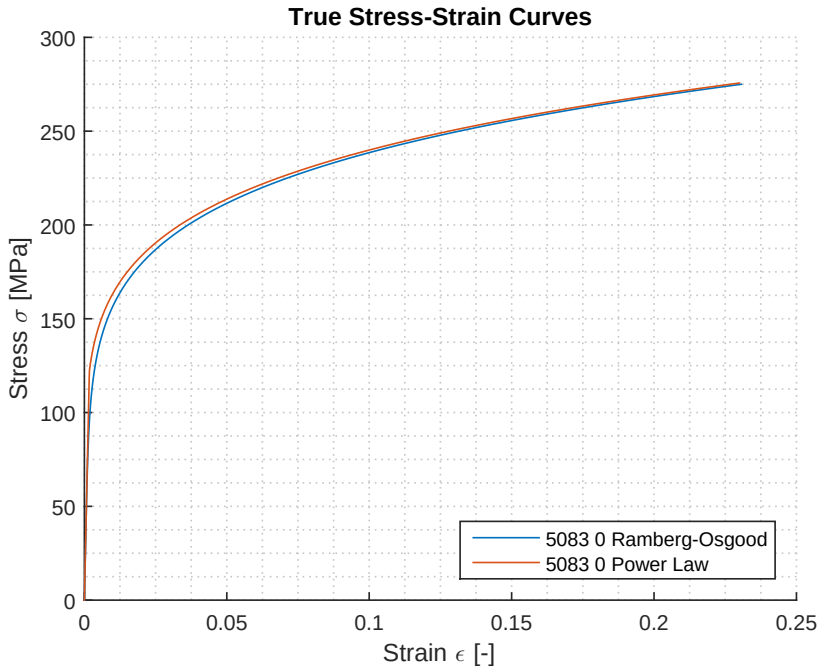

Figure 5.4: Comparison of the stress-strain curve obtained from Ramberg-Osgood equation and from the modified power law expression used for the user defined material model for aluminium alloy 5083-O

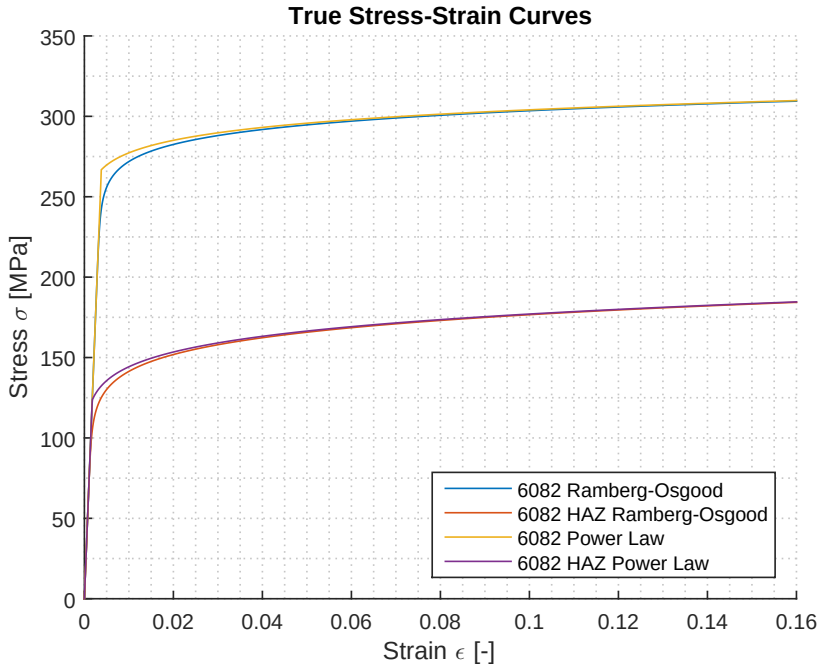

Figure 5.5: Comparison of the stress strain curve obtained from Ramberg-Osgood equation and from the modified power law expression used for the user defined material model for aluminium alloy 6082-T6

By investigating Figure 5.4 and Figure 5.5 it is seen that the curves based on Ramberg-Osgood

equation (equation (3.1)) and the power law equation drawn according to equation (5.5) looks quite similar. The hardening area of the Ramberg-Osgood curve starts at a lower stress level, the reason is as stated above that to estimate the power law parameter the Ramberg-Osgood equation have been split into two equations and that the hardening phase of this curve first act after the elastic region. Therefore the plastic contribution before the material reach yielding which applies for the Ramberg-Osgood curve has been disregarded when establishing the power law parameters. Another differences between the curve from Ramberg-Osgood equation and the power law equation is according to the difference discussed above, the area below the curves are larger when the power law equation is applied. Therefore the energy dissipated are slightly larger when applying the modified power law expression.

Table 5.3: Material properties for aluminium using MAT_046 User Defined Material Model

	5083-O	6082-T6 base	6082-T6 HAZ	Global material model
ρ $[kg/m^3]$	2 700	2700	2 700	68 780
E [MPa]	70 000	70 000	70 000	70 000
σ_Y [MPA]	125	260	125	125
ν Poisson's ratio	0.33	0.33	0.33	0.33
Bulk modulus B [MPa]	68 627	68 627	68 627	68 627
Shear modulus G [MPa]	26 315	26 315	26 315	26 315
Power law coefficient K [MPA]	352	330	217	352
Power law exponent n_{pow}	0.1667	0.04	0.24	0.1667
Strain plateau exit $\epsilon_{plat} = \epsilon_Y$	0.00178	0.00371	0.00178	0.00178
Critical strain ϵ_{crit}	0.23	0.16	0.16	0.23

The aluminium alloys have been assumed to be homogeneous isotropic linearly elastic material, even that this not always is the case for aluminium alloys. This assumption is in accordance with use of the user defined material model which originally used and developed for mild steel. By using this assumption the shear and bulk modulus could be calculated by the following equations.

Shear modulus:

$$E = \frac{E}{2 \cdot (1 + \nu)} \tag{5.13}$$

Bulk modulus:

$$B = K = \frac{E}{3 \cdot (1 - 2 \cdot \nu)} \tag{5.14}$$

5.1.5 Fracture model and mesh scaling, user defined material model

In chapter 3 the fracture criterion applied for the stiffened plate was a simple criterion based on effective equivalent strain. Such a simple fracture criterion will for instances not cover failure in compression. Therefore in order to obtain a more realistic representation of the fracture it is preferable to apply a more advanced fracture criterion. Such criterion could for instance the Rice-Tracy-Cockcroft-Latham damage criterion (RTCL) or the Bressan-William-Hill instability criterion (BWH). For the user defined material model applied for the shell elements it is the RTCL damage criterion which is implemented. This criterion will briefly be covered in the next section.

To account for for local instabilities in finite element analysis the mesh size should not exceed two times the plate thickness. Such small element size is unpractical for large models. Therefore the user defined material model includes a mesh scaling to account for local necking. How this is accounted for is described below.

The RTCL damage criterion

The RTCL damage criterion is composed of the modified Cockcroft-Latham-Oh damage criterion and the Rice-Tracey damage criterion. Both criterion are a function of the hydrostatic stress state and expressed by the stress triaxiality, see equation (5.15).

$$T = \frac{\sigma_m}{\sigma_{eq}} \tag{5.15}$$

Where:

T: Stress triaxiality

σ_m: Hydrostatic stress

σ_{eq}: Equivalent stress

The value calculated from equation (5.15), gives what type of failure that is governing for the structure.

$T < -\frac{1}{3}$: Cut-off value, fracture will not occur

$-\frac{1}{3} < T < \frac{1}{3}$: Damage evolution in the shear domain and represented by the Cockcroft-Latham-Oh damage criterion

Otherwise, $T > \frac{1}{3}$: Void growth domain, calculated according to Rice and Tracey damage criterion

Based on a combination of the statements above, the damage criterion applied for the user defined material model (Alsos et al., 2009) may the be expressed mathematically by the evolution rule:

$$\dot{D} = \begin{cases} 0 & \text{if } T < -\frac{1}{3} \\ \frac{\sigma_1}{\sigma_{eq}} \cdot \dot{\epsilon}_{eq} & \text{if } -\frac{1}{3} < T < \frac{1}{3} \\ \exp(\frac{3 \cdot T - 1}{2}) \cdot \dot{\epsilon}_{eq} & \text{Otherwise} \end{cases} \tag{5.16}$$

Where:

$\dot{D}$: Rate of damage

σ_1: Major principal stress

$\dot{\epsilon}_{eq}$: Rate of the equivalent plastic strain

The criterion is stated such a way that fracture is initiated once the accumulated damage reaches a critical level ($D > D_{cr}$). An important feature of the RTCL damage criterion is relating to how to determine the critical damage. For proportional loading in uniaxial tension (T=0.33), the damage evolution $\dot{D}$ is exactly matched by the rate of equivalent plastic strain $\dot{\epsilon}_{eq}$. Then the critical damage D_{cr} can easily be found from a uniaxial tensile test. From this statements a normalised damage criterion can be found, see equation (5.17).

$$D = \frac{1}{\epsilon_{cr}} \cdot \int \dot{D} \cdot dt \tag{5.17}$$

In the article (Alsos et al., 2009), the RTCL criterion applied for shell elements. The shell elements utilises a two-dimensional process, while in reality void growth is a three-dimensional process. Therefore the through thickness crack growth is described by reducing the resistance and stiffness in each through thickness integration point. When the the damage D is larger than the critical damage D_{cr} in all through thickness integration points, then the elements are removed.

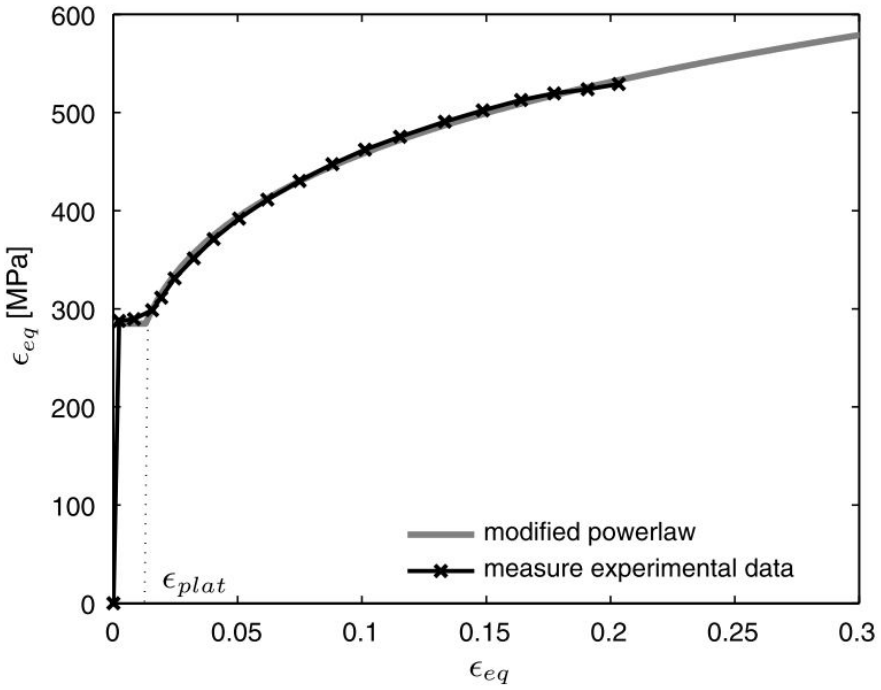

Figure 5.6: Comparison of experimental true stress-strain curve and a stress-strain curve obtained from the modified power law expression, the comparison is performed for mild steel (EN 10025 S275) (Alsos et al., 2008)

Influence of elements size, mesh scaling

One of the major concerns related to finite element analysis is related to mesh sensitivity. Specially the mesh sensitivity close to fracture, this means in zones with large strains; close to crack tips, structural joints and welds, in post necking zones. Shell elements have a plane stress formulation and is therefore especially sensitive to this effect. In solid elements the through thickness stress is stabilized by neighbouring elements. While shell elements have only one element through the thickness and the straining in thickness direction in a narrow band close to the failure can be excessively. This effect is especially a concern when small elements are applied. For large elements the concern is rather related to that the strain concentration may not be captured.

If small elements are used relative to the shell thickness, non-local methods may be applied and give reasonable results. However such methods makes only sense when the elements are smaller than the shell thickness. For analysis related to ship collision the element length is typical in the range of 5-15 times the shell thickness.

In the material model implemented in LS-DYNA by Hagbart S. Alsos Alsos et al. (2009), it is utilised a engineering correction derived by considering a deformed material element, see Figure 5.7. V_n represent the volume of the neck and V_r is the volume of the element outside the necking area. The total volume of the element is the sum of V_n and V_r and is denoted V_{el}.

The average strain ϵ_{cr} in Figure 5.7 can then be calculated by using volume weighting average strain by applying the known volumes and the corresponding strains ϵ_n and ϵ_r, see equation (5.18). Equation (5.18) is only valid for shell elements and is referring to the elements initial configurations.

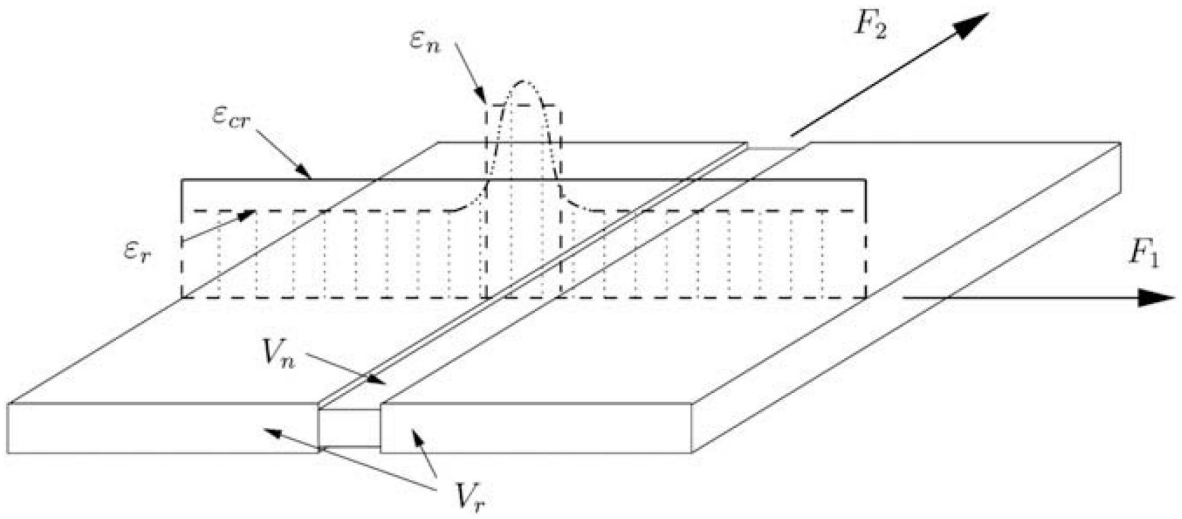

Figure 5.7: Volume averaged strain when necking has occurred (Alsos et al., 2009)

$$\epsilon_{cr} = \frac{\epsilon_r \cdot V_r + \epsilon_n \cdot V_n}{V_{el}} \tag{5.18}$$

The volumes included in equation (5.18) is given by the following equations.

$$V_n = t^2 \cdot l_e \tag{5.19}$$

$$V_{el} = t \cdot l_e^2 \tag{5.20}$$

$$V_r = V_{el} - V_n = t \cdot l_e^2 - t^2 \cdot l_e \tag{5.21}$$

By further substituting those three equations into equation (5.18).

$$\epsilon_{cr}(l_e) = \epsilon_r + (\epsilon_n - \epsilon_r) \cdot \frac{t}{l_e} \tag{5.22}$$

An uniaxial tensile test can be used to calibrate the failure criterion and hence also the user define material model. Equation (5.22) can by this assumption be simplified further. When the element length, l_e goes to infinite ($l_e = \infty$), then $\epsilon_c r = \epsilon_r$. If then assuming that a power law material model will be used, see equation (5.2), then the ϵ_r becomes equal to the power law exponent, n. Correspondingly $\epsilon_{cr} = \epsilon_n$ when $l_e = t$ and this value can be determined from numerical reproduction of uniaxial tensile tests. The equation (5.22) can then be rewritten as equation (5.23). Equation (5.23) is referred to as a "fracture scaling law" and may be applied to calibration of the RTCl criterion and for calibration of equivalent strain criterion.

$$\epsilon_{cr}(l_e) = n + (\epsilon_n - n) \cdot \frac{t}{l_e} \tag{5.23}$$

As a concluding remark related to the influence on elements size for NFEA, equation (5.23) should be used with caution. The reason is that it could be dangerous to correct the failure criterion as a function of the element size. This since the local deformation mechanism could possibly take part before fracture.

5.1.6 Contact modelling in LS-DYNA

Two different contact definitions are used for the ship barrier collision events. Automatic Single Surface contact are used to account for self-contact in the ship and the barrier respectively. The other contact definitions applied is Automatic Surface to Surface contact. This contact definitions account for contact between the ship and the barrier.

The automatic contact definitions are the most commonly used contact models in LS-DYNA. This definition is penalty based, which means that LS-DYNA search for slave nodes penetrating master segments at each time step. If a penetration is detected, a force proportional to the penetration depth is added and pushing the element back and eventually eliminate the penetration. The beneficial to use a contact method utilising a penalty based contact model is great in contrast to a constraint method. The reason is that the penalty method approach is found to excite little if any mesh hourglassing (Hallquist, 2006).

5.2 Modelling

The modelling process for each model is divided into several steps. First the geometry, meshing and section properties are created by MSC. Patran 2012, which is a pre-processor. Secondly the material properties, boundary conditions, contact properties etc. were added in the pre-processor LS-PrePost. Then the analysis is run by the NLFEA-solver LS-DYNA. The results is further investigated and post processed in the post-processor LS-PrePost.

In principal the whole pre-processing could be performed in LS-PrePost, but Patran is a stronger pre-processor and therefore allowing for significant better control with respect to modelling and meshing. As have already been mentioned in earlier chapter are finite element analysis extremely mesh sensitive and a strong pre-processor is therefore preferable in order to ensure a good representation of the physical problem. The reason why the aforementioned programs are utilised compared to other competing programs, is because those programs is commonly used at NTNU.

Matlab have been applied to creating journal files which could be read by Patran to create the models. This means that Patran has only been applied to read an input file created with Matlab.

It is the case 4 in Figure 4.5 which is considered for the models. This is the cross section consisting of two internal decks and two internal vertical bulkheads.

5.2.1 Ship

The ship model used in this thesis is the same model as applied by Konstali (2014). The model was provided for Konstali (2014) upon the start of his master thesis. The model was slightly modified by Konstali in order to fit to the nonlinear finite element program LS-DYNA. This section contains information about this bow model. For further details regarding the bow model reference is made to Konstali (2014).

The design ship parameters are given in Table 4.1. Approximately values for the bow model utilised in this thesis are given in Table 5.4. From this table it is clearly shown that the bow model represent a smaller ship compared to the design ship with respect to displacement and draft, but the remaining parameters are approximately equal to the design ship. Therefore it sounds reasonable to assume that the bow model will give a decent representation of the strength of the bow strength in the actual design ship. The bow model was originally made by Frank Klæbo at Marintek for a study performed some years back. The drawings provided in conjunction with that project is confidential and the exact dimension could therefore not be reproduced, but as already mentioned the dimension is approximately as given in Table 5.4.

Table 5.4: Approximate dimensions of the ship used for the bow model (Konstali, 2014)

Length [m]	195
Breadth [m]	25
Displacement [metric ton]	11000
GT	24000
Speed [knots]	17
Draught [m]	5.5

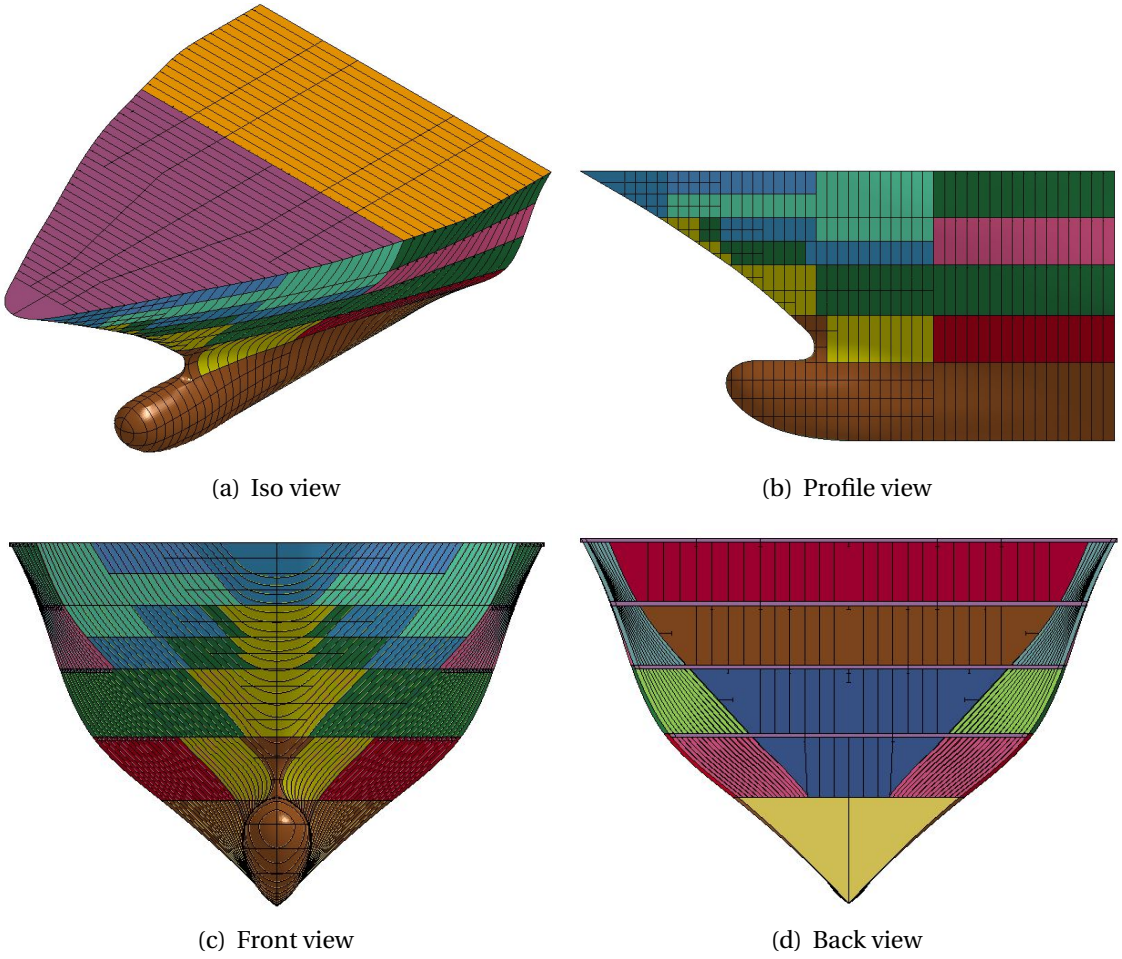

(a) Iso view (b) Profile view

(c) Front view (d) Back view

Figure 5.8: Bow model shown with different views (a)

Figure 5.8 shows the general arrangement of the bow model. The bow model is detailed modelled in front of the collision bulkhead, which is placed at the transition between the yellow and blue colour in Figure 5.8 d). The part astern for the collision bulkhead is made in a simplified manner. The purpose of modelling the area astern for the collision bulkhead is mainly related to the boundary condition. It is preferable to apply the boundary condition away from the area which undergo large deformations. This way of modelling the bow model is a reasonable representation since the ship astern for the collision bulkhead is not allowed to undergo significant deformations in order to keep the ship intact and floating after a collision.

More concrete on the dimensions used in the bow model. The stiffener spacing in front of the collision bulkhead is 610 mm and astern of the bulkhead the spacing are 650 mm. The thickness of different elements ranging from 14.5 mm at the bulbous bow to 7 mm at the aft part of the top deck. The colours in Figure 5.8 represents element with different thickness. The bulbous stiffener which was original utilised in the bow model were not compatible with LS-DYNA and therefore converted to L-stiffeners for most of the stiffeners and to flatirons for the smallest one by Konstali (2014). The way this was handled for the L-stiffeners was to keep the web height constant and converting the bulbous part into a flange. The cross section area is hence remained constant and also the bending stiffness is ensured to be approximately constant. For the flatirons the bulbous part where smeared out to the web in order to keep the cross section area constant. See Figure 5.9.

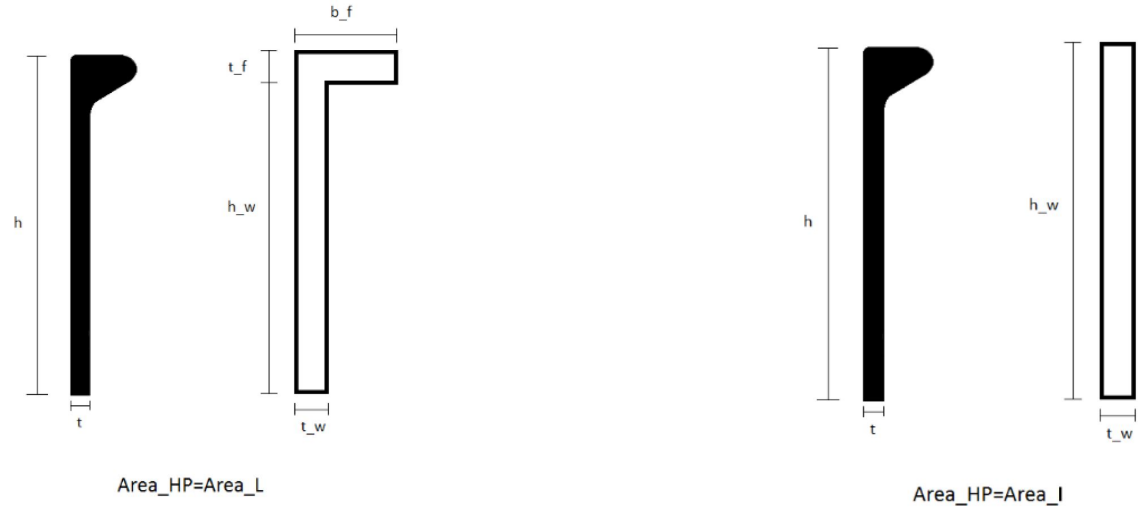

Figure 5.9: Converting of bulbous stiffeners (Konstali, 2014)

The real bow includes several cutouts/manholes, see Figure 5.10. To account for this manholes the the plate thickness was reduced, such that the correct volume is being deformed. This is the common way to treat cutouts in large finite element models. By applying this simplification the globally absorbed energy will be represented correct according to Minorsky rule of simplifications, but the local effect for instance large stress concentration around the cutouts will not be captured. However, for such large models the mesh are relatively course with respect to local effects. Therefore local effects such as stress concentrations will not have been covered even if the cutouts where modelled in detail. By the aforementioned statements it is clear that the error introduced when modelling cutouts by reducing the plate thickness will be limited.

The bow model is mostly built up by Belytschko-Lin-Tsay shell elements, but in addition 17 beams in the upper decks of the bow model are introduced. The bow model is mainly meshed by four-node shell elements, but three-node shell elements are used where one edge has more

or fewer elements seeded than its opposite edge. The seed value for the element length is 120 mm. A commonly used rule of thumb is that the element length should not exceed 5-10 times the element thickness in order to give a good physical representation of the plate folding. The thinnest elements are as stated 7 mm, may therefore a seed value of 120 mm be too course mesh. However, for most of the elements the element length will be within the range of 5-10 times the thickness. It is also stated that it should be at least three integration point over the thickness, this to ensure that the shell elements are able to represent curvature. For this particular ship bow five integration points through the thickness is applied. For further details regarding the bow model references is done to Konstali (2014).

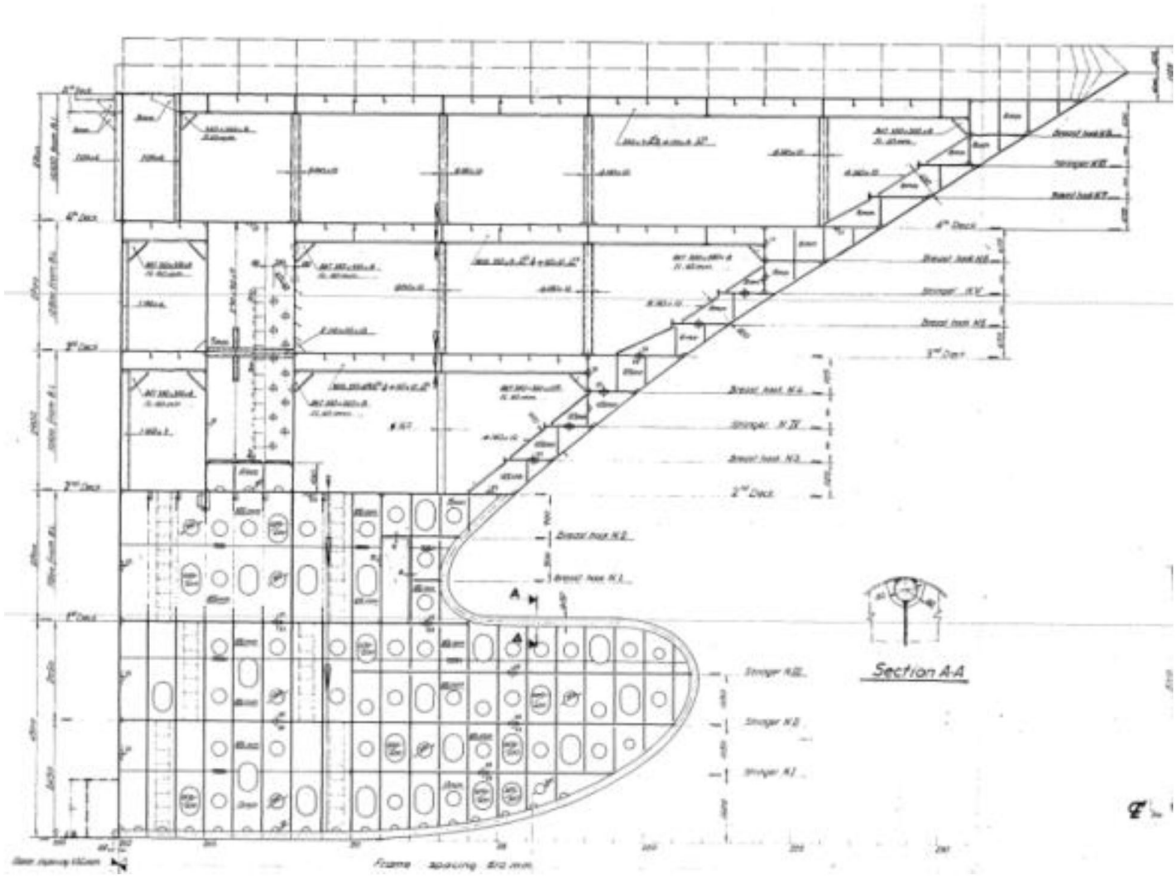

Figure 5.10: Bow model (Konstali, 2014)

5.2.2 Barrier Design

The barrier design is split into two pieces, a global design and a local design. The purpose are to have a detailed modelled cross section in the region where the bow impacts the barrier and to have a courser simplified cross section in the rest of the barrier. The properties of the simplified cross section should be the same or close to the same regarding strength and other cross section properties as for he detailed local model. The reason why not have a detailed modelled cross section along the whole barrier is due to computation demanding. It is only

in a region close to the impact position where the barrier undergoes large deformations and that the rest of the barrier length is mainly interesting with respect to the global behaviour. Therefore it will probably be satisfying to apply a courser cross section and mesh for the structural part away from the impact position. The transition from the local to the global model should be performed carefully in order to ensure that forces, stresses and deformations will be distributed in a correct way between the local to the global model.

Local Barrier Design

This barrier model is a detailed modelled cross section, where all structural members have been included; decks, vertical and transverse bulkheads and stiffeners on all the bulkheads, see Figure 5.11. The model is based on the discussion performed in section 4.2.2.

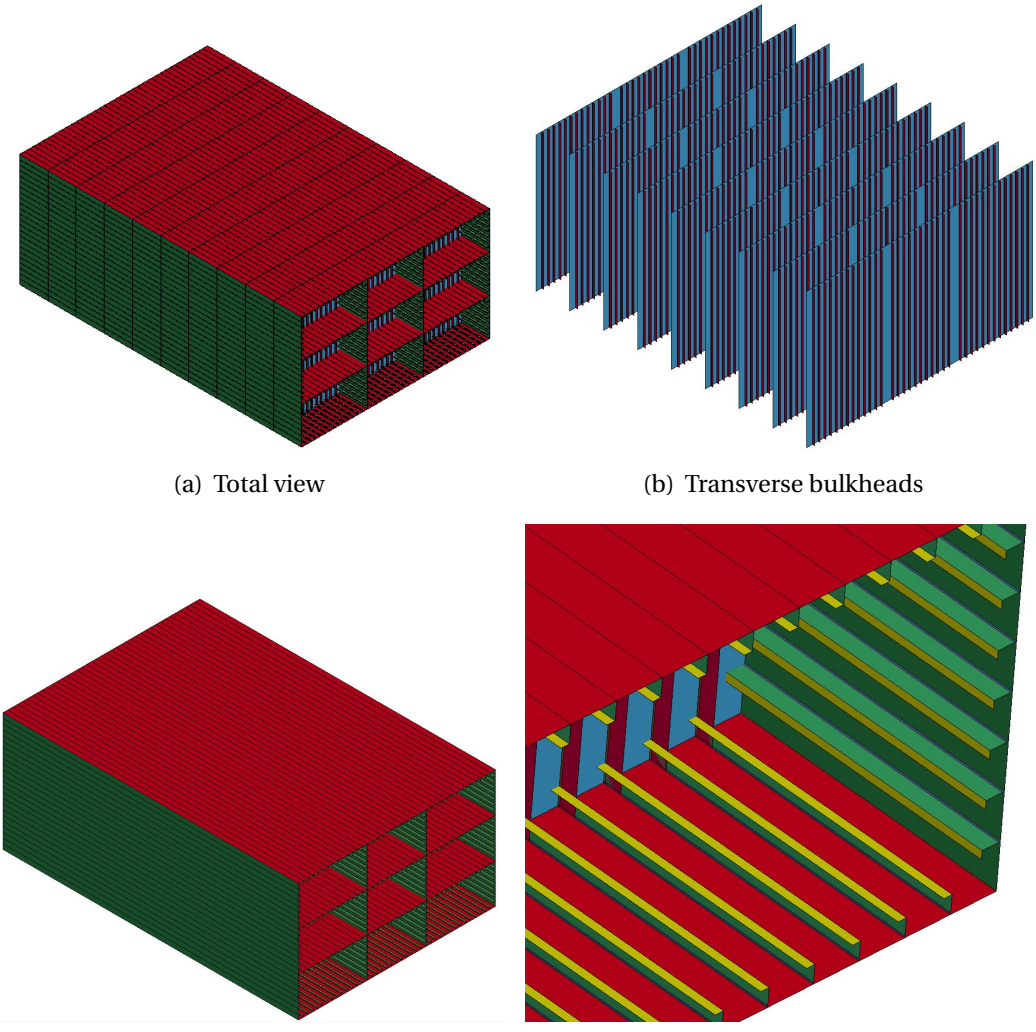

(a) Total view

(b) Transverse bulkheads

(c) Vertical bulkheads and decks

(d) Detailed stiffener view

Figure 5.11: Local barrier design, total view (a) transverse bulkheads with stiffeners (b), vertical bulkheads and decks with stiffeners (c), detailed view of a corner (d)

All dimensions and relevant parameters are given in Table 5.5. All stiffeners are applied with a spacing of $500mm$. It is applied flatiron at the transverse bulkheads in order to counteract buckling of those bulkheads, see Figure 5.11(b). The dimension of the flatirons applied are $200 \times 10mm$. Both the decks and the vertical bulkheads have the same kind of stiffeners and similar stiffener dimensions. It is used L-stiffeners with dimension $200 \times 90 \times 11.5 \times 15mm$.

The stiffener web was originally modelled with a region equal to $20mm$ close to the plate flange, the reason was to be able to apply a different material in this region in order to account for HAZ, see Figure 5.12. However, at a later state as will be discussed further in chapter 8 it was decided to omit the $20mm$ wide HAZ region. The reason was that the element in HAZ was governing with respect to the critical time step, since those elements were the smallest element in the ship collision barrier.

The mesh applied for the local model are a constant square mesh for the whole model with dimension $100 \times 100mm$, but in areas close to joints and element ends some element are smaller in order to fit to the dimensions. As have been mentioned before it is recommended to apply a mesh in the range of 5-10 times the thickness as a rule of thumb. For this particular local model the decided mesh size implies a mesh equal to 10 times the thickness for the thinnest part, the flatirons ($10mmm$), and about 6.7 times the thickness for the thickest parts, stiffener flange, decks and vertical and transverse bulkheads ($15mm$).

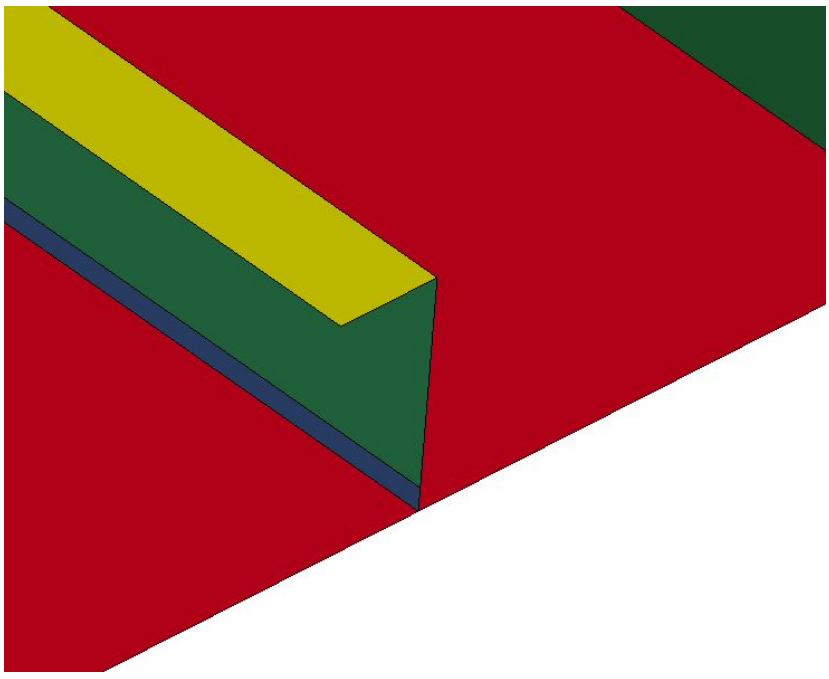

Figure 5.12: The Figure shows the modelling of stiffeners in the local model, the blue region is equal to $20mm$ height and represent the HAZ region

Table 5.5: Model input for the local detailed model

Length of local model [m]	30
Breadth [m]	20
Height [m]	12
Number of decks n_{hb}	4
Number of vertical bulkheads n_{vb}	4
Spacing of transverse bulkheads $[mm]$	3 000
Thickness of decks t_{hb} $[mm]$	15
Thickness of vertical bulkheads t_{vb} $[mm]$	15
Thickness of transverse bulkheads t_{tb} $[mm]$	15
Stiffener spacing for all stiffeners $[mm]$	500
Flatirons stiffener dimension $[mm]$	200×10
L-stiffeners dimension $[mm]$	$200 \times 90 \times 11.5 \times 15$
Height of HAZ region in the stiffener web $[mm]$	20

In order to account for inertia forces due to ballast and hydrodynamic added mass the density of the material are artificial increased as will be discussed in section 5.2.5. However, the local cross section discussed in this section is not accounted for inertia forces. The reason is to not get any spurious contact forces, which could happen if the density of the material is artificial increased.

Global Barrier Design

If the whole barrier were modelled as detailed as the local model, the nonlinear finite element model had been large and the computational time would then had been unreasonable long. A first simplification could be to reduce the mesh size outside the impact region, but even then the model would be large and the required computation resources will still be severe. Therefore there have been decided to perform additional simplifications to the model. Such simplification needs to be done with caution. It should therefore be verified that the results obtained are reasonable and physical. The error introduced should be verified and be limited. How the simplified cross section have been created will be discussed below.

Konstali (2014) made some experience when modelling the global barrier model in the master thesis during the spring of 2014. The barrier was tried to be modelled with a beam model, using a hollow profile without inside decks and bulkheads. Those experience is taken into consideration when the global model was created in this master thesis. The main experience done by Konstali (2014) was that it was preferable to include both decks, vertical and transverse bulkheads in order to obtain correct global mode for the barrier.

The main simplification performed to the global model are to omit all the stiffeners. It was decided to keep all the vertical and transverse bulkheads and the decks. The transverse bulkheads were included in order to let the structure carry the shear loads in a proper and correct

manner. The vertical bulkheads was necessary in order to both could keep the area and the buckling stiffness equal in the global and local model. Both those properties were preferable to keep constant in order to get a correct global behaviour of the ship collision barrier. The area relevant in connection with the membrane forces and stresses. The bending stiffness is related to how the structure carry the bending forces and stresses.

The global simplified model applied for the analysis was therefore decided to have the same area and the same bending stiffness about the vertical axis. The correct area can be found just by smearing the stiffeners, but since the stiffeners have eccentricity the smearing will not implies the correct bending stiffness. Therefore the position of the inside bulkheads must either be changed or the vertical bulkheads needs to have different thickness. The latter case is applied in this thesis, this means that the decks, transverse and vertical bulkheads are positioned at the same places for both the local and global model.

Table 5.6: Global model

Number of decks n_{decks}	4
Number of vertical bulkheads n_{vb}	4
Spacing between transverse bulkheads $[mm]$	3 000
Thickness of decks t_{hb} $[mm]$	22
Thickness of vertical bulkheads t_{vb} $[mm]$	21
Thickness of transverse bulkheads t_{tb} $[mm]$	19
Total length of global model $[m]$	$380 - 30 = 350$

Table 5.7: Comparison of cross section properties in the global and local model

	Local model	Global model	ratio $\frac{Local}{Global}$
Area A $[m^2]$	2.767	2.768	1.000
Section of modulus I $[m^4]$	113.973	113.603	1.003

The ship collision barrier in this master thesis is made of two different aluminium alloys.For the global simplified model where the stiffeners are omitted some additional simplification is done with respect to the material model. The yield stress, σ_Y, is taken according to the aluminium alloy 5083-O which is used for the plates in the local model discussed in the previously section. Also most of the other material properties for the global model are taken similar to the aluminium alloy 5083-O. The reason why to use those material properties to represent the material properties for the whole global model compared to for instance the alloy 6082-T6, is that the alloy 5083-O dominate the cross section since it is applied to the largest amount of the cross section area.

The density of the material model in the global model is artificial increase to take into account the hydrodynamic added mass and the weight of ballast in order to get a correct representation of the inertia forces. This is briefly discussed in section 5.2.5.

The mesh applied to the global model is a coarser mesh compared to the mesh applied to the local model since the local effects are less critical for the global model. A distributed drag load should be applied to the structure as a load distributed to the nodes at the front surface of the barrier, for more information see section 5.2.6. Due to the introduction of drag forces and related to how a distributed load are defined in LS-DYNA it is preferable to have a evenly distributed mesh for the global model. The way this is accounted for is to have a transition mesh between the mesh for the local model and the mesh for the global model in the region where the two models are connected. For the rest of the global model a coarse evenly distributed mesh is applied.

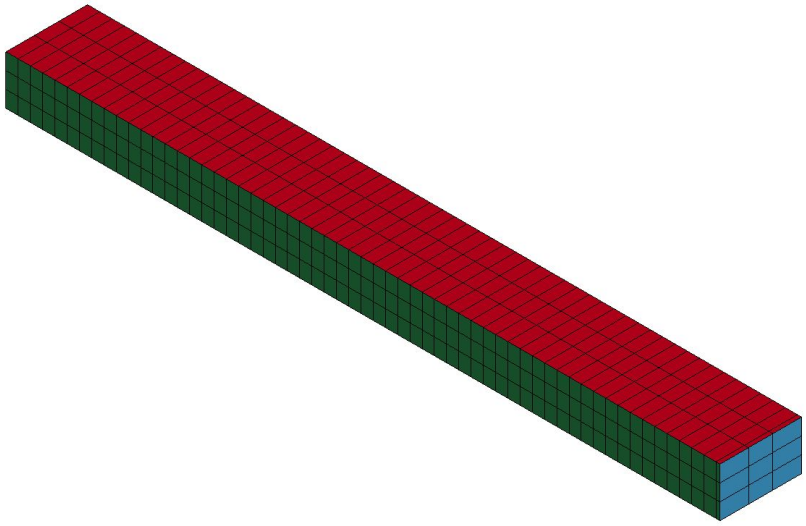

Figure 5.13: The figure shows the global model which will be attached to the local model

5.2.3 Total finite element models

The total finite element models consist of a combination of the three models discussed in previously sections, bow model, local and global model. Which models included in the total model depends on the analysis. As have been mentioned in chapter 2 there are three different analysis which is relevant to take into consideration when designing against ship collision. This is strength design, ductility design and shared energy analysis. Since the barrier is to be taken as a freely floating structure different impact position of the struct ship should be considered. In this thesis it has been created two models for shared energy analysis, one for impact at the center position of the ship collision barrier and one for impact at the barrier end. It will also have been preferable to analyse situation where the ship hits the barrier with an angle different from ninety degrees. As will be discussed in section 5.2.4 relevant finite element theory was not yet available during the work with this master thesis, but it is under development at the Department of Marine Technology.

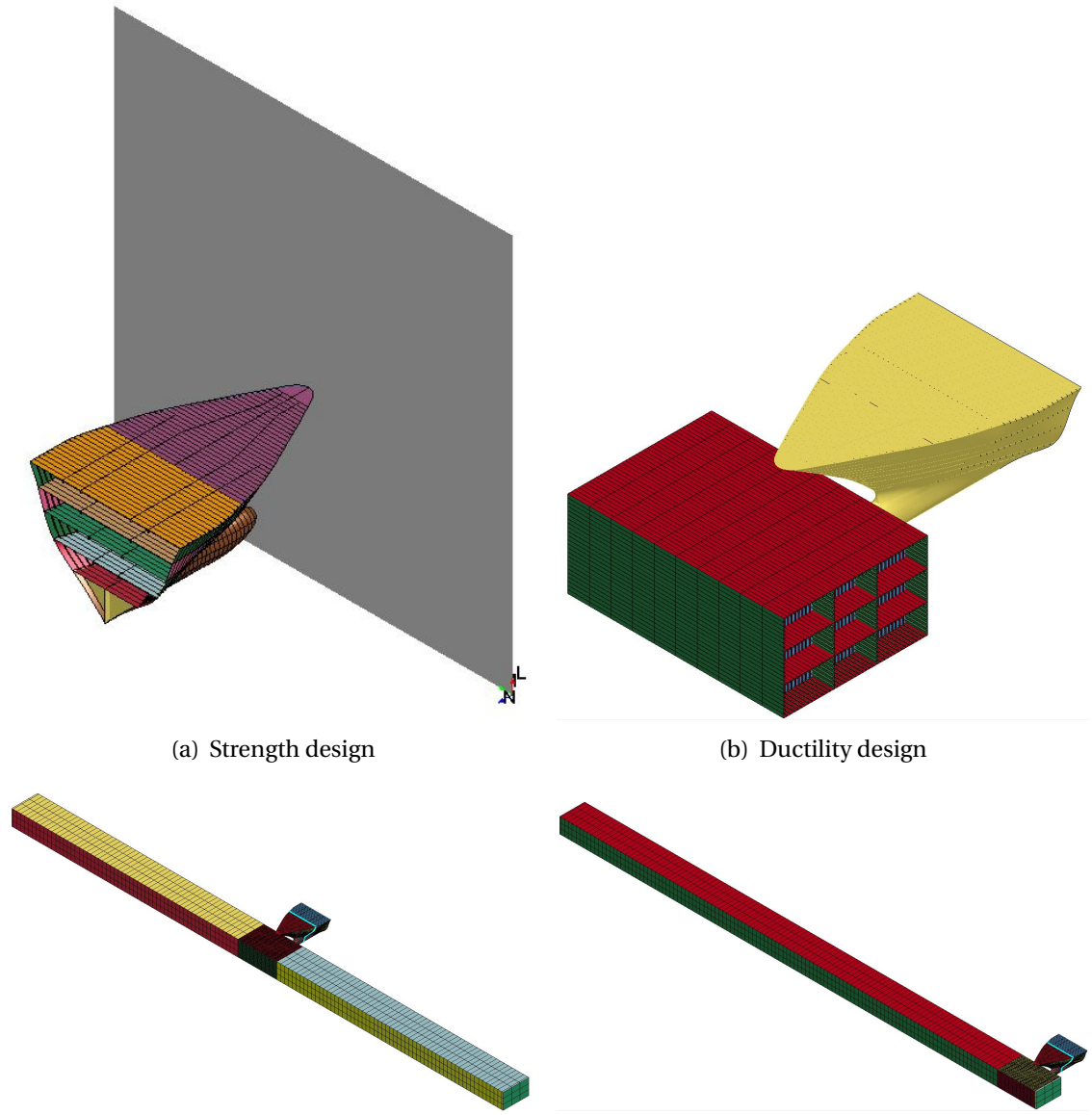

(a) Strength design

(b) Ductility design

(c) Shared energy design, impact at the center position

(d) Shared energy design, impact at the barrier end

Figure 5.14: The different total models used for the finite element analysis

5.2.4 Global Motion Interaction

The global motion of the barrier and the ship can be handled in different manner, some different methods of how this can be done are briefly discussed bellow.

If both the ship and the barrier are modelled with its full length, the fluid environment could then also be modelled around the structures. In such a way the analysis will be an integrated fluid structure analysis. If the water element is modelled correctly the forces from the fluid at the structure will then have been modelled correct and such give the global motion of the ship and the barrier. Such a model may sounds reasonable in theory, but in order to get a

correct fluid environmental it will regards a really fine mesh which also needs to be updated at each time step. Therefore a model which account for fluid structure interaction will be way too time consuming for such big models as a ship collision event.

An alternative and more simplified method, is to model the global motion with use of manoeuvring equations and theory. Such a model will be time efficient compared to the method described above and it will give reasonable results. This method utilises hydrodynamic coefficients from a similar to describe the behaviour of the ship in an analysis. The hydrodynamic forces could then be calculated according to those coefficients and the velocity found in the analysis. To be able to get a correct representation of the global motion of the ship it will be necessary to model the total ship, but the details outside the contact zone could be modelled in a simplified manner. In principle it will be possible to model the barrier in a similar manner, but the difficulties here will be related to find the correct representation of coefficient. For instance experimental value obtained for a barge will probably have could been adopted for the barrier. Another difficulties of applying this method for the barrier is related to how it should be applied to the barrier when it has formed a global mode.

Of the two aforementioned method the methods regarding use of manoeuvring equations will be preferable due to its simplicity and time efficiency compared to an integrated fluid structure method. At the moment when this master thesis is written a model to account for the global motion based on manoeuvring equation is under development at the Department of Marine Technology. The model has shown to give reasonable results. The model was not yet available for the author during the work with this master thesis. By that reason global motion have not been accounted for in the analysis performed in this master thesis. As a recommendation for further work analysis where global motion is accounted for is preferable to be performed.

One of the biggest advantage of using a model accounting for global motion is that it will be easier to investigate and get a more realistic behaviour of a collision scenarios where the heading of the ship relative to the barrier is different from 90 degrees.

5.2.5 Inertia forces

The models applied for the shared energy analysis are assumed to be freely floating structures. This means that the barrier is only supported by inertia forces and drag forces. A discussion of the applied drag forces are discussed in section 5.2.6.

The inertia forces of the barrier includes the contribution from the mass of the structure, the mass of the ballast and added mass. The added mass coefficient is assumed to be 0.8. The inertia forces is accounted for in the analysis by artificially increase the density of the material. The density is only increased for the area outside the collision point in order to not get spurious contact forces at the collision point.

In the following steps there are shown how the artificial density for the material model in the global model have been calculated:

$$V_{al} = A_{cs} \cdot L + n_{tb} \cdot B \cdot H \cdot t_{tb} \tag{5.24}$$

$$m_{total} = B \cdot d \cdot L \cdot \rho_{sw} \cdot (1 + C_m) \tag{5.25}$$

$$\rho_{eff} = \frac{m_{total}}{V_{al}} \tag{5.26}$$

Where:

V_{al}: Total volume of aluminium in the barrier $[m^3]$

A_{cs}: Cross section area of the barrier $[m^2]$

L: Total length of the barrier $[m]$

n_{tb}: Number of transverse bulkheads

B: Breadth of the barrier $[m]$

H: Height of the barrier $[m]$

t_{tb}: Thickness of transverse bulkheads $[m]$

m_{total}: Mass of the whole barrier including ballast water and added mass [kg]

d: Draft of the barrier $[m]$

ρ_{sw}: Density of seawater $[kg/m^3]$

C_m: Added mass coefficient

ρ_{eff}: Artificial density of the material model applied for the global cross section $[kg/m^3]$

5.2.6 Drag forces

The drag force is calculated by use of the drag equation, see equation (5.27). The drag force is a force which act in the opposite direction as the motion. It will act as a distributed load

on the part of the body which is submerged in water. In the next section a discussion will be done with respect to how the drag force have been added to the analysis in LS-DYNA.

$$F_d = \frac{1}{2} \cdot \rho \cdot A \cdot C_d \cdot v^2 \tag{5.27}$$

Where:

F_d: Drag Force [N]

ρ: Density of seawater [kg/m^3]

A: Area [m^2]

C_d: Drag coefficient [-]

v: Velocity [m/s]

Implementation of drag forces in LS-DYNA

The drag forces is implemented in LS-DYNA in a simplified manner. This will however be a good enough approach since it is the drag force contribution to the global structural behaviour which is relevant. This includes how the drag forces contributes to the retardation of the barrier.

Equation (5.27) gives the total drag force on the body if the area A is the projected area of the submerged part. This is correct when the drag force are assumed to act in 2D, which is the assumption done for the drag force in this master thesis. However the 3D effect could some how be accounted for by increasing the drag coefficient C_d.

In a finite element model the load needs to be assigned to the nodes. Therefore the drag forces in the finite element analysis is distributed as an equally distributed load at all the nodes submerged into water (8 meter draft) at the front side of the barrier. Since a different mesh size is used for the global model compared to the local model, the nodal force will differs, but the force per area are kept according to equation (5.27) at the whole model. Figure 5.16 and 5.15 shows which nodes the drag forces were applied to.

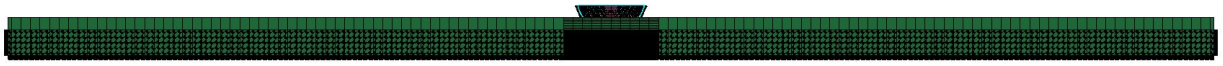

Figure 5.15: The nodes where the drag forces are applied to the structure for the centric collision scenarios, (the black points represents the nodes where the drag force are attached)

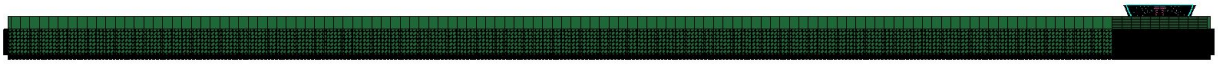

Figure 5.16: The nodes where the drag forces are applied to the structure for the collision scenarios where the ships hits at one of the barrier ends, (the black points represents the nodes where the drag force are attached)

In reality the the drag force at a node will depend on the velocity of this node. Such a formulation was not able to be done in LS-DYNA in a simply and cost effective way. Therefore it was instead picked three nodes at each structural part for the centric collision scenarios, local part and the two global part at each end of the barrier. For the collision scenarios with collision at one of the barrier end it was taken three velocity nodes at the local barrier and three at the global part. The velocity components for each part were then averaged to calculate the drag component for each node. Figure 5.17 and 5.18 shows the nodes used for averaging the velocity.

Figure 5.17: A representative velocity for each barrier part er calculated by taking the average of the nodes shown by the yellow point in the figure

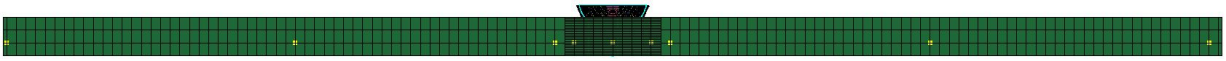

Figure 5.18: A representative velocity for each barrier part er calculated by taking the average of the nodes shown by the yellow point in the figure

The value of the nodal drag force are calculated according to equation (5.27). The area A is taking according to the mesh size. The density of seawater is taken as $1025 kg/m^3$ and the drag coefficient, C_d is assumed to be 1.3. It is related a amount of uncertainty to the value taken for the drag coefficient. An earlier experiment for a tank ship gave this value with respect to translation in beam direction, but since the barrier have abrupt ends with sharp corners it will probably have a larger drag coefficient compared to a tank ship.

Resultant drag force from the analysis

As have been discussed before it is expected that the inertia forces will dominate at the time where the impact occur and until the emerged structure consisting of the barrier and the ship have got a significant velocity. When the velocity increases the drag forces will increase since as can been seen from equation (5.27) the drag force is dependent on the velocity squared.

In order to determine a significant drag force from the analysis performed in LS-DYNA, a long simulation time required. The shared energy analysis have not been carried out in this master thesis. Therefore the results to discuss the importance of drag forces are limited.

Figure 5.19 confirms that the drag force first will be important after long time. However, this figure is just an illustration and has been determined for a centric collision scenarios where mass scaling is applied for the bow. Hence the bow model will be too strong and the conservation of energy in the analysis will not be kept constant. This is further discussed in section 6.3.

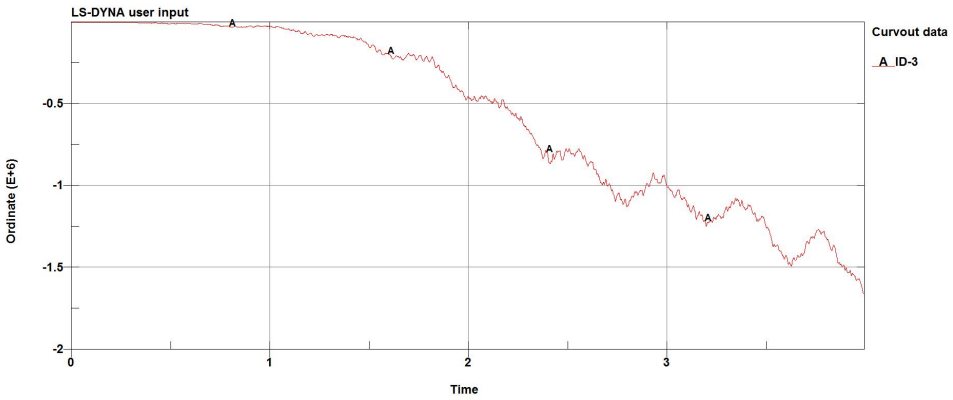

Figure 5.19: The Figure shows an illustration of the drag load. The load will first be significant after the barrier have got a significant velocity. This curve is only an illustration since it is drawn for a case where mass scaling is applied.

6 Analysis and Results

The analyses and results conducted in this chapter is related to a collision event between the ship and the ship collision protection barrier. The modelling process with respect to each analysis is discussed in chapter 5. The results is in particularity discussed as they are presented.

Different analysis have been conducted for the ship barrier impact. Those includes bow against rigid wall (strength design) and rigid bow against local barrier cross section (ductility design). The analyses connected to the shared energy approach have not been fulfilled and is therefore only briefly discussed.

6.1 Bow against rigid wall, strength design

The purpose of this analysis is to determine the collision force from the bow, when assuming collision against a rigid structure. The energy dissipated as strain energy is also determined by deforming the bow into the collision bulkhead, see Figure 6.1(f). A further deformation is unwanted in order to avoid seriously damage to the ship. If the deformations is increased further the ship could sink and the risk of human life is severe.

A time collapse of a ship colliding with a rigid wall is shown in Figure 6.1. All the nodes behind the collision bulkheads are applied this constant velocities, the force should not be to larger in order to get quasi-static results. For this analysis the velocity applied is $5 m/s$. Figure 6.1(c) to Figure 6.1(f) are all plotted with the same height hence the relative indentation between the figures are real. Figure 6.1(f) is equal to an indentation close to the collision bulkhead, further indentations will not give good results since such a large indentation will influence the boundary conditions.

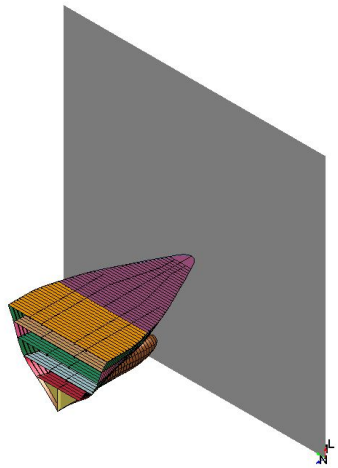

(a) Initial position, iso view

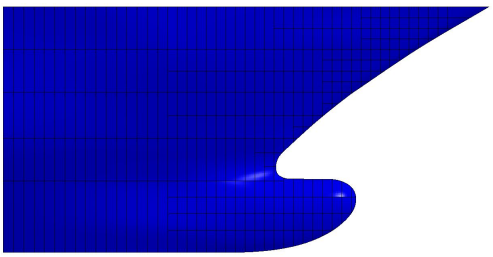

(b) Initial position, left view

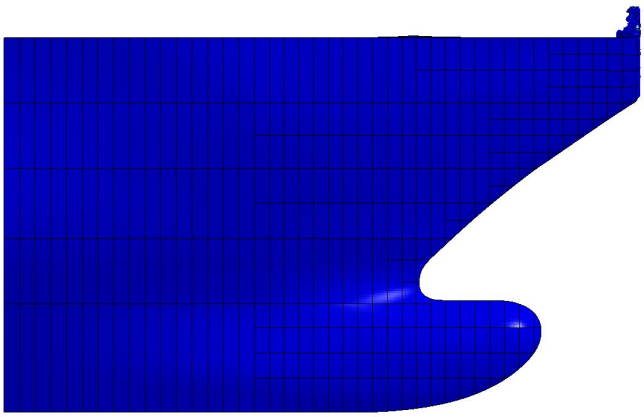

(c) Position at 1 sec

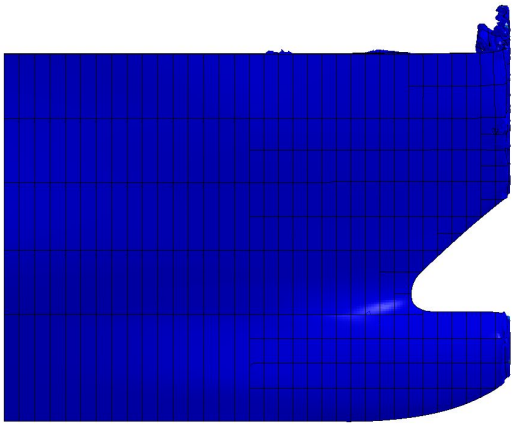

(d) Position at 2 sec

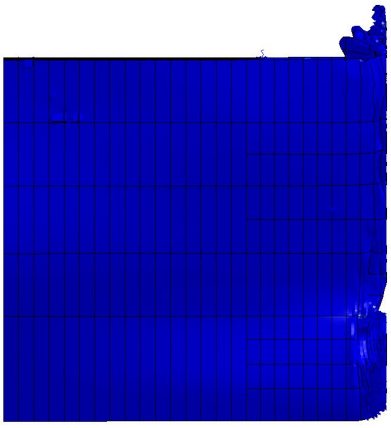

(e) Position at 3 sec

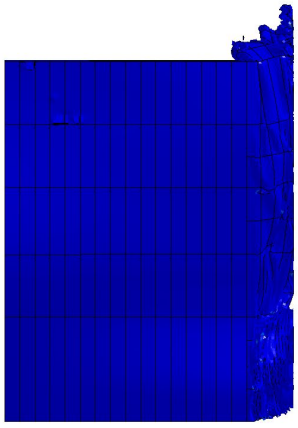

(f) Position at end

Figure 6.1: Time collapse of collision between ship and rigid wall, the figures (c)-(f) are plotted with the same height so the relative indentations is clearly shown

The force indentation curve and the force time curve for this particular collision scenarios is included in Figure 6.2(a) and Figure 6.2(b). The reference node for the deformation is the node which hits the rigid wall first.

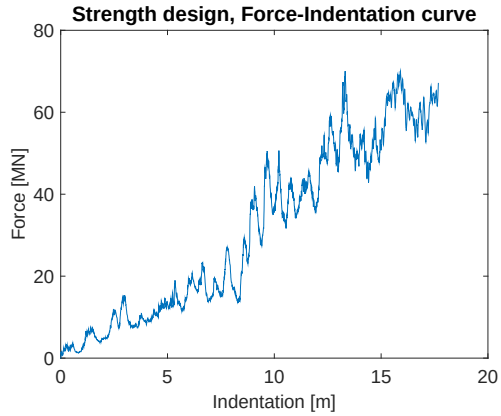

(a) Force-indentation bow against rigid wall

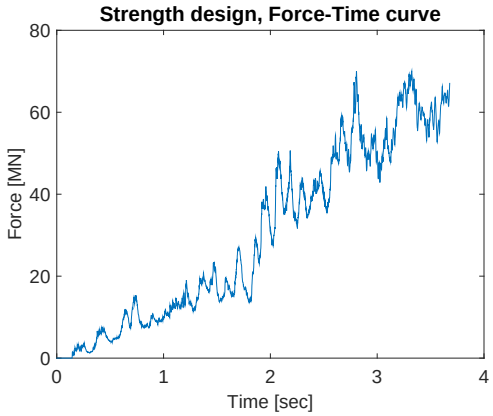

(b) Force-time bow against rigid wall

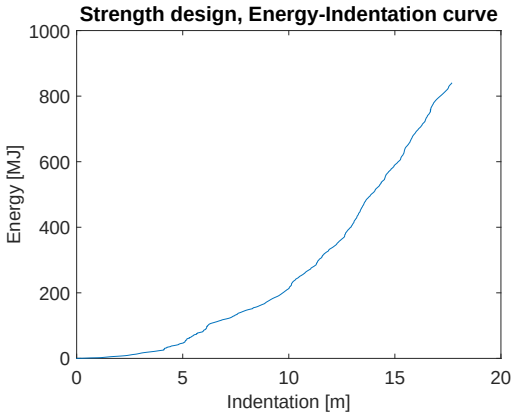

(c) Energy-indentation bow against rigid wall

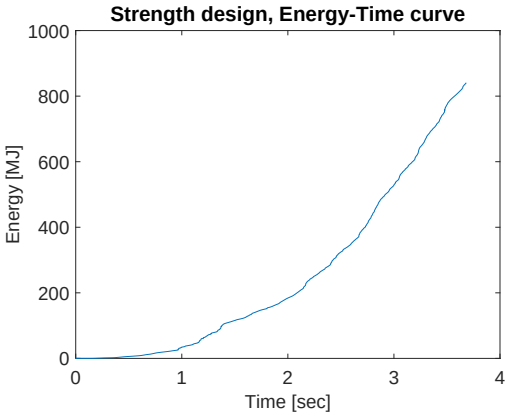

(d) Energy-time bow against rigid wall

Figure 6.2: Force and energy curves for collision of a bow against a rigid wall

From Figure 6.2(a) it is seen a suddenly increase in the force after an indentation close to $8m$. This increase is because the strongest part of the bow, the bulbous part hits the wall and contribute to the collision force. It is also seen in Figure 6.2(c) that this curve gets a larger rate of change from about $8m$ which of course also is due to the contribution from the bow.

In Figure 6.2 it is shown that the maximum collision force is approximately $60MN$. The amount of energy which could be taken by the bow before it reach the collision bulkhead is approximately $800MJ$. In other word this means that the bow does not could dissipate the total kinetic energy in the design ship ($1565MJ$). The remaining energy need to be dissipated by the barrier locally and/or by the boundary condition.

This analysis have taken into account that the total bow is crushed. However in a collision scenarios it is not likely that the total bow will be crushed, the upper part of the barrier may not hit the structure and will therefore not contribute to energy dissipation. When the total bow is crushed and those values are applied in design the energy dissipation in the barrier will be non-conservative, but the collision force will be conservative with respect to predicting failure in the barrier. A model where only the relevant bow part is crushed are shown in Figure

6.3. However, this analysis have not been conducted in this master thesis. Such an anlysis were performed for the bow by Konstali (2014) showed that the collision force are reduced from $60MN$ and down to about $50MN$, hence also the energy dissipation was reduced.

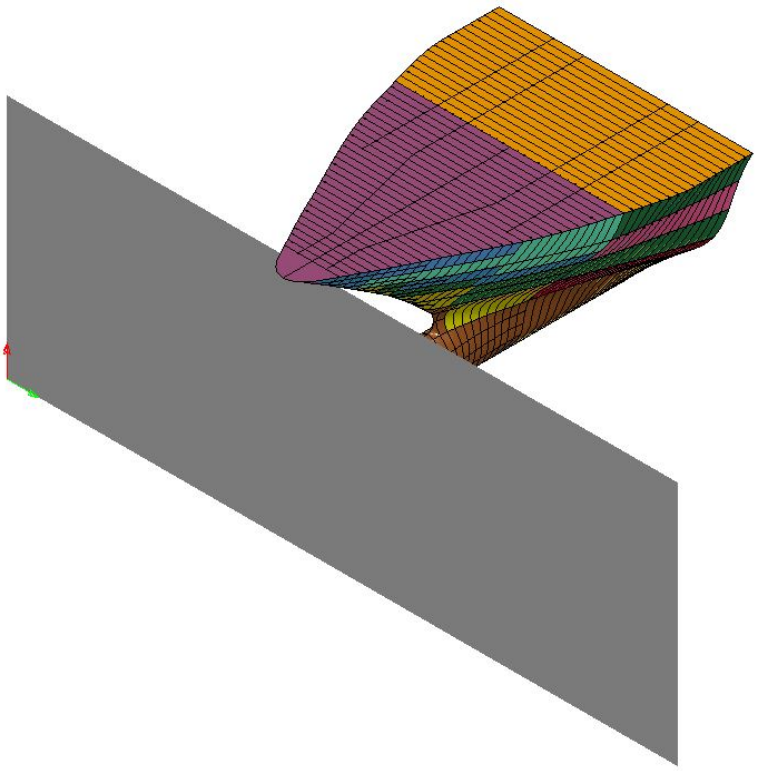

Figure 6.3: Illustration of the bow against a rigid wall where only a part of the model is crushed

6.2 Rigid bow against local barrier cross section, ductility design

For this case the the bow is assumed rigid and the barrier is allowed to deform. The material parameters for the bow is modelled in order to account for sliding energy between the rigid bow and the barrier. For this analysis only the local detailed model of the barrier is included, this means that a part of only $30m$ is modelled. The boundary condition applied for the barrier is that the end nodes on each sides are all assumed to be constraint in five degree of freedom. All degree of freedoms except for the translation in longitudinal direction, y-direction. The choice of boundary condition may be questionable. By letting the barrier be able to translate in y-direction, contraction of the barrier ends are allowed and local membrane force will hence not be introduced. The rotational stiffness is due to stiffness from contribution from the rest of the barrier. However, this may be slightly non-conservative.

From the previous section the bow have been calculated to be able to dissipate around a max-

imum of $800MJ$, the barrier have then to be able to dissipate a minimum of $800MJ$. This is valid if all the kinetic energy in the ship should be dissipated as strain energy in the ship and the barrier.

In order to get proper design of the barrier cross section it will be necessary to perform an iteration with respect to different cross sectional properties in order to get a proper cross section which satisfy the requirements. A couple of different configurations with respect to the plate thickness and stiffener dimensions where therefore investigated. The results are summarised bellow.

The aluminium alloys considered in this master thesis will have poorer material properties with respect to energy absorption compared to ordinary mild construction steel as for instance s235 considered for the bow. This was the steel grade considered for the barrier by Konstali (2014). By that reason it was not practical to consider any weaker cross section compared to the cross section considered by Konstali (2014). This cross section utilised a stiffener spacing of $500mm$, which is slightly less than the common value used for ship structure $(600-700mm)$, and a spacing between the transverse bulkheads of only $3m$, which in fact is quite small. Therefore it was decided to not decrease does values in order to increase the strength of the cross section. The cross section was instead increased by utilising stronger stiffeners and increasing the plate thickness in the decks and bulkheads.

The iteration process is time demanding and number of iteration steps were therefore limited. Only a few different cross section were determined by use of finite element analysis.

First the cross section considered in section 4.2.2 was considered. This is a cross section with a slightly increased thickness and stiffener strength compared to the cross section considered by Konstali (2014). The second cross section was a cross section with even further increase of the plate thickness. The intention was to perform a third analysis with an increase in number of vertical bulkheads and decks, this analysis have not been completed and will therefore only briefly be covered. A time laps of the ductility design analysis is shown in Figure 6.4.

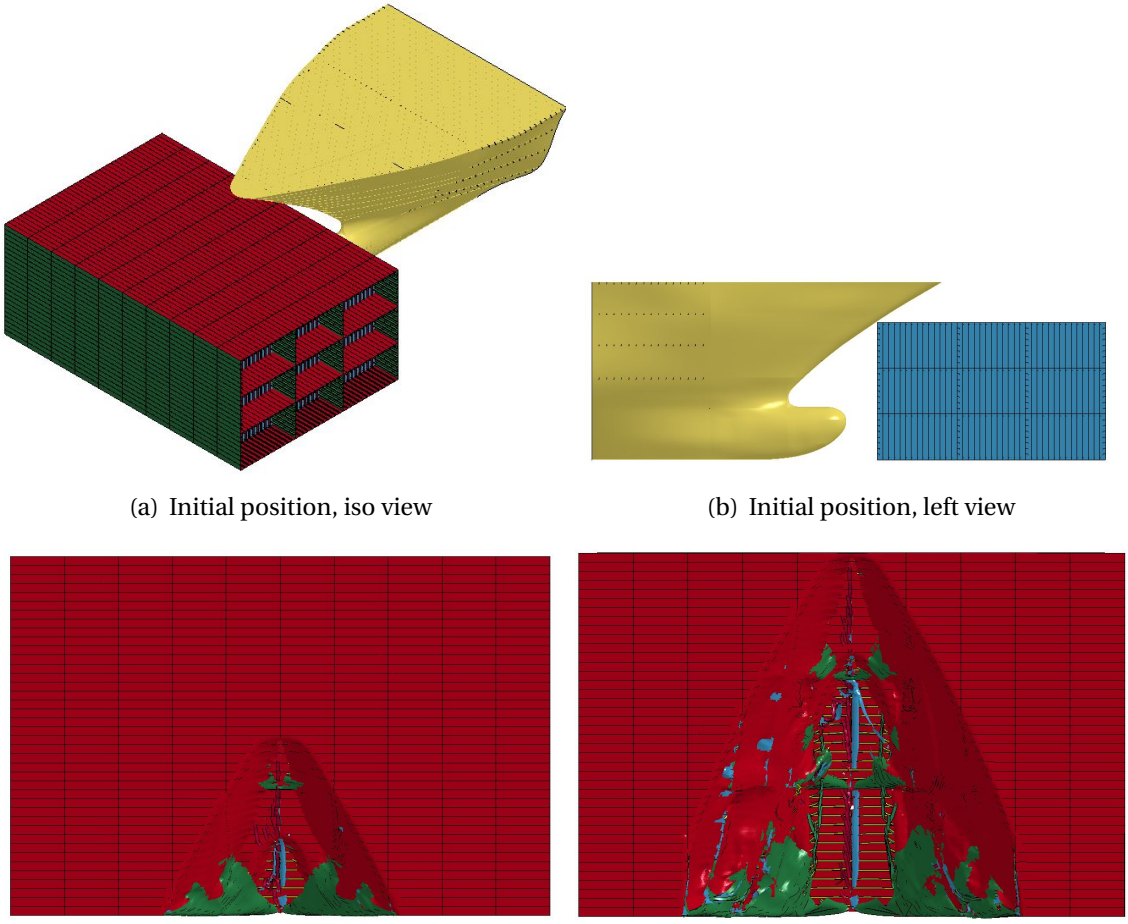

(a) Initial position, iso view

(b) Initial position, left view

(c) Position at 1 sec

(d) Position at 2 sec

Figure 6.4: Time collapse of collision between rigid ship and local barrier cross section, (c) and(d) is plotted from top without displaying the rigid ship

The deformation utilised for plotting the force-deformation and the energy-deformation curves shown for each case, are plotted against indentation of the first point which hits the barrier. It is from that moment the force start to increase from zero.

6.2.1 Case 1, original cross section

The force-deformation and energy-deformation curve according to the local barrier cross section discussed in section 4.2.2, the curves is shown in Figure 6.5.

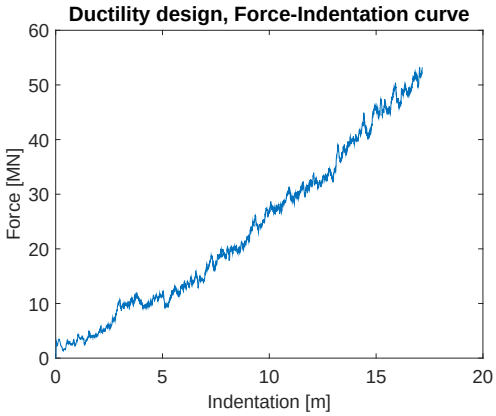

(a) Resultant force-indentation

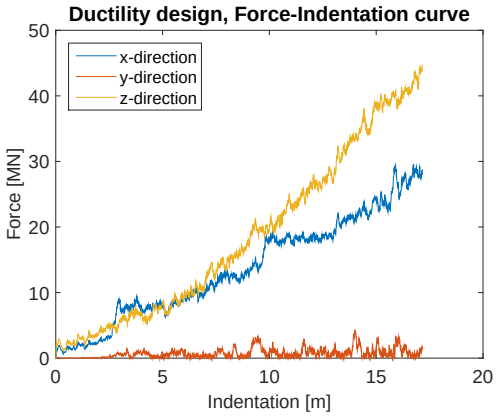

(b) Absolute value of the contact force in different direction-indentation

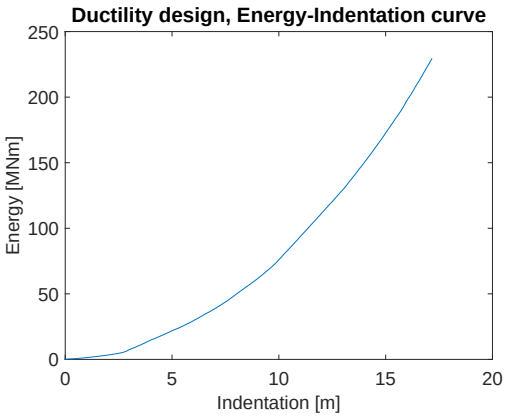

(c) Internal energy-indentation

Figure 6.5: The figure shows the curves for the cross section discussed in 4.2.2

6.2.2 Case 2, further increased plate thickness

The energy dissipation in the local barrier cross section need to be increased further. The most easily way is to increase the shell thickness of the different compartments. All the global parameters and also the mesh could hence be kept constant, and the model is then created with only a few modification to the original model. Therefore the time regarding modelling of the slightly modified barrier was limited. The modified cross section will therefore looks similar to the barrier in Figure 6.4(a). The thickness of each bulkheads and decks have been increased form $15mm$ to $20mm$ for the barrier considered in this section. Force-deformation and energy-deformation curves are shown in Figure 6.6.

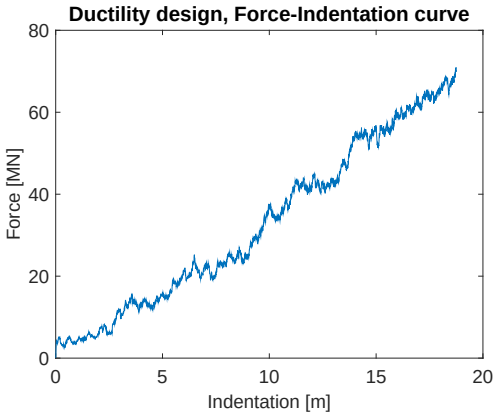

(a) Resultant force-indentation

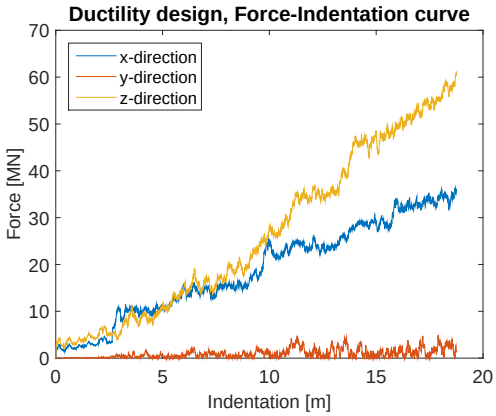

(b) Absolute value of the contact force in different direction-indentation

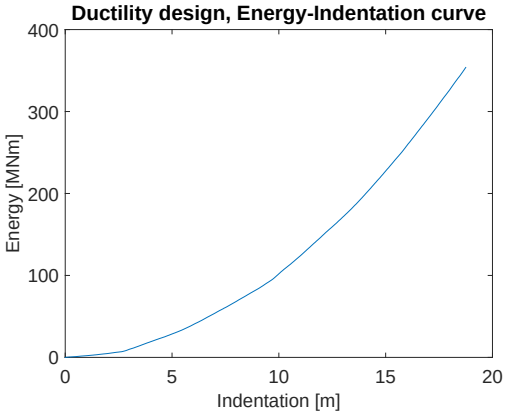

(c) Internal energy-indentation

Figure 6.6: The figure shows the curves for a cross section with increased plate thickness

6.2.3 Case 3, increased number of decks and bulkheads

In order to increase the energy dissipation and contact force for the barrier, it was decided to apply a local cross section with increased number of decks and vertical bulkheads. The cross section is shown in Figure 6.7. However due to limited time this analysis was not conducted.

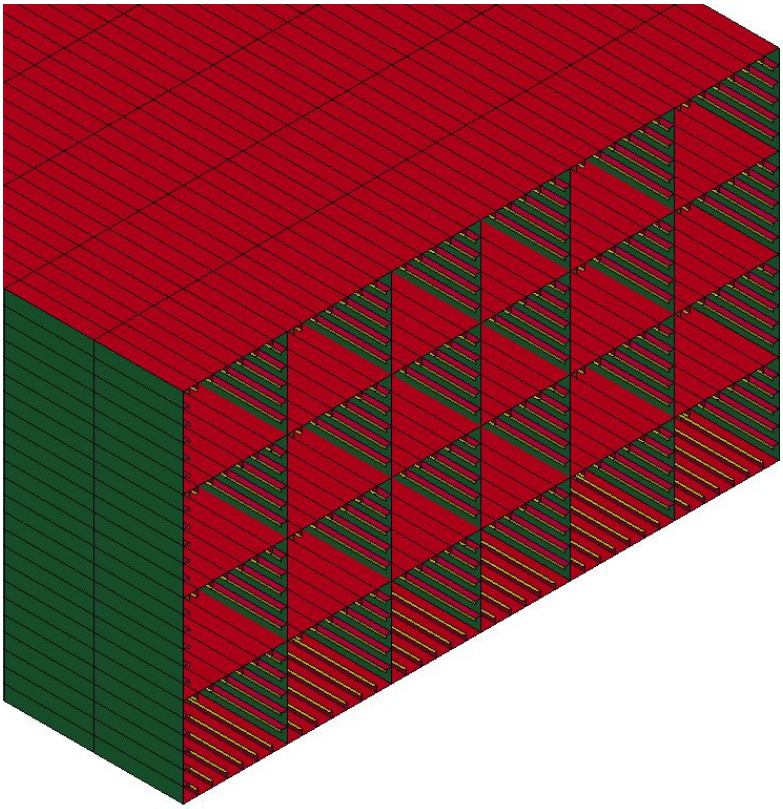

Figure 6.7: The figure shows the local barrier which intentional should be considered with respect to energy dissipation

6.3 Shared energy design, both structural parts deformable

For shared energy design both structural parts are assumed to dissipate energy. In order to let this happen, both structure needs to have about the same strength. In strength design and ductility design approach it is assumed that one of the structures are strong compared to the other. If so not is the case, a shared energy analysis needs to be performed. In such analysis the deformations in both structural members are accounted for. The shared energy analyses are as have been mentioned earlier not been completed and are therefore only briefly discussed in this section

To account for correct kinematic energy in the ship at the time of impact ($1565MJ$), lumped mass nodes were added to the bow model. Since the bow is to be taken as a part of large ship, the nodes behind the collision bulkhead have been applied constraint in all directions except for the surge direction.

In order to get some results for the shared energy design, selective mass scaling was applied to the bow in order to increase the time step. Mass scaling increase the density of the elements critical with respect to time step, therefore the energy relations in such analysis is bad. By that reason final results can not be conducted from the analysis utilising mass scaling. However,

the general trend shown from those analysis may be reasonable.

6.3.1 Centric collision

As could been seen in Figure 6.8, the global mode formed will be similar as the mode utilised for the plastic hinge calculation in section 4.2.1. Since mass scaling is applied for the bow in Figure 6.8 the deformation is not real. However, it is likely to assume that the real configuration will looks quite similarly.

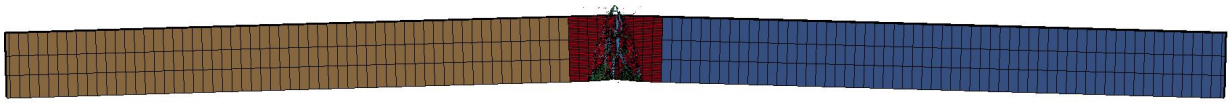

Figure 6.8: The figure shows the global mode for the centric collision scenarios. Mass scaling has been applied for the bow so the shown deformation is not real.

6.3.2 Collision at the barrier end

In Figure 6.9 the global mode for the collision scenarios where the bow hits at barrier end is shown. The mode occurring is that the barrier form an arch with largest translation at the impact position.

Figure 6.9: The figure shows the global mode for the collision scenario at the barrier end. Mass scaling has been applied for the bow so the shown deformation is not real.

7 Discussion

The results have been briefly been discussed as the results are presented in the previous chapters. In spite of this some topics needs a further discussion, such a discussion is performed in this chapter. In addition a discussion of a comparison of the results with simplified approaches are included.

7.1 General

In the analyses performed in this master thesis the ship collision barrier for protection of the transition zone between the floating bridge and the submerged floating tunnel are assumed to be made of aluminium. The author have therefore had some issue in how to handle and use aluminium alloys compared to for instance ordinary construction mild steel. In spite of accurate description of the material curves for aluminium alloys it was decided to use the values given as typical values in Eurocode 9: Part 1-1 (2007). The main difficulties and uncertainties of applying the aluminium alloys were therefore related to the modelling of a fracture criterion. The fracture criterion in connection with the user defined material model in LS-DYNA is only validated for mild construction steel. It was therefore necessary to make the assumption that this fracture criterion also was valid to aluminium alloys. This however is questionable and in principle it should have been validated. The differences between aluminium alloys and mild construction steel is more comprehensive than just change the material properties. Earlier research have shown that aluminium alloys structures fails in a different manner than steel structure.

7.2 Element size and HAZ considerations

As have been discussed before the HAZ area in the stiffeners was modelled by using an element size equal to $20mm$ in the lower part of the stiffener web, see Figure 7.1(a) and Figure 7.1(b). As a consequence of the HAZ part the mesh for the stiffener web consist of three elements and the smallest is then placed in the HAZ area with its smallest edge length equal to $20mm$.

When the ship collision analysis is run through it turns out that does elements, which are the smallest elements in the barrier, will be critical in respect to the critical necessary time step in order to keep the analysis stable.

It was by the aforementioned argument decided to omit the HAZ area from the analysis. Then the smallest elements in the barrier were omitted and the critical time step will hence also increase. The stiffeners were now modelled with only two elements over the stiffener web, see Figure 7.1(c) and Figure 7.1(d).

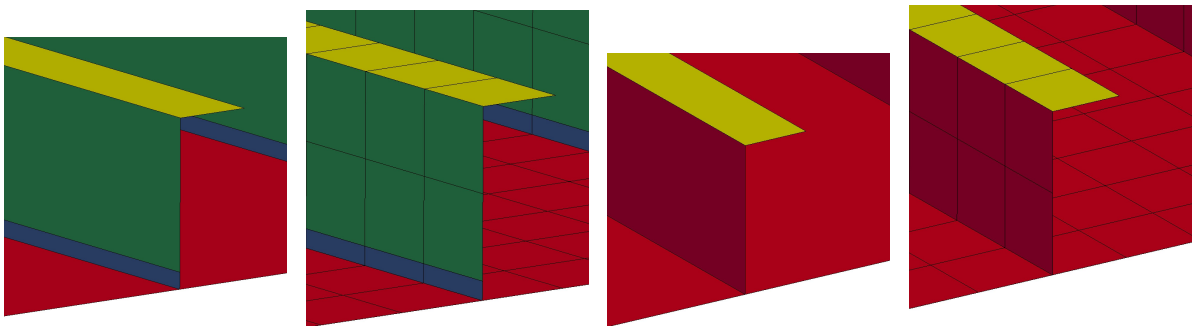

(a) With HAZ, part (b) With HAZ, mesh (c) Without HAZ, part (d) Without HAZ, mesh

Figure 7.1: The figures shows the difference in the stiffeners when HAZ is modelled or not

As have been described above was the HAZ not included in the analysis of the aluminium alloys in the barrier. The result of the analysis could therefore be questionable. When omitting the HAZ area, an area in the stiffener web which in reality will have reduced material properties will be omitted.

However, the results may still be reasonable and representable. As was shown in chapter 3, it is the plate which here is assumed to be made of aluminium alloy 5083 O which have no HAZ region, which take most of the load and energy through membrane forces. The stiffeners main effect is to counteract against local buckling. Hence when looking globally at the barrier the total absorbed energy and and the contact forces between the ship and the barrier will give good results even when the HAZ is omitted.

In spit of the discussion above it would been preferable to include HAZ. It had been better to apply a bigger element so the critical time step had been increased. This could be achieved in different ways. The user defined material model discussed in chapter 5 which is developed at the department of marine technology is already using mesh scaling in order to account for local necking. Somehow it may be possible to include a kind of mesh scaling in order account for the reduction in HAZ. This will not be any further discussed in this master thesis.

7.3 Comparison of piecewise linear and the user defined material model

As have already been mentioned the main difference between the piecewise linear and user defined power law material model is related to how fracture is accounted for. For the local

barrier model the element size is in the range of 5-10 times the plate thickness. Therefore the mesh scaling which is implemented in the user defined power law material model to account for local necking will have a great influence on the results. In chapter 5 the difference in material curves between the Ramberg-Osgood and the modified power law equation have been discussed.

A comparison between the models are done with respect to ductility design for the barrier cross section discussed in section 4.2.2. The HAZ area is omitted in the power law material model, however as discussed in chapter 3 the stiffener have small influence on the total globally dissipated strain energy and contact force.

7.3.1 Piecewise linear material model

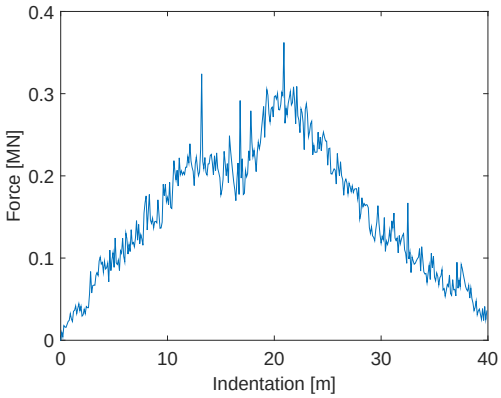

(a) Resultant contact force-Translation of the bow

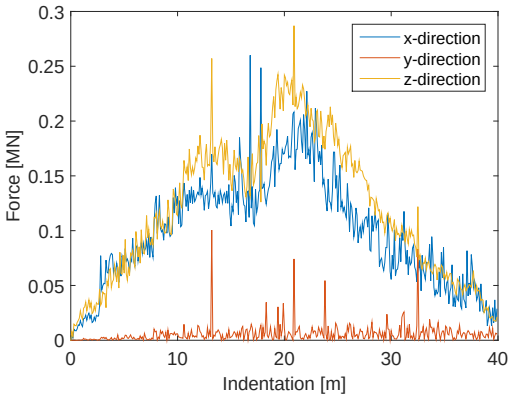

(b) Absolute value of the contact forces in different direction-Translation of the bow

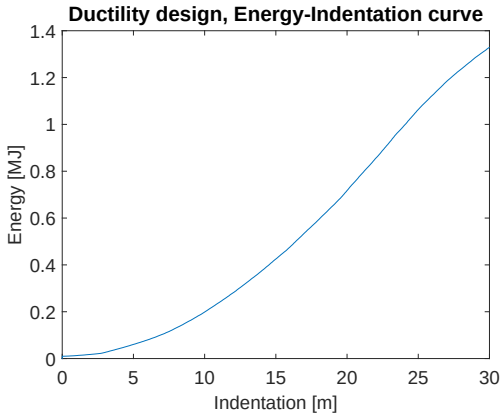

(c) Internal energy-indentation

Figure 7.2: Curves for collision a rigid bow against the barrier, when the piecewise linear material model is applied without mesh scaling and only a simplified fracture criterion

As clearly shown in the Figure 7.2 both the contact forces and the energy dissipation in the local barrier cross section is very small. It is way to small to be able to dissipate a significant

amount of the total energy in the design ship, $1565MJ$.

7.3.2 User defined power law material model

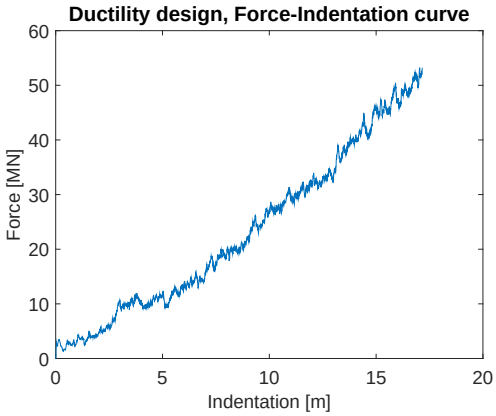

(a) Resultant contact force-Translation of the bow

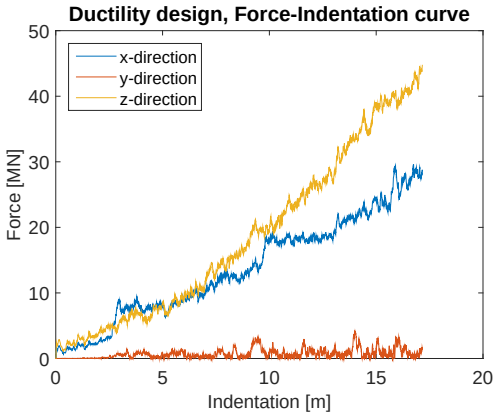

(b) Absolute value of the contact forces in different direction-Translation of the bow

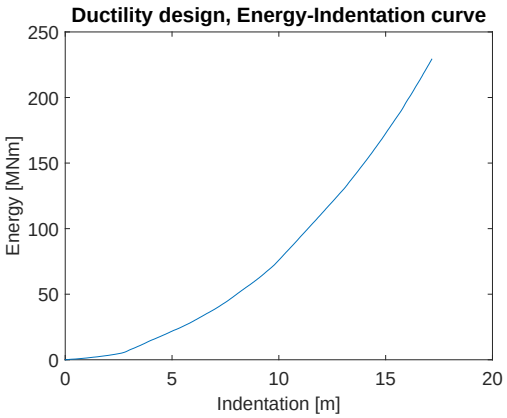

(c) Internal energy-indentation

Figure 7.3: Curves for collision a rigid bow against the barrier, when the modified power law material model is applied utilising mesh scaling and a RTCL fracture criterion

The analysis for the case where the user defined material model is applied (Figure 7.3), has been analysed for a smaller simulation time. Hence the bow have not been able to sail straight through the barrier. The drop which could be found in 7.2 for the case where the piecewise linear material definition is applied, is related to that the ship have sailed straight through the barrier and strength of the barrier is hence lost.

7.3.3 Conclusion

By comparing Figure 7.2 and Figure 7.3 there are clearly shown that almost no energy will be dissipated locally when the piecewise linear model with no mesh scaling and a simplified

fracture criterion are applied. Some differences between the two figures was as stated above expected. The parameters included in the user defined power law expression is extrapolated from the Ramberg-Osgood curve. The validation of those parameters are limited to comparison of stress-strain curves. Therefore it is recommended as further work to do a more cohesive validation of the parameters used in the user defined material model.

The values found in Figure 7.2 are unrealistic low compared to Figure 7.3. The conclusion is therefore if a simplified material model should be applied to the structure, the mesh should then be small. Preferable in the range 1-2 times the plate thickness. However, for large finite element models such small element size is unwanted, because of the accordingly small time step. Therefore a material model utilising mesh scaling is necessary to be applied in order to get satisfying results when a mesh size equal to 5-10 times the thickness is utilised for the structure.

7.4 Discussion of the nonlinear finite element analysis

The original intention of this master thesis was to discuss energy dissipation in the ship and the barrier. In order to do so it should have been done an integrated analysis with large simulation time. This to be able to determine how much energy which are dissipated through the translation of the barrier. The energy dissipated through the inertia and the drag forces could be determined. Since such long simulations not have been completed in this master thesis it is not possible to determine the force which will be transferred to the bridge and/or the force which will be taken by the supports after the barrier has translated a given distance. Further investigation are recommended to be performed on this scenario.

7.4.1 General

The collision force found for collision of a bow against a rigid wall was about $60MN$. If the collision force between the ship and the barrier is much smaller than $60MN$ a ductility design approach will give satisfying results. If the opposite is the case, a contact force much larger than $60MN$ strength design approach will give reasonable results. However, if the contact force is in the range of $60MN$ a shared energy approach have to be considered.

For the particular collision event discussed in this thesis, the strength of the ship collision barrier is unknown. However, since the design ship have large amount of kinetic energy at the time impact occur ($1565MJ$) and that the design ship only can dissipate about $800MJ$, only ductility design and shared energy design are therefore relevant for this impact scenario.

7.4.2 Shared energy design, both structural parts deformable

Originally the plan for this master thesis was to carry out a shared energy analysis in LS-DYNA where both the structural parts were allowed to deform. When a such finite element analysis is performed the relative deformation of the bow and the barrier is determined in a correct manner. However, such analysis have not been completed.

In lack of results from shared energy analysis it was decide to create force-deformation curves for both the ship and the barrier in the same figure, similarly as Figure 2.2 which is picked from NORSOK N-004 (2004). The method is described in chapter 2.

Force-deformation curves for a simplified shared energy approach

In the following figures the force-deformation curves obtain from the strength design and ductility design analysis have been plotted together in the same figures. This method of treating shared energy design is acceptable as a first approach. However, at a later stage in the design a detailed finite element analysis have to be performed in order to determine the correct energy dissipated in each of the structures. This is in particular necessary when a strength design and a ductility design approach does not can be utilise, which means in the cases where both structures have about the same strength, which is the case for this ship collision barrier as is shown in the Figure 7.4. The reason why a simplified method does not is satisfying when the structure have about the same strength are discussed in chapter 2. The method will generally overestimate the deformation in the stronger part and underestimate the deformation in the weaker part. The reason is that a larger deformation in the stronger part will give a larger contact area and hence also the force will be distributed over a larger are. Hence the force-deformation curve of the strong structure increases and therefore it is not fully valid.

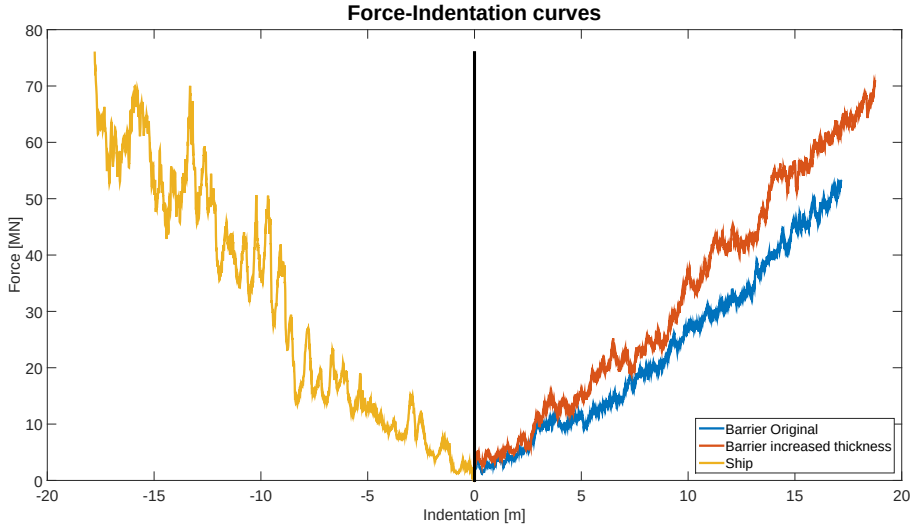

Figure 7.4: Force-deformation curve for the ship and barrier. Both the barrier cross section considered are included

As seen from Figure 7.4. The maximum force for original barrier cross section is about $50MN$. While for the ship and the barrier cross section with increased plate thickness both have a maximum force equal to approximately $60MN$.

Based on the statement that the collision force in the barrier and the ship needs to be equal, the maximum indentation for each part is shown in Figure 7.5. For the case where the weakest barrier is applied the indentation is $13.4m$ and $16.6m$ for the bow and the barrier respectively. In the case where the thickness of the plate in the barrier is increased the indentation of bow and the barrier was measured to be $16.4m$ and $16.6m$.

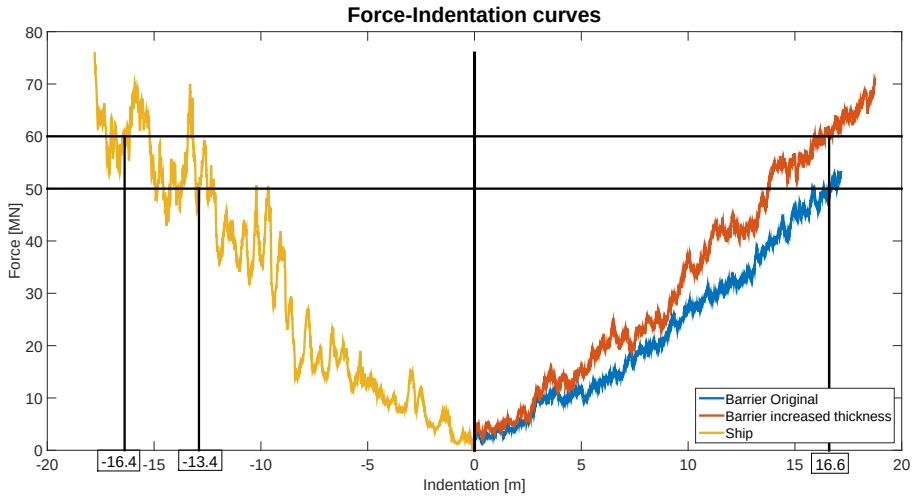

Figure 7.5: Force-deformation curve for the ship and barrier. The measured indentation of each structural parts at the end of the analysis is shown.

Energy-deformation curves for a simplified shared energy approach

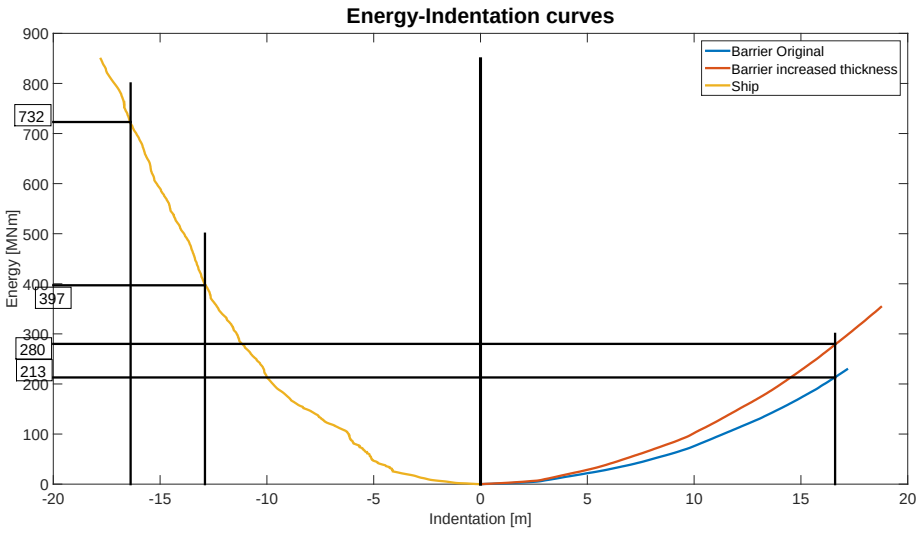

Figure 7.6: Energy-deformation curve for the ship and barrier. Both the barrier cross section considered are included

In Figure 7.6 the strain energy of receptively the barrier and ship have been plotted against indentation of each structural part.

Comparing the force-deformation curve in Figure 7.5 with the energy-deformation curve in Figure 7.6. If Figure 7.5 had been a real force-deformation the energy dissipation for each structural part could be found by simply integrated the area below the force-deformation curve. However, since the contact area between the rigid part and the deformable structure various during the analysis and the fact that the contact forces act in three directions, such a simple relations between the curves could not be established.

By using the indentation level found in Figure 7.5 discussed in the previous section, the energy level according to this indentation can be found from Figure 7.6. Then summing the energy dissipated as strain energy locally in the barrier and the strain energy dissipated in the ship. For the weakest barrier cross section the total strain energy dissipated by applying this method is only $610MJ$. For the barrier cross section with increased thickness the total strain energy dissipated is $1012MJ$. In both cases the dissipated energy is smaller than the kinetic energy in the design ship, (1565).

Concluding remarks

For the measurement and discussion performed in this section it have been assumed that the maximum indentation allowed for the barrier is $16.6m$. This is slightly underestimating the total capacity of the barrier. However, it is only a couple of meter before the bow had sailed

straight through the barrier which is unwanted and therefore the value 16.6m was picked in order to ensure to be on the safe side with respect to the integrity of the barrier.

Based on the method discussed in this section, all the kinetic energy in the design ship will not be possible to be dissipated as strain energy in either of the two barrier cross section discussed. However, the increase in strength from the first barrier to the other barrier cross section with increased plate thickness is severe. It will therefore be likely to expect that a stronger barrier cross section will be able to dissipate all the energy, for instance see Figure 6.7. As a further step it will be necessary to perform integrated shared energy analysis in order get a more correct results of how the energy is dissipated in the two structural parts. With an integrated analysis it will also be possible to take into account the energy dissipated globally. This means energy used to formation of global modes, through translation of the barrier.

7.5 Comparison with Codes and Simplified Methods

The comparison with simplified methods are limited. The reason is mainly that the integrated shared energy approach have not been completed. Therefore the discussion of the shared energy approach based on the results conducted from strength design and ductility design have been discussed in section 7.4.2. This is itself a simplified method. However, some simplified approach will be discussed with respect to the analysis performed in this master thesis. First a comparison to some simplified strain equation taken from NORSOK N-004 (2004). Thereafter a discussion of the collision force in comparison with different design codes.

7.5.1 Comparison with strain energy equations in NORSOK N-004 (2004)

Two equations which calculate the amount of kinetic energy which need to be dissipated as strain energy in the ship and the installation is given in NORSOK N-004 (2004). The theory related to those equations were discussed in chapter 2.The two equations represents a compliant and a fixed installation, see equation (2.4) and equation (2.5). Those equations are reprinted below.

Compliant installations:

$$E_{strain} = \frac{1}{2} \cdot (m_s + a_s) \cdot v_s^2 \cdot \frac{(1 - \frac{v_i}{v_s})^2}{1 + \frac{m_s + a_s}{m_i + a_i}} \tag{7.1}$$

Fixed installations:

$$E_{strain} = \frac{1}{2} \cdot (m_s + a_s) \cdot v_s^2 \tag{7.2}$$

For the case of a fixed installation (equation (7.2)), the total kinetic energy have to be dissipated as strain energy. As have been shown in section 7.4.2 will this not be possible for the considered local barrier cross section if the ship does not are allowed to be further deformed after the deformations have reached the collision bulkhead. However, the case considered in this master thesis is in reality a compliant installation. The barrier is considered as a freely floating structure. Therefore some of the kinetic energy considered in connection with the impact are allowed to remain as kinetic impact after impact and some energy will be dissipated through translation. Hence the strain energy necessary to be dissipated as strain energy are lower than for the case with a fixed installation.

By inserting the relevant parameters into equation (7.1) and utilise that the velocity of the barrier at impact is zero ($v_i = 0$), the amount of energy which is necessary to be dissipated as strain energy are calculated to $1170.9MJ$. Comparing this value with the values determined in section 7.4.2 ($1012MJ$) it is slightly higher. The differences is only about $150MJ$. This means that it is likely to expect that for stronger cross section all the strain energy could be dissipated by the two structures and that the structures will still remain intact after collision. This means that the risk of human life is reduced.

7.5.2 Comparison of Ship Collision Forces with Different Design Codes

In the following are a briefly comparison of the collision force between the foce conducted from the analysis compared with the codes requirement in NORSOK N-004 (2004) and AASHTO American (Association of State Highway and Transportation Officials), (AASHTO Guide specification, 2009, AASHTO LRFD, 2012). In addition also the collision force recommended in design from Eurocode 1: Part 1-7 (2006) is also included.

In NORSOK N-004 (2004) the curve for force-deformation of 125 000 DWT tanker is included. This is a large ship compared to the ship used in this master thesis. The design ship is assumed to be a cruise ship with tonnages 31 456 DWT, however the bow model applied in the analysis have a tonnage of only approximately 11 000 DWT. NORSOK N-004 (2004) divides the structure into a bulb and the substructure which is the rest of the structure when the bulb is omitted. The total collision force is then approximately around $100MN$, which is nearly 50% larger force compared to the force conducted from strength design approach in section 6.1. However it is not practical to compare a 125 000 DWT ship with a ship with tonnage of 11 000 DWT. Further comparison with collision forces in NORSOK N-004 (2004) is therefore not performed.

AASHTO suggest a static ship impact force formula, see equation (7.3).

$$P_s = 220 \cdot (DWT)^{1/2} \cdot (V/27) \tag{7.3}$$

Where;

P_s: Equivalent static impact force [kips]

DWT: Deadweight tonnage of the ship [metric tonnes]

V: Ship impact velocity [feet per second]

By inserting the relevant parameters for the design ship, 31 456 DWT, 10 m/s and using relevant conversion factors. The static ship impact force for this particular design ship is calculated to be $211MN$. This force is a lot larger than the force conducted from the strength design approach ($60MN$).

In section C.4.4 in Eurocode 1: Part 1-7 (2006) equations to calculate the bow impact force, the corresponding indentation and the duration of the impact are included.

$$F_{bow} = \begin{cases} F_0 \cdot \overline{L} \cdot [\overline{E}_{imp} + (5.0 - \overline{L}) \cdot \overline{L}^{1.6}]^{0.5} & \text{for } \overline{E}_{imp} \geq \overline{L}^{2.6} \\ 2.24 \cdot F_0 \cdot [\overline{E}_{imp} \cdot \overline{L}]^{0.5} & \text{for } \overline{E}_{imp} < \overline{L}^{2.6} \end{cases} \tag{7.4}$$

Where:

$$\overline{L} = L_{pp}/275m \tag{7.5}$$

$$\overline{E}_{imp} = E_{imp}/1425MNm \tag{7.6}$$

$$E_{imp} = \frac{1}{2} \cdot m_X \cdot v_0^2 \tag{7.7}$$

F_{bow}: Largest bow impact force [MN]

F_0: Reference collision force = 210 MN

E_{imp}: Energy which have to be absorbed by plastic deformations

L_{pp}: Length between perpendicular

m_X: Mass plus added mass

v_0: Velocity before impact

Further Eurocode 1 suggest that the largest indentation s_{max} is calculated according to equa-

tion (7.8) and the duration T_0 is calculated according to equation (7.9).

$$s_{max} = \frac{\pi \cdot E_{imp}}{2 \cdot F_{bow}} \tag{7.8}$$

$$T_0 \approx 1.67 \cdot \frac{s_{max}}{v_0} \tag{7.9}$$

When I insert the relevant parameter for the design ship according to table 4.1 into the above equations I get $F_{bow} \approx 300MN$, $s_{max} \approx 8m$ and $T_0 \approx 1.5s$.

As a concluding remark on the collision forces proposed by AASHTO and Eurocode 1 are that both is depending on the impact velocity. Both will over predict the actual ship collision force obtained from the nonlinear finite element analysis of the strength design approach in chapter 6.1. The reason is that a analysis of a bow against rigid wall have the purpose of predicting the quasi-static strength of the bow. Therefore the ship impact forces calculated from equations in AASHTO and/or Eurocode 1 should be compared and discussed with relation to the contact forces occurred for the integrated shared energy analysis. Since those analysis does not have been fulfilled this will not be possible. However by comparing with the results obtained by Konstali (2014), it is clearly seen that AASHTO and Eurocode 1 over predict the collision force. They gives more than twice the value from the finite element analysis.

A further discussion of the ship collision forces proposed in the different design codes and a comparison between the codes were performed in the author's project thesis (Hansen, 2014).

8 Conclusion and Further Work

This chapter shortly summarise and conclude on the work carried out in this master thesis. The work is based on reasonable assumptions. However, points in the design of the ship collision barrier should be analysed in more detail and such considerations is included as recommendation for further work.

8.1 Conclusion

The ship collision barrier needs to be designed for dissipation of large amount of energy. Due to the larger amount of kinetic energy in the design ship ($1565MJ$), the ship is not able to dissipate the total energy alone. The reason is due to the risk of human life, the bow is not allowed to be crushed further behind than to the position of the collision bulkhead. At this position the amount of strain energy dissipated is determined to be a maximum of $800MJ$. In other word this means that a strength design, where the total amount of energy is dissipated in the bow is not possible. By those reason the ship collision protection barrier had to be designed in order to dissipate large amount of energy.

The ship collision barrier investigated in this master thesis was provided to be built up of aluminium alloys. Aluminium is in general a poorer material compared to ordinary steel material in relation to accidental limit state. One of the reason is related to the stress-strain curves. Most aluminium alloys have a small and steep plastic zone. This means that the difference between the yield stress and ultimate stress is relatively small. Therefore the redistribution of forces from the elastic to the plastic zone may not occur in a proper way. Hence the structure may fail at a lower strain level compared to a case where the redistributed of forces is satisfying. Most of aluminium alloys have a severe drop in the material properties in the heat affected zone (HAZ). This is the case for the aluminium alloy picked for the stiffeners (alloy 6082-T6), but for the alloy suggested for the plates (alloy 5083-O) have no reduction in HAZ. Analysis conducted for a stiffened plate showed for large deformations the plate carry all the loads and energy as membrane forces and stresses. The stiffeners contributes to the strength is mainly related to carry the life loads in the elastic range and to prevent buckling. Therefore it is the material properties of the plates which are governing with respect to the total energy dissipation in the structure. Hence, the choice of a material with HAZ for the stiffeners (alloy 6082-T6) and a alloy where the HAZ was omitted for the plates (alloy 5083-O) sounds reasonable.

Two different local barrier cross sections were considered. The difference between the two cross sections were related to the plate thickness. From the ductility design analysis the strongest cross section considered was only able to dissipate about $300MJ$. By simply comparing the results from the strength design and the ductility design as a simplified approach. The total energy dissipated by the ship and the barrier would hence have been $1100MJ$. Therefore by this simple comparison the total kinetic energy in the design ship can not be dissipated as strain energy in the ship and the barrier. In a real collision event some energy will be lost to the environment and therefore the cross section may be strong enough to carry the energy in the design ship. Energy will be dissipated due to the translation of the barrier. This should have been investigated further by performing integrated shared energy analysis. However, such analysis have not been completed and it is therefore not possible to give a general conclusion related to the necessary strength of the barrier.

From the few analysis carried out in this thesis with alloy 5083-O and 6082-T6 it sound feasible to apply aluminium alloys to design the ship collision barrier. However, more research needs to be done in order to verify this statement. In order to perform the nonlinear finite element analysis in this thesis, it was necessary to apply several assumptions related to the behaviour of the aluminium alloys. One of the main assumptions were that the aluminium structure will fails in a similar manner with respect to fracture propagation as a steel structure. However, research have shown that this is not usually the case. Therefore it should be verified that the fracture criterion applied for the aluminium structure gives reasonable results.

The production cost and the cost of the material itself have only qualitative been discussed in this thesis as a factor which should be taken into account. The cost should be investigated more in detail. Due to the cost of different aluminium alloys and tempers it may then be necessary to consider other alloys and tempers.

The intact stability of the barrier was determined to be good. For the damaged stability only a simplified qualitative discussion and simplified equations were applied. The damaged stability for the cross section applied was determined to be satisfying. However, more comprehensive calculation should be carried out in order to verify those results.

8.2 Recommendation for further work

- Integrated shared energy analysis should be conducted in order to get a more correct representation of the energy distribution between the barrier and ship.
- A total analysis with long simulation time should be conducted in order to measure the amount of energy dissipated by the drag force as a function of the global translation of the barrier.
- An impact scenarios where the ship hits at the barrier end should be investigated more in detail in order to measure the rotational stiffness of the barrier.
- A longer local cross section is preferable to be modelled in order to have a correct distribution of the forces and stresses in a larger area around the impact position.
- The fracture criterion applied for the aluminium structure should be verified to be valid for aluminium structures.
- The material properties of the aluminium alloys should be verified. It is preferable to have data which describes the stress-strain curves more in detail. Special concerns should be done with respect to HAZ. The characterisation of the properties in HAZ have only be found through curve fittings in this thesis.
- A cost estimate of the production cost should be performed. Then it may be shown that other aluminium alloys are more preferable with respect to cost and hence design and analysis should be performed with respect to those alloys.
- The bow model applied is in fact valid for a smaller ship. Therefore it should be verified that this bow model actually gives reasonable representation of the strength of the actual design ship.
- It is preferable to carry out shared energy analysis where the heading of the ship are different from 90 degrees. A code accounting for global motion should then be applied. At the moment code to allow such modelling based on manoeuvring equation with LS-DYNA is under development.
- Damage stability of the barrier should be verified by using an advanced computer program.
- The HAZ should be included in the analysis.

Bibliography

AASHTO Guide specification (2009). AASHTO (2009), Guide specification and commentary for vessel collision design of highway bridges. Volume I: Final report. Am. Assoc. of State Hwy. and Transp. Officials (AASHTO). Washington D.C.

AASHTO LRFD (2012). AASHTO, LRFD Bridge Design Specifications and Commentary, American Association of State Highway and Transportation Officials, Washington, D.C., 2012.

Alsos, H. S., Amdahl, J. r., and Hopperstad, O. S. (2009). On the resistance to penetration of stiffened plates, Part II: Numerical analysis. *International Journal of Impact Engineering*, 36(7):875–887.

Alsos, H. S., Hopperstad, O. S., Törnqvist, R., and Amdahl, J. r. (2008). Analytical and numerical analysis of sheet metal instability using a stress based criterion. *International Journal of Solids and Structures*, 45(7-8):2042–2055.

Chen, Q. (2011). *Ultimate strength of aluminium panels, considering HAZ effects* , volume 2011:326. Norges teknisk-naturvitenskapelige universitet, Trondheim.

Eurocode 1: Part 1-7 (2006). Eurocode 1: Actions on structures - Part 1-7: General actions - Accidental Action.

Eurocode 9: Part 1-1 (2007). Eurocode 9: Design of aluminium structures - Part 1-1: General structural rules.

Hallquist, J. (2006). *LS-DYNA theory manual.*

Hansen, J. L. (2014). Analysis and Design of Ship Collision Barriers on a Submerged Floating Tunnel subjected to Large Ship Collisions. (Project Thesis NTNU).

Hatch, J. E. (1984). *Aluminum: properties and physical metallurgy* . American Society for Metals, Metals Park, Ohio.

Konstali, Ø. (2014). Analysis and Design of Ship Collision Barriers on a Submerged Floating Tunnel Subjected to Large Ship Collisions. (Master Thesis NTNU).

Kristensen, O. H. H. (2001). Ultimate Capacity of Aluminium Plates under Multiple Loads, Considering HAZ Properties. *Department of Marine Structures*, Dr. Ing Th(1307).

Mazzolani, F. M. (1995). Aluminium alloy structures .

Moan, T. . (2003). *Finite element modelling and analysis of marine structures*, volume UK-03-98. Marinteknisk senter., Trondheim.

NORSOK N-004 (2004). Design of Steel Structures NORSOK N-004 Rev. 2.

Ramboll (2011). Design ship. (Presentation).

Appendix A Retardation of the barrier after impact

This appendix gives a short review of the discussion an establishment of an analytical expression for the retardation of the barrier due to drag forces when the barrier is assumed to remain straight after impact. This was performed in the author's project thesis (Hansen, 2014).

The discussion was performed with use of analytical equations and with the barrier draft as a variable. and performed for different drafts of the barrier. Two different cross section was considered, one closed cross section and on with a skirt. Those two cross sections is shown in Figure 4.1 and reprinted as A.1 in this appendix. An expression was deducted only for the centric collision scenarios and hence only this expression is reprinted here. It was also discussed how the mooring forces could be included.

The derivations regards that both conservation of momentum (equation (2.2)) and the conservation of energy (equation (2.3)) have to be satisfied.

Centric collision

In the first analysis, head on collision at center of the barrier is assumed. This will gives a situation with pure translation of the barrier. It is assumed that impact duration is short. The velocity after impact can therefore be calculated from conservation of momentum, equation (2.2). After impact the ship and the barrier have equal velocity and act as one body.

Some addition simplification have been done to be able to carry out the calculation in a simplified way. The added mass and drag coefficient are assumed to be constant, but in the real world this values are both frequency dependent. The drag coefficient in the analysis is taken to be 1.2 and the added mass for the barrier is assumed to be equal to the mass of the barrier for the closed cross-section. The cross-section with skirt is assumed to have the same added mass as the closed cross-section for a given draft. The rest of the parameters are given in Table A.1. The loss of momentum and energy to the environmental have been neglected.

Length [m]	380
Breadth [m]	20
Draft [m]	d [Variable]
Mass ship [tonne]	31456
Added mass ship [kg]	$0.2 \cdot m_{ship}$
Mass barrier [kg]	$L \cdot B \cdot \rho \cdot d$
Added mass barrier [kg]	$1.0 \cdot m_{barrier}$
Drag coefficient, C_D	1.2

Table A.1: Input parameter for the simplified analysis

The energy in the body consisting of the ship and the collision barrier need to be retarded by drag forces and possibly mooring forces. As a first approach it is assumed that the barrier is freely floating and have no mooring forces. The sequence to calculate the velocity of the barrier and ship as a function of the translated distance are given in the following.

Only drag forces:

$$\sum F = m \cdot a \tag{A.1}$$

$$(m_s + a_s + m_i + a_i) \cdot a = -\frac{1}{2} \cdot \rho \cdot C_D \cdot A_p \cdot v^2 \tag{A.2}$$

$$a = \frac{dv}{dt} = \frac{ds}{dt} \cdot \frac{dv}{ds} = v \cdot \frac{dv}{ds} \tag{A.3}$$

$$(m_s + a_s + m_i + a_i) \cdot v \cdot \frac{dv}{ds} = -\frac{1}{2} \cdot \rho \cdot C_D \cdot A_p \cdot v^2 \tag{A.4}$$

For simplicity introducing $m = (m_s + a_s + m_i + a_i)$

$$\frac{1}{v} \cdot dv = -\frac{1}{2 \cdot m} \cdot \rho \cdot\cdot C_D \cdot A_p \cdot ds \tag{A.5}$$

Integrate on both side of the equation:

$$ln(v) = -\frac{1}{2 \cdot m} \cdot \rho \cdot C_D \cdot A_p \cdot s + C \tag{A.6}$$

$$v = C \cdot \exp(-\frac{1}{2 \cdot m} \cdot \rho \cdot C_D \cdot A_p \cdot s) \tag{A.7}$$

Using the boundary condition $v(0) = v_{b,i}$ and $v(\infty) = 0$, which gives $C = v_{b,i}$. Then

$$v(s) = v_{b,i} \cdot \exp(-\frac{1}{2 \cdot m} \cdot \rho \cdot C_D \cdot A_p \cdot s) \tag{A.8}$$

Where:

a: Acceleration

m_s: Mass ship

a_s: Added mass ship

m_i: Mass installation/barrier

a_i: Added mass installation/barrier

ρ: Density seawater

C_D: Drag coefficient

A_p: Projected area

s: Distance translated

v: Velocity of the barrier

Draft is taken as a variable which varies between 8 and 20 meter. The velocity as a function of distance according to equation (A.8) have been calculated for two different barrier design, one closed cross-section and one which consist of a cross-section with a skirt below. The purpose of the skirt is to increasing the projected area and hence the drag force with a minor increase in the mass. For illustration see Figure A.1. For the case with skirt the draft of the main body is taken equal to 8 meter and the total draft of the barrier varies between 8 and 20 meter.

Figure A.2 and A.3 shows the result for both cross-sections. From equation (A.8) it is clear that the velocity decays exponentially with respect to the distance. This could also clearly be seen from the figures. It is also clear that a cross-section with skirt will have a larger velocity

straight after the impact due to smaller mass. The kinetic energy will then also be larger since the velocity is a factor of power two and mass is only of power one when calculating kinetic energy. Therefore less energy have to be taken locally by the barrier and the ship. In addition we see that the velocity is decreasing faster by using a cross-section with skirt, compared to the closed cross-section with the same draft. For plot showing the kinetic energy and drag force as a function of distance see Figure A.4, A.5, A.6 and A.7.

Figure A.1: Cross section of the barrier with and without skirt

A dimensionless plot as a function of the characteristic value is shown in Figure A.8. Here the y-axis is $\frac{v(s)}{v_{b,i}}$ and the x-axis is $\frac{1}{2 \cdot m} \cdot \rho \cdot C_D \cdot A_p \cdot s$.

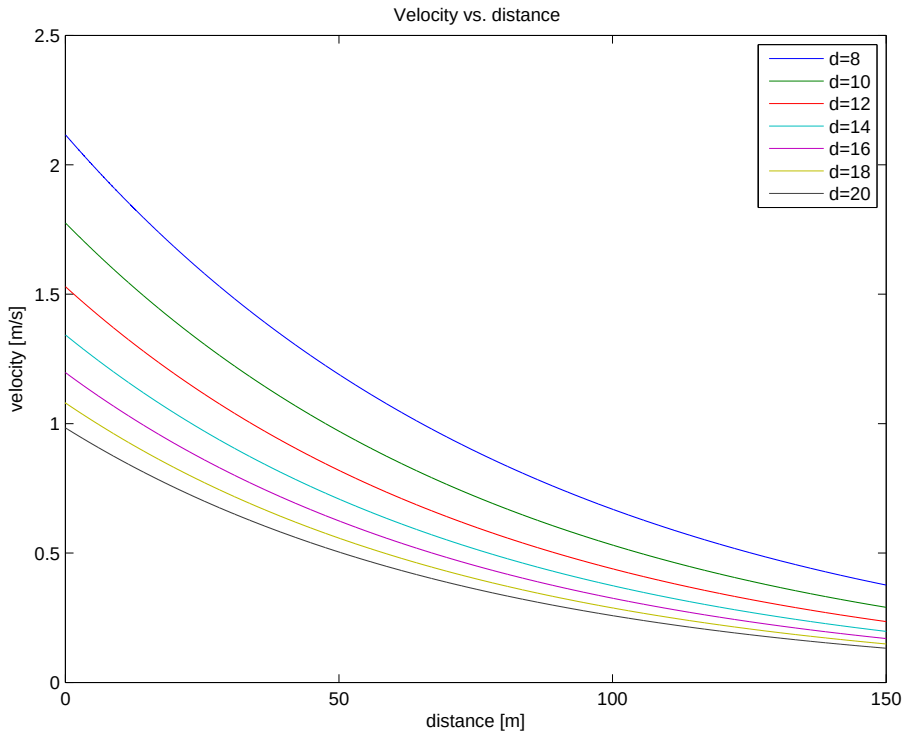

Figure A.2: Velocity vs. distance plot for a closed-cross section with different drafts

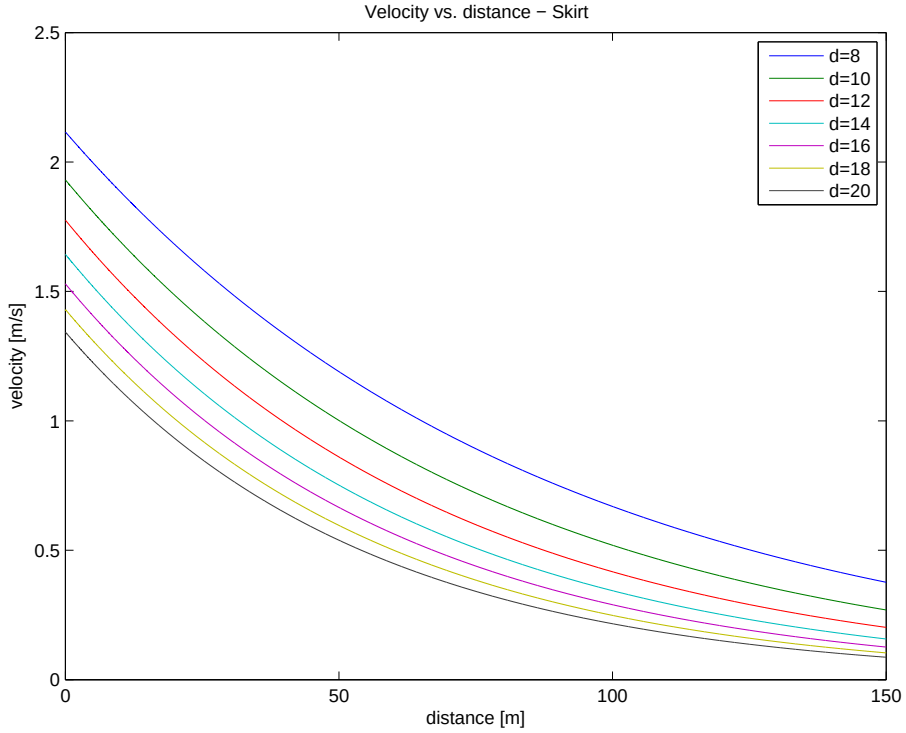

Figure A.3: Velocity vs. distance plot for a closed cross-section with draft 8 meter and with variable effective draft of the included skirt

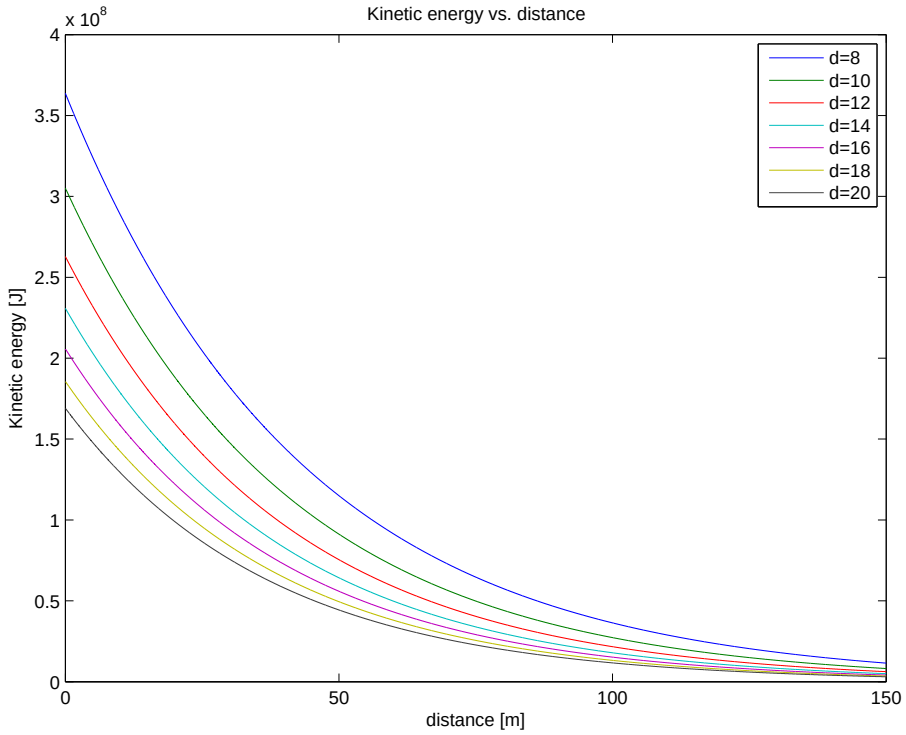

Figure A.4: Kinetic energy vs. distance for different drafts

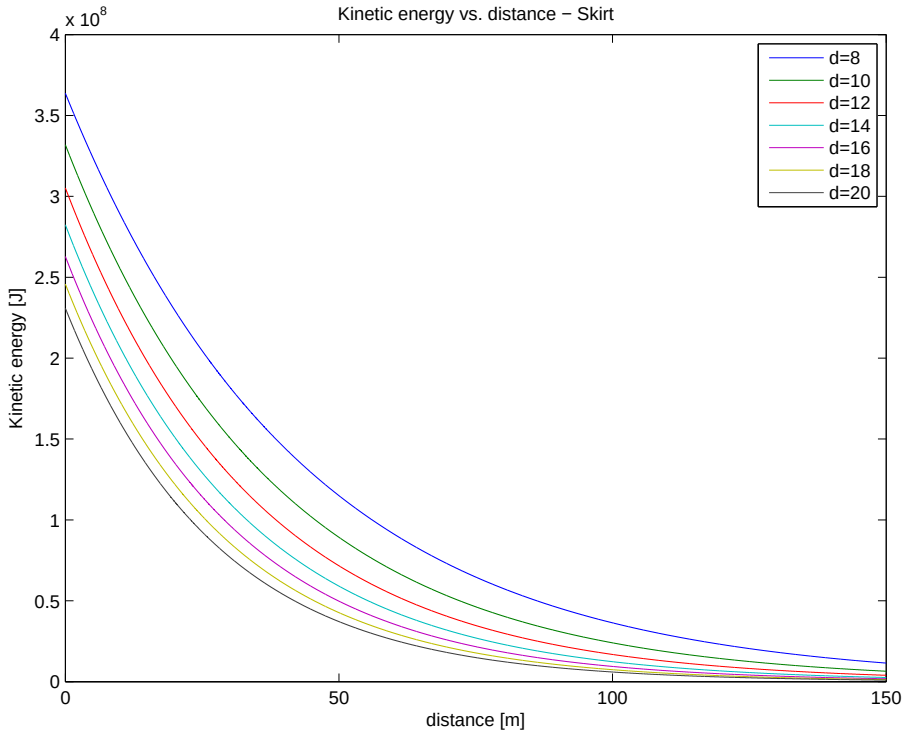

Figure A.5: Kinetic energy vs. distance for different drafts with skirt

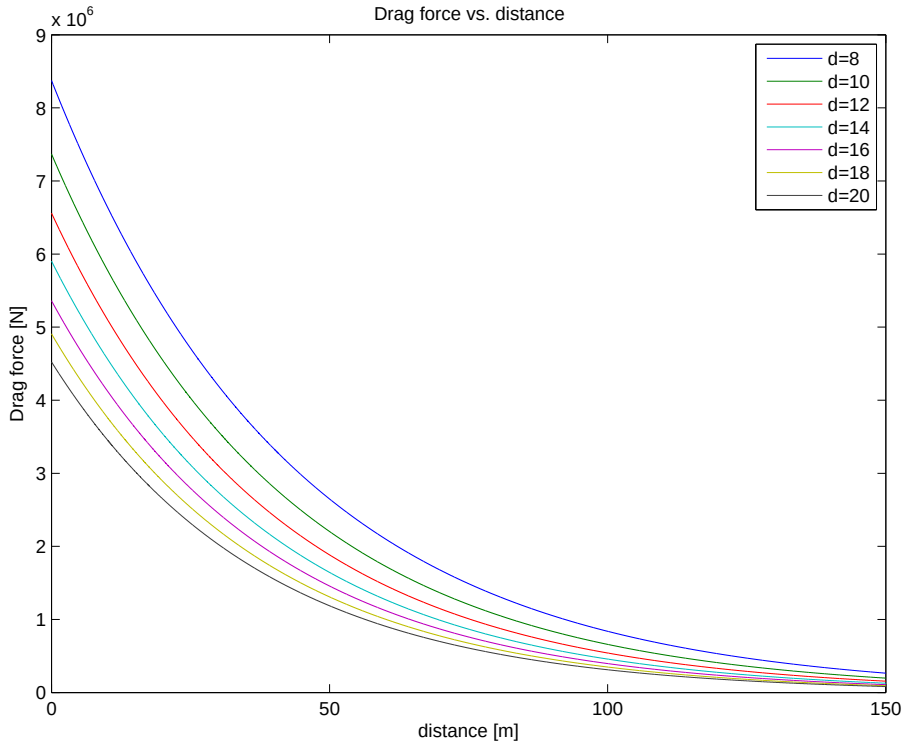

Figure A.6: Drag force vs. distance for different drafts

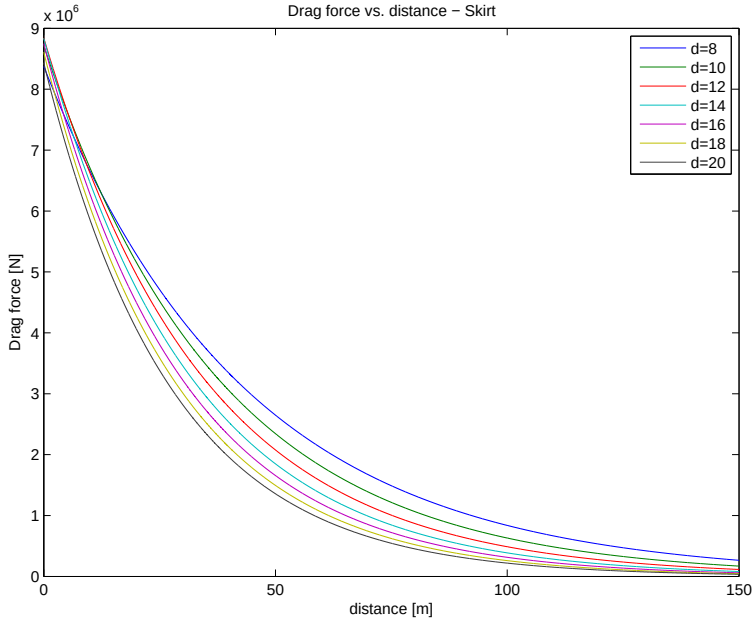

Figure A.7: Drag force vs. distance for different drafts with skirt

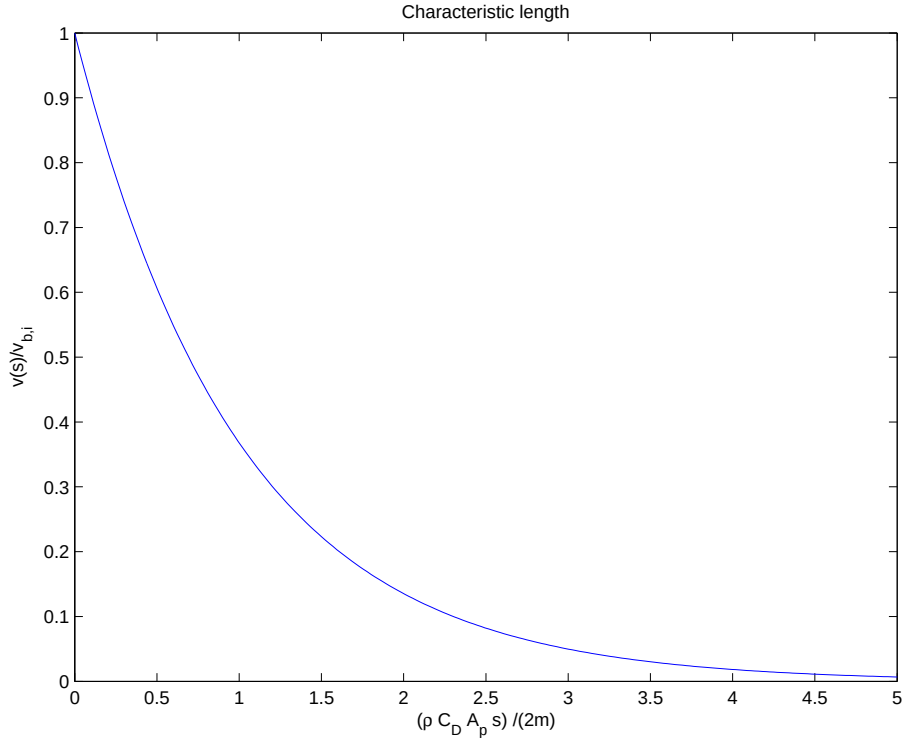

Figure A.8: Characteristic velocity vs. distance plot as a function of the parameters

Includes mooring forces: The mooring force is depending on the displacement. Hence the differential equation will be more complex, it will be a non-linear ordinary differential equa-

tion.

$$\sum F = m \cdot a \tag{A.9}$$

$$(m_s + a_s + m_i + a_i) \cdot a = -F_D(v) - F_{anchoring}(s) \tag{A.10}$$

Assuming a linear anchoring force, $F_{anchoring}(s) = k \cdot s$ where k is the stiffness of the anchoring system, then:

$$(m_s + a_s + m_i + a_i) \cdot a = -\frac{1}{2} \cdot \rho \cdot C_D \cdot A_p \cdot v^2 - k \cdot s \tag{A.11}$$

$$a = \frac{dv}{dt} = \frac{ds}{dt} \cdot \frac{dv}{ds} = v \cdot \frac{dv}{ds} \tag{A.12}$$

For simplicity introducing, $m = (m_s + a_s + m_i + a_i)$

$$\frac{dv}{ds} = -\frac{1}{2 \cdot m} \cdot \rho \cdot C_D \cdot A_p \cdot v - \frac{k \cdot s}{m \cdot v} \tag{A.13}$$

This is a first order non-linear ordinary differential equation. The solution with boundary condition $v(0) = v_{b,i}$ is given below for $k, m, \rho, C_D, A_p \geq 0$. The simplification $c = \frac{1}{2 \cdot m} \cdot \rho \cdot C_D \cdot A_p$ are introduced.

$$v(s) = \sqrt{\frac{\exp(-\frac{2 \cdot c \cdot s}{m}) \cdot (2 \cdot c^2 \cdot v_{b,i}^2 - k \cdot m) - 2 \cdot c \cdot k \cdot s + k \cdot m}{2 \cdot c^2}} \tag{A.14}$$

Due to large kinetic energy straight after the impact it may not be feasible to activate the mooring at $s = 0$. It may be a better solution to assume that the barrier is moored with a weak-link at $s = 0$ and that the primary mooring is activated at a position $s = s_1$. The way to treat this

will then be a combination of equation (A.8) and (A.14), see equation (A.15).

$$v(s) = \begin{cases} v_{b,i} \cdot \exp(-\frac{1}{2 \cdot m} \cdot \rho \cdot C_D \cdot A_p \cdot s) & \text{for } s < s_1 \\ \sqrt{\frac{\exp(-\frac{2 \cdot c \cdot s}{m}) \cdot (2 \cdot c^2 \cdot v(s_1)^2 - k \cdot m) - 2 \cdot c \cdot k \cdot s + k \cdot m}{2 \cdot c^2}} & \text{for } s \geq s_1 \end{cases} \tag{A.15}$$

Another way to treat the anchoring force is to assume that we can neglect the drag force when the mooring force is activated. This may be a good assumption since the mooring force will probably be much larger than the drag force short time after it has been activated. The deduction of this solution is given in the following steps. First the differential equation for only the mooring force have been solved.

$$\sum F = m \cdot a \tag{A.16}$$

$$(m_s + a_s + m_i + a_i) \cdot a = -F_{anchoring}(s) \tag{A.17}$$

Assuming a linear anchoring force, $F_{anchoring}(s) = k \cdot s$ where k is the stiffness of the anchoring system, then:

$$(m_s + a_s + m_i + a_i) \cdot a = -k \cdot s \tag{A.18}$$

$$a = \frac{dv}{dt} = \frac{ds}{dt} \cdot \frac{dv}{ds} = v \cdot \frac{dv}{ds} \tag{A.19}$$

For simplicity introducing, $m = (m_s + a_s + m_i + a_i)$

$$m \cdot v \cdot \frac{dv}{ds} = -k \cdot s \tag{A.20}$$

Integrating on both sides of the equation gives the solution for the velocity as a function of

the translation s. (Only the positive solution are of interest.)

$$v(s) = \sqrt{-\frac{k}{m} \cdot s^2 + C} \tag{A.21}$$

Using the boundary condition that equation (A.8) and (A.21) gives the same velocity at a distance $s = s_1$, where the mooring force are activated.

$$v(s) = \sqrt{-\frac{k}{m} \cdot s^2 + \frac{k}{m} \cdot s_1^2 + v_{b,i}^2 \cdot \exp(-\frac{1}{m} \cdot \rho \cdot C_D \cdot A_p \cdot s_1)} \tag{A.22}$$

Combining equation (A.8) and (A.22).

$$v(s) = \begin{cases} v_{b,i} \cdot \exp(-\frac{1}{2 \cdot m} \cdot \rho \cdot C_D \cdot A_p \cdot s) & \text{for } s < s_1 \\ \sqrt{-\frac{k}{m} \cdot s^2 + \frac{k}{m} \cdot s_1^2 + v_{b,i}^2 \cdot \exp(-\frac{1}{m} \cdot \rho \cdot C_D \cdot A_p \cdot s_1)} & \text{for } s \geq s_1 \end{cases} \tag{A.23}$$

Equation (A.15) and (A.23) have not been treated any further in this thesis. By use of one of those equations the regarded stiffness of the mooring system can be calculated if the position of the barrier before impact relative to the bridge and the position where the mooring forces are activated are know. In additional it needs to be known how much energy, if any, the barrier and ship could have when/if it hits the submerged floating tunnel.

Appendix B Plastic moment capacity for the barrier

This appendix shows the calculation of plastic moment capacity for the straight barrier. It is assumed that the ship can hit at an arbitrary position along the barrier. This example are used to show which position which will be most severe with respect to the global strength of the barrier, see section 4.2.1.

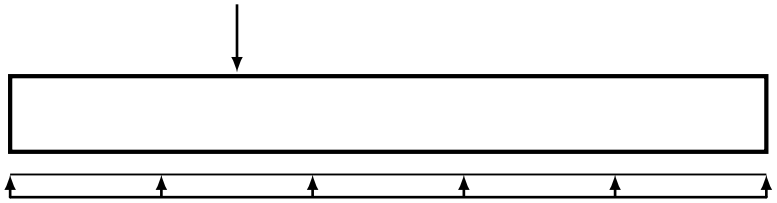

Figure B.1: Simplified model for the global analysis

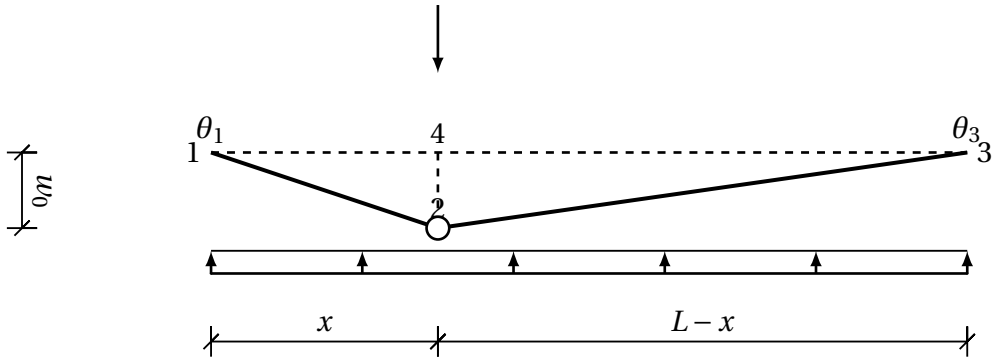

Figure B.2: Deformed shape when plastic hinge have been formed

Firstly establishing the geometrical relations between the different parameters:

$$w_0 = \theta_1 \cdot x = \theta_2 \cdot (L-x) \qquad \Rightarrow \theta_2 = \theta_1 \cdot \frac{x}{L-x} \tag{B.1}$$

Internal virtual work:

$$W_i = M_P \cdot \theta_1 + M_P \cdot \theta_2 = M_P \cdot (\theta_1 + \theta_2) = M_P \cdot \theta_1 \cdot \left(1 + \frac{x}{L-x}\right) \tag{B.2}$$

External virtual work:

$$W_e = \int_0^L \cdot q \cdot w(x) \cdot dx = q \cdot x \cdot w_0 \cdot \frac{1}{2} + q \cdot (L-x) \cdot w_0 \cdot \frac{1}{2} = \frac{1}{2} \cdot q \cdot x \cdot w_0 + \frac{1}{2} \cdot L \cdot w_0 \cdot q - \frac{1}{2} \cdot q \cdot x \cdot w_0$$
$$= \frac{1}{2} \cdot L \cdot w_0 \cdot q = \frac{1}{2} \cdot L \cdot x \cdot q \cdot \theta_1 \tag{B.3}$$

Combining the equation for internal and external energy, see equation (B.2) and equation (B.3).

$$W_i = W_e \tag{B.4}$$

Insert:

$$M_P \cdot \theta_1 \cdot \left(1 + \frac{x}{L-x}\right) = \frac{1}{2} \cdot L \cdot x \cdot q \cdot \theta_1 \tag{B.5}$$

Gives:

$$M_P = \frac{1}{2} \cdot q \cdot x \cdot (L-x) \tag{B.6}$$

To calculate the most critical impact position with respect to global strength, it is necessary to find the minimum of equation (B.6). Therefore finding the zero point of the derivative of this equation.

$$\frac{\partial M_P}{\partial x} = \frac{1}{2} \cdot q \cdot (L - 2 \cdot x) = 0 \qquad \Rightarrow x = \frac{1}{2} \tag{B.7}$$

The most critical impact position is at the middle position of the barrier $L/2$.

Appendix C Additional results

C.1 Shared energy approach based on strength design and ductility design

C.1.1 Force-indentation curves for a simplified shared energy approach

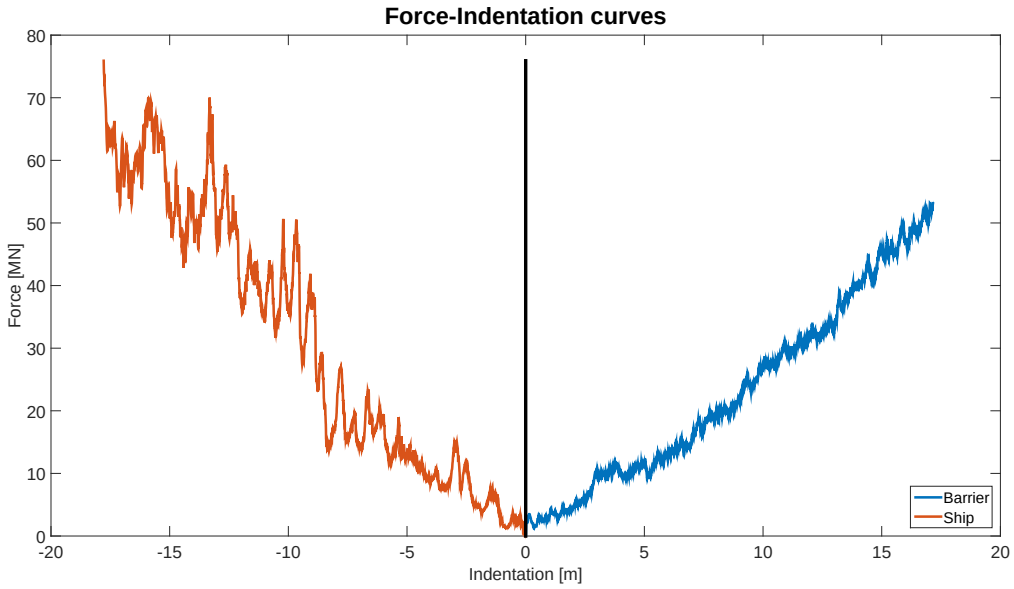

Figure C.1: Force-deformation curve for the ship and barrier. Each curve based on the rigid analysis. The curve for the barrier is for the cross section discussed in section 4.2.2

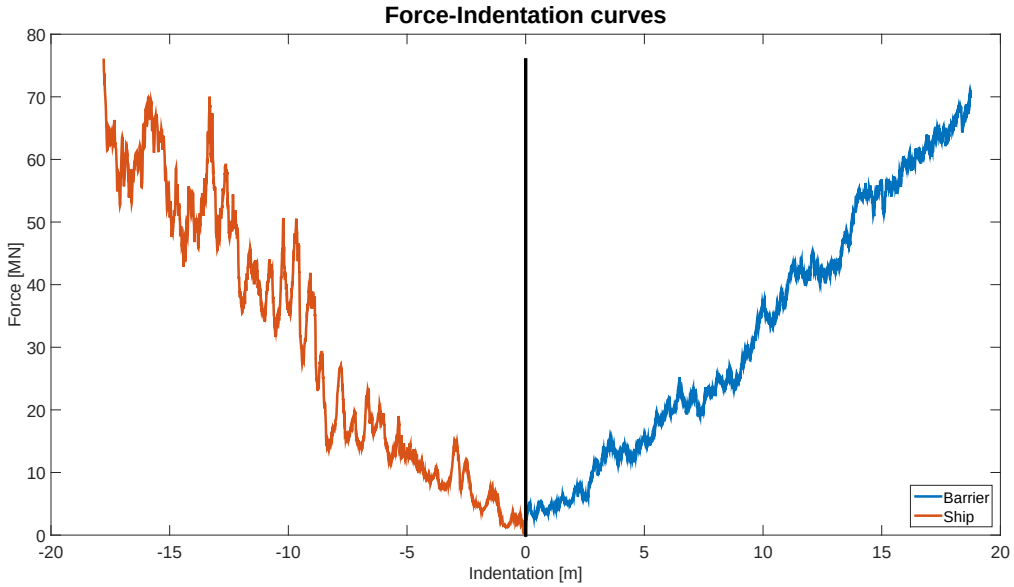

Figure C.2: Force-deformation curve for the ship and barrier. Each curve based on the rigid analysis. The curve for the barrier is for the case with increased thickness

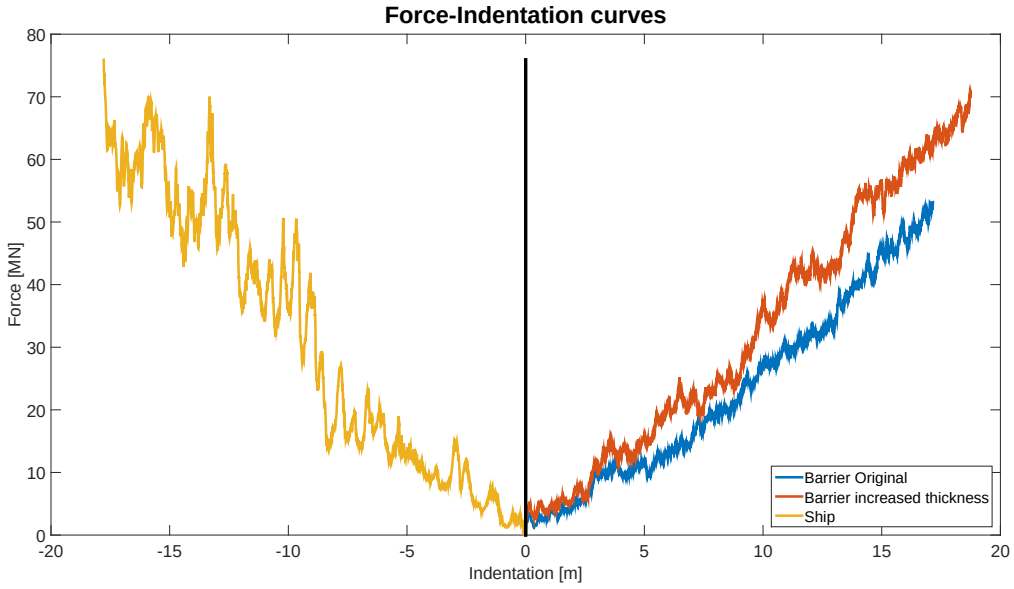

Figure C.3: Force-deformation curve for the ship and barrier. Both the barrier cross section considered are included

C.1.2 Energy-deformation curves for a simplified shared energy approach

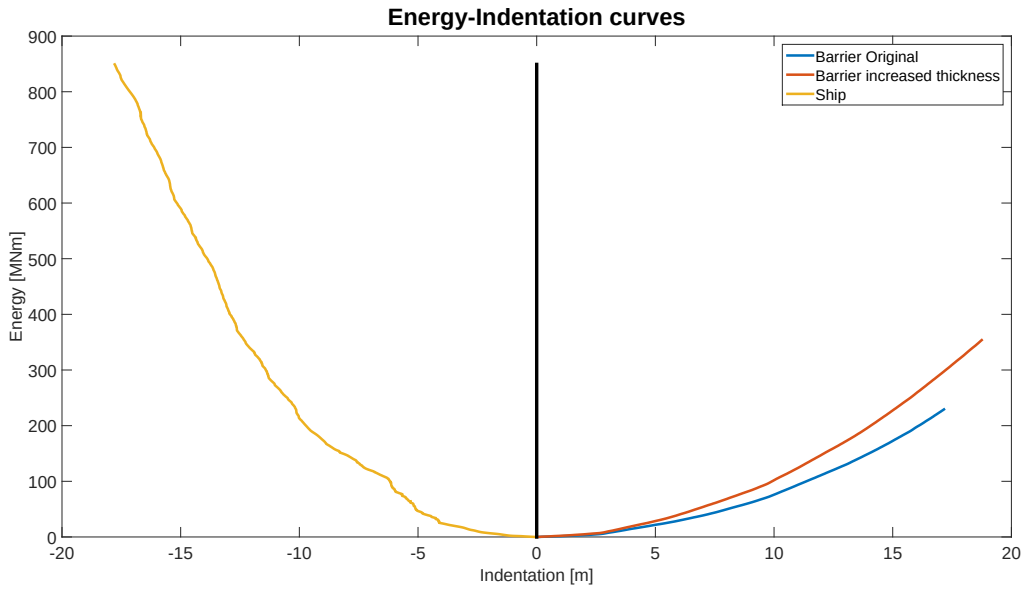

Figure C.4: Energy-deformation curve for the ship and barrier. Both the barrier cross section considered are included